University of Strathclyde Glasgow

Thermal modelling of wind turbine gearboxes for condition monitoring

PhD Thesis

Becky Corley

Wind Energy and Control

Department of Electronic and Electrical Engineering

University of Strathclyde, Glasgow

December 8, 2025

This thesis is the result of the author's original research. It has been composed by the author and has not been previously submitted for examination which has led to the award of a degree.

Abstract

This thesis explores wind farm reliability research which identifies the gearbox as having the most detrimental influence on wind turbine (WT) reliability. This research brings together theoretical thermal modelling, experimental research, and machine learning data analysis applied specifically for WT gearbox condition monitoring. Existing condition monitoring techniques were explored and many of these data driven models required significant amounts of historical data.

A thermal model was created for a experimental WT test rig and faults were simulated in the form of losses to analyse changes in thermal behaviour. The design of the WT test rig experimental data acquisition set-up is outlined and the results used to validate the thermal model.

Inverse thermal modelling was then applied to real life WT data to estimate changes in losses at particular components, between when a gearbox is healthy, or is one month from a known failure. It was found that there was a potential to detect failure, but efficacy is reduced when the fault is not located near a sensor. However, when carrying out weighting analysis, it was found that combining thermal model results with temperature data, losses could prove more effective in health classification.

WT gearbox reliability analysis was carried out on a population of WTs in relation to the WT power train configuration, comparing the reliability of the gearbox when in a Doubly Fed Induction Generator (DFIG) WT or a Permanent Magnet Generator (PMG) WT. The results of the analysis presented DFIG WT as having worse overall gearbox reliability. This led to the hypothesis that the operation in relation to the grid could have an effect on gearbox loading, fatigue and thus reliability.

Contents

List of Figures

List of Tables

Definitions

SCIG: Squirrel cage induction generator

DFIG: Doubly fed induction generator

WRIG: Wound rotor induction generator

PMSG: Permanent magnet synchronous generator

EESG: Electrically excited synchronous generator

SCADA: Supervisory Control and Data Acquisition

CMS: Condition monitoring system

Cp: Coefficient of power

OEM: Original equipment manufacturer

Nomenclature

R	Rotor radius	m
k	Thermal conductivity	W/mK
A	Surface area	m^2
L	Length	m
h	Heat transfer coefficient	W/m^2K
α	Coefficeint of thermal expansion	-
c	Specific heat capacity	J/kgK
ω	Rotational speed	rad/s
ε	Emissivity	-
σ	Stefan-Boltzman constant	W/m^2K^4
H_ν	Gear loss factor	-
μ_{mz}	Friction coefficient	-
P_a	Power in	W
ϵ_a	Profile contact ratio	-
$\epsilon_{1,2}$	Tip contact ratio	1 pinion, 2 gear
u	Gear ratio	-
β	Base helix angle	^{o}
z	Number of gear teeth	-
F	Force at pitch circle	N
b	Tooth width	mm
υ_Σ	$2\upsilon_t \sin \alpha_t$	m/s
υ_t	Tangential speed at pitch circle	m/s
ρ_c	Equivalent radius of curvature at pitch point of contact	mm
ρ	Fluid density	kg/m^3
α_t	Transverse pressure angle	^{o}
μ	Dynamic viscoity	Ns/m^2
η_{oil}	Dynamic viscosity of oil at operating temperature	$mPAs$

Ra	Average roughness of pinion and gear wheel	μm
X_L	Lubrication parameter	-
υ	Kinematic viscosity	mm^2/s
υ_{oil}	Kinematic viscosity	m^2/s
l	Characteristic length	m
V	Velocity of fluid	m/s
S_m	Submerged surface area	m^2
R_p	Pitch radius	m
D_p	Pitch diameter	m
V_O	Oil volume	m^3
n_i	Rotational speed of gear stage i	rpm
$h_{e,max}$	Max.Tip circle emmersion depth with oil level stationary	mm
h_{e1}, h_{e2}	Tip circle emmersion depth with oil level stationary	mm
h_{e0}	Reference value of immersion depth =10mm	mm
h_c	Height of point of contact above the lowest point of the immersing gear	mm
ϕ	Shaft diameter	m

Acknowledgements

I would like to acknowledge the support of those in EEE department and CDT who have helped me to complete my PhD, in particular James Carroll and Alasdair McDonald, my supervisors, and Drew Smith.

I am thankful for the continued support of my treasured friends; Sofia Koukoura and the windy girls, the Lash Monkeys, Sophie Kneeshaw, SV gang and Lindsey Amos. Most importantly, my husband, Rhys, who has been with me on this journey every difficult step of the way.

I am grateful to my Mum, Brother and Sister who have helped pushed me through, and my Dad, who I wish could have seen this.

Finally, in the words of Snoop Dogg "I want to thank me for believing in me. I want to thank me for doing all this hard work[...] I want to thank me for never quitting." I'm glad it's done.

Chapter 0. Acknowledgements

Chapter 1

Introduction

1.1 Background

The climate crisis poses a huge threat to society. To address the crisis, the United Nations (UN) Framework Convention on Climate Change aims to reduce Greenhouse Gas (GHG) emissions so that global average temperatures do not exceed 2°C above pre-industrial temperatures. If possible, countries pledged to aim for a 1.5°C limit [1]. The UN 2030 Agenda for Sustainable Development calls for urgent action to combat climate change and the impacts in Sustainable Development Goal 13. Additionally, it is intrinsically linked to all 16 of the other Sustainable Development Goals [2]. To meet these goals, energy production must be sustainable through energy security, energy equity (accessibility and affordability) and environmental sustainability [3]. The European Union (EU) has set a target for at least 32% of energy being produced from renewable sources, by 2030 [4] to meet its emissions reduction commitments under the Paris Agreement.

Northern Europe has significant wind resource, meaning it can contribute significantly to meeting renewable energy and climate change targets. The USA and China also have significant installed wind energy. Wind energy has an increasing share of the installed capacity of energy generation in the UK, Europe and globally. The projection of global power generation from wind energy is expected to continue to increase from around 3% in 2015 to 8% in 2030 [5]. Global installed and projected power generation

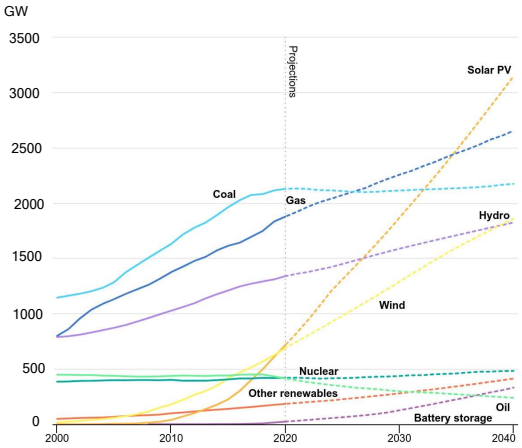

Figure 1.1: Installed and predicted power generation capacity

capacity under current stated policy scenarios is shown in Figure 1.1 [6].

1.2 Wind Turbines for Electricity Production

As the amount of energy produced from wind has increased, the Wind Turbine (WT)[1] design has developed with advancing technologies. Most notable, the size and power output of individual turbines, particularly as Wind Farms (WF) move offshore, as shown in Figure 1.2 [7].

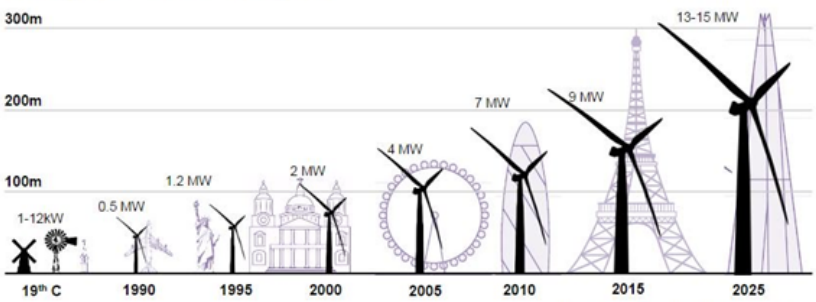

Figure 1.2: Evolution of WT size and power output

[1] horizontal axis WTs only

As a result of the changing power output and increased wind penetration in the National Grid, the reliability of WTs is of increasing importance, from an energy balancing perspective, and commercial perspective. The configuration of WTs vary in relation to the drive train and grid integration, as shown in Figure 1.3 [8].

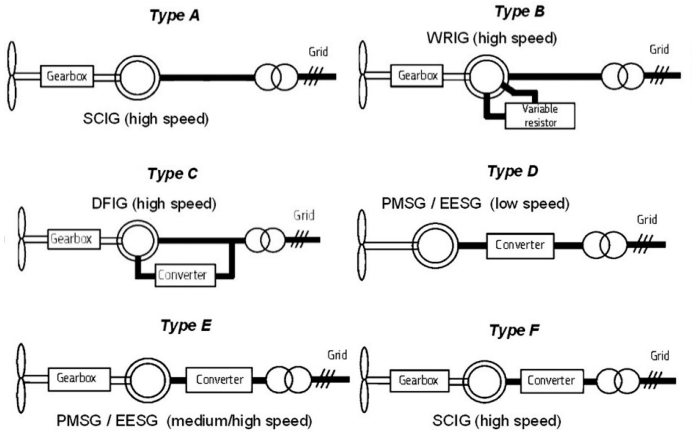

Figure 1.3: WT configurations

The traditional solution has been to place a gearbox in the drive train that will step up the rotational speed from the rotor to the generator. Reliability issues specific to the geared WT have led to increasing interest in direct drive WTs, which remove the gearbox [9], as the generator is designed to operate at much lower speeds than a conventional generator. Direct drive machines require sophisticated power electronics which can also suffer high failure rates and rely on the use of rare earth metals needed for the permanent magnets. Original Equipment Manufacturer (OEMs) are still in favour of using a gearbox, and ways of improving gearbox reliability should continue to be explored, especially as approximately 75% of all current WTs are geared [10].

The gearbox has the highest average cost per failure. The fact that the gearbox has a high major replacement failure rate and repair time also suggests that it will be one of the largest contributors to the overall operation and maintenance (O&M) costs for the offshore turbine. Gearboxes alone could be responsible for up to one third of all lost WT availability [11], each failure resulting in average downtime of around 600

hours [12]. The percentage of electricity production lost due to the gearbox downtime is the highest of all subassemblies [13].

1.2.1 Wind Turbine Gearbox

Gearboxes are needed to transfer the low speed, high torque of rotors to the high speed, low torque requirements of the generator and are made up of a number of components, most significant being the gears and bearings.

Gears

WT gearboxes generally comprise a combination of parallel axis and planetary gear stages. The parallel axis gear stage is a simpler design, whereby the input gear drives another gear, the output gear, as shown in Figure 1.4 [14]. Most of the gearboxes

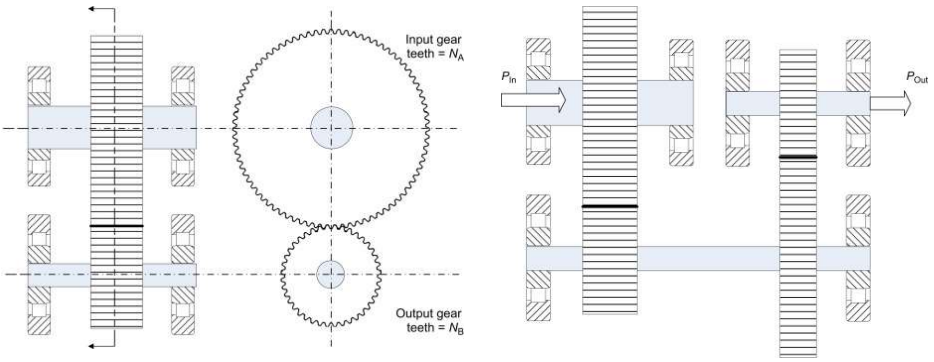

Figure 1.4: Parallel axis gear configuration

in large WTs rely on planetary gearing stages. They provide compact structure, are lightweight and have a greater power-to-weight ratio than a parallel shaft gear set while keeping the input and output shaft coaxial. An example configuration is shown

in Figure 1.5 [14]. Planetary gear stages have lower efficiency compared to simple gear systems [15].

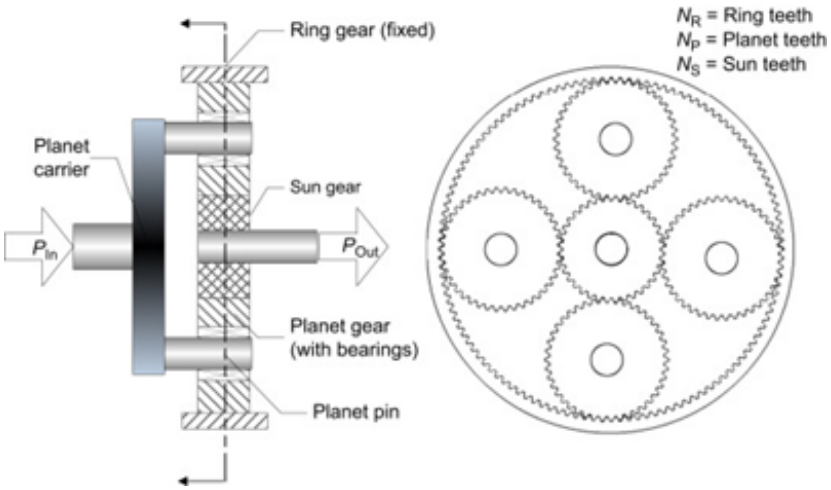

Figure 1.5: Planetary gear configuration

Bearings

WT gearbox bearings are used to support shafts in different gear stages i.e. a low-speed stage, intermediate-speed stage, and high-speed stage. For different gear stages the choices of bearings are different depending on the type of load. Low-speed stage bearings are usually the largest bearings in the gearbox where the loads supported are both radial and axial. Tapered roller bearings, cylindrical roller bearings, four-point contact bearings and tube roller bearings are suitable for this application [16].

Typical design

A typical utility scale gearbox speed ratio in large WTs may be around 30:1 to 100:1. This represents a significant change in rotational speed. A single gear stage is limited to give a speed ratio of approximately 6:1. Hence, most WT gearboxes require multiple stages to reach the desired overall speed ratios [14], an example shown in Figure 1.6 [17].

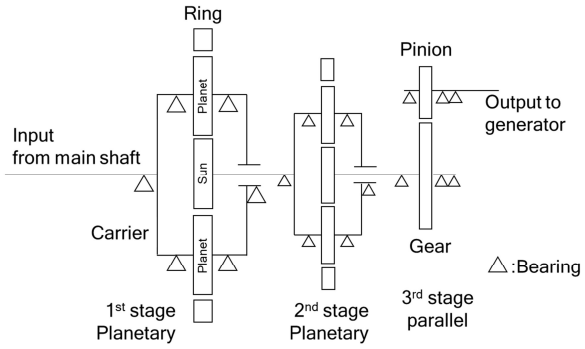

Figure 1.6: Schematic of WT gearbox

Operational Considerations

Most multi-MW WTs are variable speed, pitch regulated. This allows the turbine to operate at maximum efficiency, to capture as much energy from the wind as possible. Below rated power, the maximum Cp curve is tracked at variable wind speeds by varying the rotational speed, via a controller in the generator. This is shown by the blue curve, tracking the green, 'Max aero eff.' curve on Figure 1.7 [18].
At rated power, the rotational speed is maintained (by the generator) and the torque increases as wind speeds increase. The pitch system on the blades modulate the torque to maintain a stable power output. The operation of a WT sees torque and reaction torque fluctuate in response to the stochastic nature of wind speed. The gearbox is in the middle of these two opposing forces. WT gearboxes also have to withstand a range of shocks and loads that would not be found in most gearbox applications. As well as the bending forces on the shaft which are transmitted into the gearbox, there are sudden changes in torque caused by gusting or changes to grid frequency. Figure 1.8 shows a WT and torque loading by external factors.

Consideration of the loading on both sides of the gearbox is an idea that is explored in this thesis, and how different resource conditions or grid operating conditions can impact the gearbox reliability and its condition monitoring for fault detection.

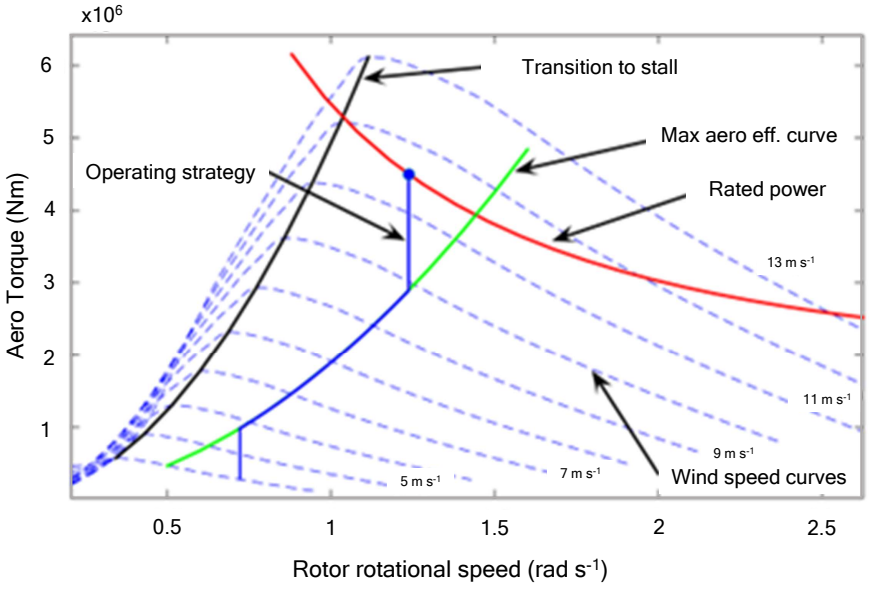

Figure 1.7: WT torque speed diagram

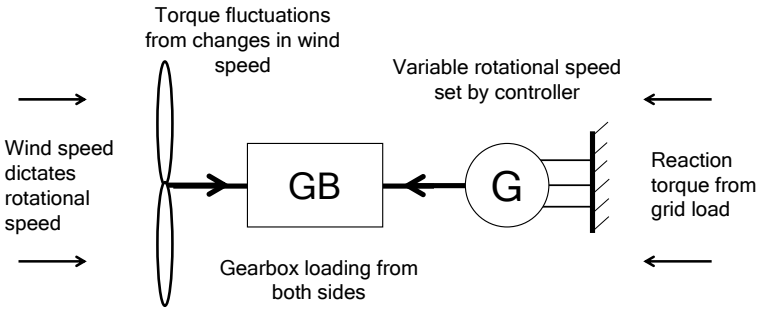

Figure 1.8: WT external torque

1.3 Operation and Maintenance

WT operation and maintenance (O&M) aims to maximise production and minimise lost energy. O&M contributes 20-30% of the total levelised cost of energy (LCOE) [19] [20] for wind energy as shown by Figure 1.9. However, the O&M expenditure for offshore WTs requiring more frequent maintenance, can reach, and even exceed 40% of the total income generated by the turbine throughout its lifetime [10].

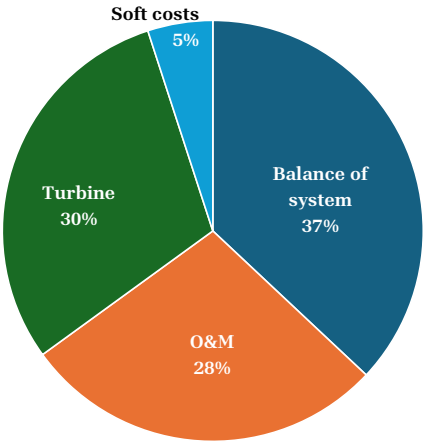

Figure 1.9: Cost breakdown of WT LCOE

The success of operating the WT turbine as a system, depends on the reliability of the turbine components [21]. The availability of a WT is a vital metric during operation and is a measure of the potential for a WT or Wind Farm to generate power [22]. WTs are exposed to extreme, variable weather conditions that generate rapid changes to temperature, air pressure, wind shear and wind speed. This results in constantly changing global and local dynamics and loads. Components must work in intense and variable mechanical stress, which can lead to failure. There is no standardised way for defining a failure in the wind energy industry. [23] defines failure as a visit to a turbine, outside of a scheduled operation, in which material is consumed. With WTs moving offshore, fault detection is more important as the likelihood of failure is higher due to

more extreme conditions. Access is also more difficult, leading to longer downtime than onshore.

1.3.1 Types of maintenance

The maintenance strategy of a WT can have a significant effect on its reliability. Ways in which maintenance is carried out has developed over the years, as technology has progressed, and as WT placement has continued to become less accessible, for example, moving further offshore.

Reactive maintenance refers to repairs that are done when equipment has already broken down, to restore it to its normal operating condition. No upfront cost is associated with reactive maintenance, and it requires far less planning than preventive maintenance. Unexpected downtime as a result of the unpredictable nature of reactive maintenance means that labour and spare parts may not be readily available when needed. Generally, reactive maintenance should be reserved for components that are inexpensive, easy to replace, and where failure does not cause further damage to the system.

Preventive maintenance can either be time-based or usage-based, where the operator is notified after a certain number of hours, or production cycles. Preventive maintenance should be implemented when a component has a critical operational function. The cost of preventive maintenance can be high when access is difficult. Planning is the biggest advantage of a preventive maintenance program over less complex strategies. Generally, preventive maintenance is carried out every 6 months for each WT, but it can vary depending on service provider and access. Oil sampling for particle counting and borescope inspection of gears and bearings [24] usually takes place as part of planned maintenance as the WT must be offline.

However, the frequency of preventive maintenance is most likely to be too high, as components will be replaced too soon where they still have some remaining useful life. Predictive maintenance allows the maintenance frequency to be as low as possible to prevent unplanned reactive maintenance, without incurring costs associated with too much preventive maintenance. Predictive maintenance [25] is a balance between

preventive and corrective maintenance to produce a most cost-effective solution by maximising resources.

Condition monitoring plays an important role in predictive maintenance by continuously monitoring the condition of components whilst the turbine is operational. Condition monitoring allows for a number of benefits:

- Premature breakdown prevention with early maintenance and component protection.
- Intact component replacement avoidance.
- Remote supervision and diagnosis.
- Maintenance planning actions during low wind seasons and increasing the overall capacity factor of WTs.

1.3.2 Condition monitoring

Many maintenance models use annual failure rates to estimate the probability of failure. The failure rates are usually calculated based on observations, collected during turbine operation. Depending on the type of turbine component, the probability of failure may change during the lifetime. For mechanical components that experience fatigue, the bathtub curve is often used to visualize the changing failure rate explained by early-operation-failures and end-of-life failures as shown in Figure 1.10 (adapted from [26]). Recent state of the art condition monitoring research methodologies apply the principle of changes in data, such as temperature or vibration, being symptomatic of a component fault. However, these methodologies predominately use data driven machine learning techniques to predict failure; so called 'black box' approaches that rely on large amounts of operational data and failure histories, with minimal need to understand the physical behaviour of the component or system.

This thesis explores gearbox reliability and how the physical behaviour of its operation can manifest in relation to external factors. This is especially useful when historical operational data is unavailable and/or models are transferred from other gearbox types.

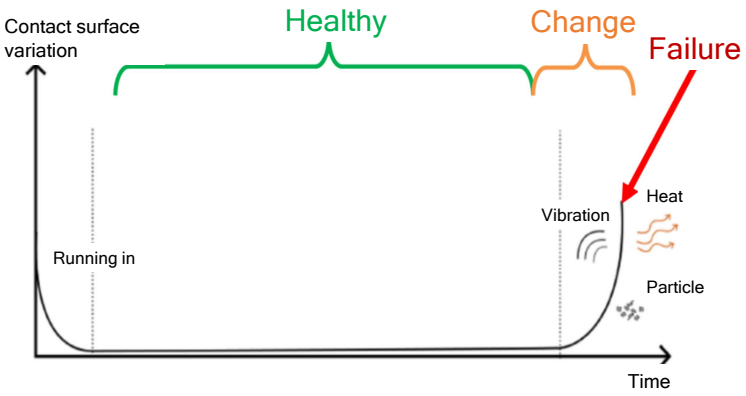

Figure 1.10: Bathtub curve

If the physical behaviour of a gearbox can be modelled, a link can be drawn between failure and changes in output data.

1.4 Thesis research question

How can thermal modelling of a wind turbine gearbox be used for condition monitoring and fault detection to improve reliability?

The hypothesis that a fault will cause an increase in heat generation is the basis for this research, which will include thermal modelling, experimentation, and data analysis. The aim of the experimental aspect is to validate and improve the thermal model. The thermal modelling concept will then be applied to real world SCADA data to test its efficacy, with machine learning techniques providing a level of validation. There will also be a focus on how external factors can affect fault detection and gearbox reliability, for example, the wind regime or interaction with the grid, demonstrating that a physical understanding of all aspects of wind turbine operation is necessary to develop ways to improve gearbox reliability. The thesis structure is shown in Figure 1.11 and demonstrates the chapter linkages, The literature review pertaining to each

chapter is contained within Chapter 2. Secondary research questions will be outlined and addressed in each chapter.

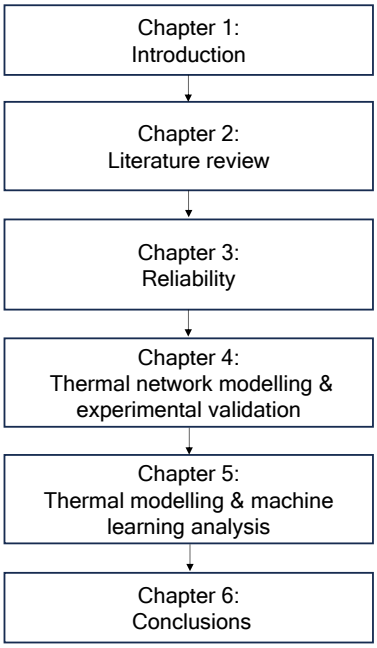

Figure 1.11: Thesis structure

1.4.1 Scope & limitations

The scope of the research conducted in this thesis is determined by the availability of access to experimental facilities, for example, the test rig gearbox available is a small scale 11kW gearbox rather than a utility scale multi-MW gearbox. The performance of the test rig has the potential to be a limiting factor. The scope of this PhD research changed significantly as a result of test rig issues and the COVID-19 pandemic, this is discussed in more detail in Chapter 4.

1.5 Novelty

The novelty of this research, based on the literature review carried out, is that the thermal modelling concepts used have yet to be applied in the context of WT gearboxes. The experimental research has focused on calculating gearbox losses, from a purely tribological perspective. This research will bring both theoretical thermal modelling, experimental research, and machine learning data analysis applied specifically for WT gearbox condition monitoring. The novelty of the research in each chapter will be outlined in the respective chapters.

1.6 Research outputs

1.6.1 Conference presentations

Output relating to Chapter 3:

- *"Gearbox reliability analysis for different Wind Turbine power train configurations"* B.Corley, J.Carroll. Wind Energy Science Conference, May 2023

Output relating to Chapter 4:

- *"Thermal modelling of a small Wind Turbine gearbox for condition monitoring"*, B. Corley, J. Carroll, and A. McDonald. IET Renewable Power Generation, September 2018

Output relating to Chapter 5:

- *"Wind Turbine condition monitoring: experimental validation of a thermal network model"* B. Corley, J. Carroll, and A. McDonald. Wind Energy Science Conference, June 2019

- *"Fault detection of Wind Turbine gearbox using thermal network modelling and SCADA data"* B. Corley, J. Carroll, and A.McDonald. Torque Conference, October 2020

1.6.2 Peer reviewed journals and publications

Output relating to Chapter 3:

- B. Corley, J. Carroll, and A. McDonald, "Gearbox reliability analysis for different Wind Turbine power train configurations" (to be submitted)

Output relating to Chapter 4:

- B. Corley, J. Carroll, and A. McDonald, "Thermal modelling of a small Wind Turbine gearbox for condition monitoring," *J. Eng.*, vol. 2019, no. 18, pp. 5335 – 5339

Output relating to Chapter 5:

- B.Corley, J.Carroll, and A.McDonald, "Fault detection of Wind Turbine gearbox using thermal network modelling and SCADA data" *J. Phys. Conf. Ser.*, vol. 1618, p. 22042, 2020

- B.Corley, S.Koukoura, J.Carroll, A.McDonald, "Combination of Thermal Modelling and Machine Learning Approaches for Fault Detection in Wind Turbine Gearboxes" *Energies*, 14, 1375, 2012

Chapter 2

Literature Review

2.1 Reliability

The majority of WT components are designed to be dependable and have no redundancy. A typical WT has thousands of parts, which can lead to numerous possible turbine failures [27]. Premature failures not only significantly reduce WTs' designed service life, but also cause unplanned shutdowns and early component replacements. Consequently, these failures reduce WT availability and increase LCOE, problems which will be exacerbated in offshore operation due to constrained accessibility and increased maintenance costs [28]. A thorough understanding of WT reliability is critical to the development of effective O&M strategies and to improved WT and WF performance.

WT reliability research is dependent on the availability of large databases of hundreds or thousands of turbines over several years of operation. Due to the limited amount of failure databases in the public domain, the majority of reliability research has been based on the same WT populations and failure databases, such as Reliawind, LWK, WMEP, WindStats and other more recent studies, outside of Europe [29]. In many cases both failure rates and downtime must be considered jointly since it is their combined result that affects the WT's availability.

[30] reviewed thirteen reliability studies which included data from turbines predominantly in Europe, and also USA and China. The purpose of the study was to draw conclusions about which components are to be considered in condition monitoring de-

sign and development. It was found that the assemblies showing the highest failure rates are the electric and control systems, whereas those with the highest downtimes belong to hub & blades and gearbox. Moreover, the study found that the reliability of main shaft, braking, yaw and sensor assemblies has improved in the most recent studies, while that of the gearbox and generator has not, when comparing new and old studies. This suggests a more in depth understanding of the cause of failures is needed.

[31] uses the same reliability studies as [30] plus five additional studies, with a focus on the effect reliability has on LCOE. The majority of databases consist of a mixture of WT types (and configurations) but in many instances, details of WTs are not revealed due to confidentiality. In terms of failure rates, the electrical, control, blades and hub, and pitch systems are the four most critical subassemblies. In terms of downtime, the gearbox, generator, blades and hub, and drivetrain are the four most critical subassemblies for both onshore and offshore WTs.

[32] uses reliability data which enables a comparison of reliability for different WT configurations, namely doubly fed induction generator (DFIG) and permanent magnet generator (PMG), and how the generator configuration effects the WT reliability. When comparing the generators alone, the DFIG has approx 40% more failures than the PMG. However, when the generator and converter failure rates are combined, PMG FRC configuration shows an overall failure rate nearly three times greater than the DFIG PRC configuration. This shows that component reliability cannot be analysed in isolation.

[33] used results from 24 reliability initiatives, which included those used in previously referenced studies. This research analyses the reliability data at a system and subsystem level. The additional datasets included enough offshore WF data to allow them to identify differences between onshore and offshore reliability. It found that for offshore, the drivetrain and rotor systems are potentially the most critical due to being associated with longer downtime, and cost of the repair. In general, the highest contributor to the hours lost per turbine per year, is the presence of a gearbox. Interestingly, this is true for the European initiatives, but the statistics from the Chinese sites contrapose a higher criticality for the control and electrical transmission system.

As a gearbox is made of numerous moving parts, there are many ways in which it can fail. The effect of different operating conditions on failure modes and failure mechanisms is explored in the context of reliability.

Failure mode and effects analysis (FMEA) can be useful in identifying why something may fail, and root cause analysis is useful for determining why something has failed. [34] conducted a FMEA and identified a number of reliability influencing factors for a WT gearbox. These factors include wind speed, maintenance strategy and environment conditions (such as humidity and high turbulence level). Similarly, [33] found that for onshore WTs, a higher number of failures is generally recorded for higher averaged wind speed, gust speed, other environmental conditions. [35] found that the gearbox was more likely to fail in variable wind conditions, with a high potential impact on the failure rates of these subassemblies offshore. This research shows that there is an established link between wind regime and gearbox failure.

A common failure mode occurring in gears and bearings is micro pitting. In bearings, it is caused by sliding or skidding of bearing rollers during varying operating conditions [36]. Similarly, bearing plastic deformation can be caused by excessive loads/overloading [16].

It has been found that the sun gears in planetary stages and pinion in parallel helical stages are those with the highest damage, primarily due to their higher number of cycles and lower number of teeth comparative to planets, rings and gear wheel in the last stage [37]. This suggests rotational speed influences gearbox damage. It was also observed that the wind speeds around rated power contributes more than other wind speeds to gear fatigue damage. Similarly, [24] found that rated wind speed has the biggest contribution in fatigue damage of the gearbox.

As demonstrated in previous paragraphs, research has been carried out to identify how and why gearbox failure occurs with a focus on the upstream operation, the wind regime. [27] identifies the interdependence of WT components but there is one study where findings specifically link the generator and gearbox operation [38]. This study explores how WT shutdown effects the gearbox. During shutdown, the variation range of the meshing force between the planet and sun gears is five to six times higher than

that in normal operation. When the aerodynamic brake is engaged the generator is turned off, to reduce the torque to zero, the aerodynamic and mechanical brakes both produce resistance torques on the drivetrain. The comparison between these two loading conditions shows that the shutdown condition is one of the most critical loading conditions that the WT gearbox components may experience which may contribute to premature failures.

There is a need to improve the knowledge of the WT from a holistic approach in order to understand the relation between different components and their failure mechanisms.

2.2 Gearbox failures

Wind turbine gearboxes are designed to have a minimum service lifetime of 20–25 years. However, most require replacement or significant refurbishment after only 6 or 7 years of operation [39]. To improve reliability, the ways in which the gearbox components fail must be understood. Historical failures can give an indication of component failure location and frequency.

Historical data has shown that the high-speed (HS) parallel stage is found to be the most unreliable module. Parallel intermediate speed stage is more reliable than an intermediate planetary stage. Planetary intermediate speed is less reliable than the planetary low speed due to higher speed [40], as shown by Figure 2.1 [41] which is based on data from WF owners and operators in the US from 2009 to 2016.

It was found that bearing and gear failures were concentrated in parallel section. Gear teeth and bearing faults were found to be caused by issues with lubrication, for example, contamination due to defective seal or a loss of oil [42]. The causes of damage can be either surface initiated damage such as pitting; or geometrical induced damage such as shaft imbalance or bearing misalignment, both of which can lead to failure [43].

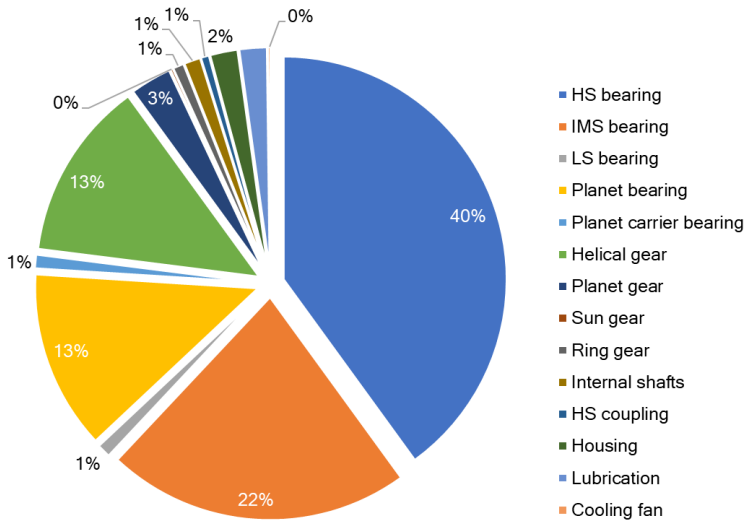

Figure 2.1: Root cause location of WT gearbox

2.2.1 Bearing failure

WT gearbox failures are predominately caused by the bearings, over 70% [44]. The high-speed bearing contributes the most to gearbox failure, and it has been found that the HS bearing furthest away from generator contributes significantly higher to failure rates than other HS bearings. Planetary bearings also experience high fatigue damage [24].

WT gearbox bearings suffer more than in other industries as the ball or roller raceway suffers from adhesive wear and high cycle fatigue/pitting caused by high edge contact stress due to traverse aerodynamic forces acting on the rotor and transferred through the drive shaft. Micro pitting, scuffing and white structure flaking initiate many gearbox failures [45].

Bearings are scaled up when the size of WT machine is increased. As described in previously, WT bearings operate in unique conditions, so to just scale up, without any further design considerations, is inappropriate. Design requirements can be conflicting, e.g., increasing rolling element size will increase the load carrying capacity but simultaneously increase the risk of cage and roller slip and sliding damage [46]. As

the size increases, the amount of loading, both static and dynamic increase. Design considerations should be made to reduce sliding and improve system stiffness. For example [47] suggests an alternative to the "scaled up" conventional Spherical Roller Bearings (SRBs). Tapered Double Inner (TDI) Roller Bearing, that are pre-loaded, can manage the combination of radial and thrust loads much better than the SRB.

Micro pitting occurs when the lubricant film between contacting surfaces is not thick enough and the surfaces have high amounts of sliding action. This results in a frosted or matte finish surface which increases friction. Macro pitting occurs when the contact stress in the bearing exceeds the fatigue strength of the material. Macro pitting results in craters on the bearing ring (or roller) surface. Fretting corrosion is a surface-wear phenomenon that occurs when two contacting surfaces have small oscillating relative motions, with no lubricant film between the surfaces. It often occurs in WT gearboxes due to transportation or spending extended periods of time with no rotation. Fretting corrosion can be identified by the presence of ruts along the lines of contact, along with the presence of reddish brown or black wear debris.

Axial cracks on inner rings of high speed and intermediate speed bearings have become a leading cause of WT gearbox life issues.

Bearing temperature sensors are generally located in the bearing housing or close to the outer ring, depending on how the gearbox is designed. The sensor will be inside a protection tube to ensure consistent metallic contact with the bearing, enhancing measurement accuracy. Temperature monitoring is therefore only representative of the outer part of the bearing. Sensors won't be embedded inside the bearing due to the harsh operating environment and difficulty of maintenance. Temperature data combined with vibration data can be more useful, as vibration data can provide additional prognostic information e.g. increased vibration at fault frequencies of inner race. Alternatively, oil temperature is used as a proxy for bearing temperature, where sensors are installed in the lubrication path, which would provide, more of an average bearing temperature.

2.2.2 Gear failure

Gears were identified as the second leading cause of failures. Gear failure is when the gear geometry or surface changes causing an increase in friction, the root cause is commonly found to be [43]:

- Subsurface initiated bending fatigue
- Micro/macro pitting
- Fretting corrosion (sun pinion)
- Scuffing

Scuffing accelerates the tooth surface destruction and even causes failure [48]. The physical manifestation of scuffing is the sudden rise in friction. The friction rises by a factor of three, typically from a coefficient of approximately 0.07 to one of approximately 0.2. The rise is very abrupt and appears to coincide with the sudden increase in noise and vibration [49], and an increase in frictional heat.

Frictional heat generation during gear meshing is determined by the applied load, rotational speed and lubrication on the tooth flank. The frictional heat flux varies over the tooth flank due to changes of sliding velocity, normal contact pressure and the coefficient of friction along the contact path [50].

The mechanical stress from the contact point and resulting peak in temperature can have a negative effect on lubrication fatigue life. The fatigue effect on gearbox lubrication fluid refers to how the properties of the lubricant degrade over time due to mechanical, thermal, and chemical stresses during operation [51]. High-speed gear meshing and turbulence cause the lubricant molecules to shear repeatedly. Over time, this can break down the molecular structure, reducing viscosity. Continuous operation raises oil temperature. Heat accelerates oxidation and additive depletion, affecting lubricity and chemical stability [52].

2.2.3 Lubrication failure

An effective lubricant reduces wear, transports heat generated by friction away and keeps contamination away from bearings. Too much or too little lubrication can have a detrimental effect on bearings and lubrication contamination can lead to scuffing [16].

Lubricant failure causes equipment failure and vice-versa. Lubricating oil carries a great deal of information about the operating condition of the equipment as well as provides a leading indicator of what could be the condition if no corrective action is taken [53]. Harsh environmental conditions such as, temperature, dust and moisture promote tribological issues (scuffing, micropitting, wear, corrosion). Issues can also be caused by lubricant compromise between needs of gears and bearings as well as between low and high speed stages, insufficient oil drains and refill intervals.

WT has higher requirements for gear oil than typical industrial applications. [54] found during the periodic analysis the gearbox lubrication was found highly contaminated, moisture content and degraded due to the load change, temperature and other environmental factors. Higher level of particulate contaminants in oil not only reduces its efficiency in carrying away heat from localised contact areas, but generates additional dispersed particles. It also reduces the fluidity of lubricating oil.

Studies show that the wear which affects the main bearing service life is primarily caused by micropitting. And a poor lubrication condition leads to an insufficient local lubrication film thickness, allowing direct interaction of the asperities on rollers and raceway. Therefore, lubrication significantly affects the main bearing's lifetime [55].

At high temperatures, grease can lose its structure causing lubrication failure and damages on rolling element bearings [56]. Viscosity can change over time which can affect all components of the gearbox. Lubrication can cause catastrophic failure if whole system fails. Whilst subtle issues with lubrication can have a knock-on effect on other components.

An understanding of failure modes and component reliability can help guide which techniques to use for early detection, helping to prevent failure. Existing condition monitoring techniques will be explored.

2.3 Existing condition monitoring techniques

Current state-of-the-art fault detection research uses data science techniques applied to WT data. This takes the form of SCADA (Supervisory Control and Data Acquisition) data and additional condition monitoring systems (CMS) data which vary depending on the turbine type, size and operator. A range of techniques can be used for the CMS; acoustic measurement, electrical effect monitoring, power quality, temperature, oil debris monitoring and vibration analysis. As the nature of these variables differ, so does the way the signal is treated and analysed. These techniques and applications will briefly be explored.

2.3.1 Vibration

Vibration as a fault indicator has received a lot of attention in recent research. Data from accelerometers express vibration signals and it is known that characteristics of a "healthy" vibration can be demonstrated, so in theory faults in gearbox components would result in changes to vibration data in the frequency or time-frequency domains [57]. A number of processing methods have been applied successfully such as Envelope Analysis, Wavelet-Transform and Artificial Neural Networks. However, this analysis requires advanced signal processing as the data is noisy. Rotational speed and load condition are both time-varying due to the uncertain wind speed and wind intensity [58]. [59] was able to show a change in vibration signatures from intermediate speed shaft data, prior to failure, shown in Figure 2.2.
Most vibration-based fault detection is focused on HS and IMS stages, as detecting faults in LS stage is difficult due to weak fault signals [16]. Vibration based fault detection can detect earlier than oil debris analysis, however, it is challenging to detect damage to planetary stage bearings and gears [43].

A comparison of independent vibration and oil debris particle count against energy produced can give early detection of incipient gearbox damage [13], and could produce a severity factor if calibrated against other incidents to reduce the number of false alarms. A study conducted by NREL found the average detection accuracy of existing vibration

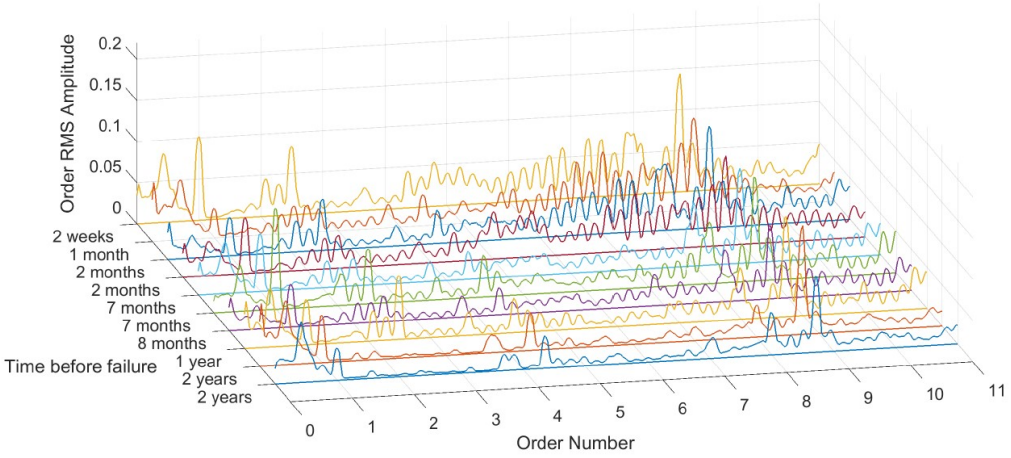

Figure 2.2: Vibration waterfall plot

monitoring system to be about 50% [60]. Vibration analysis requires expensive sensory systems, and their maintenance and repair are added cost.

2.3.2 Acoustic emissions

Acoustic emission (AE) is a transient impulse caused by a rapid release of strain energy in solid material under stress conditions such as mechanical or thermal loading [16]. The main application of AE is the detection of cracks. Therefore, this technique can be used as a tool for condition monitoring of bearing faults and shaft cracks. Typically, the accuracy of these methods depends on sound pressure and sound intensity data [44].

Compared with vibration data, AE has advantages: it is more sensitive to fault activities; AE monitoring has been proven to be able to detect faulty roller bearings at extremely low-speeds, such as 0.5 RPM [10], something that vibrational data can struggle with. [61] states it is insensitive to structural resonances and unaffected by typical mechanical background noise. As demonstrated by [62], who found that AE-

based approach has the potential to differentiate gear tooth damage levels in comparison with the vibration-based approach. The partial tooth cut faults seeded in a gearbox test rig and experimentally tested, found that while vibration signals are easily affected by mechanical resonance, the AE signals show more stable performance using same sampling rate. Similarly, [63] carried out a comparison of the vibration and AE analysis using a large bearing defect, and small bearing defect. Both measurements were able to identify the presence of the large bearing defect. For the small defect condition, the vibration data was dominated by the gear mesh frequencies and their harmonics, and as such the bearing defect frequencies were not evident. However, AE analysis was able to identify both the small and large defect conditions.

The analysis of both types of data relied on advance signal processing techniques to extract defect information. A drawback of AE technology is that most sensors and instruments available on the market have high power consumption, and perform data transmission and operation control through wired connection [64], something which is problematic for most WFs.

2.3.3 Electrical signal analysis

Electrical signal analysis has the potential to reduce WT operation cost by reducing the number of sensors and therefore the need for maintenance and repair [57], as current and voltage signals are already monitored for operation. It has been found that vibrations inside the mechanical components appear in the electrical signatures of the WT generator [57] [65]. Defects in bearings or gears will cause torsional/radial vibrations, which are transmitted into the generator via the mechanical drivetrain transmission path.

Fault detection uses similar approaches to vibration analysis, such as Wavelet Transform, Fourier Transform and Time Synchronous Averaging [57]. Researchers in [66][60] use current signature with vibration data to improve detection and diagnosis accuracy. [67] combines the gearbox vibration and the generator current signals for successful WT gearbox bearing fault diagnosis.

2.3.4 Oil analysis

Oil sample analysis takes a sample from the operational gearbox and investigates the oil chemical properties, viscosity, particle count and debris analysis. Oil monitoring can detect gear and bearing failure as damaged gearboxes have much higher debris generation rates than healthy gearboxes [68].

Lubricant parameters can be indicators for lubricant degradation, which would lead to further failures. Lubricant temperature is linked to condition. An increase in the oil temperature causes a decrease in the oil viscosity, which causes the oil film thickness between contact bodies to decrease [69]. Temperature also has the biggest effect on oxidation. Oxidation reaction rates double for every 10^oC increase in temperature [70]. Oxidation causes changes in viscosity, additive depletion, base oil breakdown, filter plugging, and corrosion. Oil temperature could in theory be used to monitor condition, but oil temperature is generally controlled. However, the oil inlet temperature can be useful, before it enters the cooling system. In some configurations there is inlet temperature and sump temperature, the difference between the two could be used; an increase in the delta could indicate additional heat is being generated by a component in the gearbox, before the cooling system actively controls the oil temperature. Other cooling systems are not actively controlled, in technologies that use a thermal bypass value, the oil temperature could be monitored to indicate the effectiveness of the cooling system.

Oil sample analysis is usually carried out offline, which can incur costs for access and may detect faults too late. It can be carried out online but it requires an additional measurement system. For real-time monitoring, the challenge is to correctly interpret the real-time oil condition sensor readings, as operational conditions have significant impacts. Moreover, there is no single standard set for all WTs, as different turbine manufacturers or lubrication oil suppliers may require a unique set of analyses in order to obtain credible results [71]. Filter element analysis can also give information not included in oil sample analysis [43].

2.3.5 SCADA data

All turbines use SCADA data of varying quality to relate WT operating and environmental conditions; wind speed, temperature, and power with the condition of the system [45] [72] as standard.

Using SCADA temperature data for fault detection can be successful [40] [73] [74] as it does not require complex signal processing. However, accurate fault detection and reliable prognosis in WT gearboxes remain challenging due to the inherent complexities in their mechanical systems and operation conditions. Additionally, an important drawback of SCADA data is low temporal resolution, which results in a loss of information about the dynamic behaviour of the WTs and can lead to a loss of detection capabilities. [75] found that high-frequency data provides a deeper understanding of WT condition and improves the detection capabilities. However, the issue of noise in data becomes more prominent with very high sampling rates, which can lead to misclassified anomalies, resulting in false/missed alarms so more complex methods are needed, undermining one of the benefits of using SCADA data. As a result, SCADA data analysis has become more complex, as an increasing amount of data is collected.

Techniques for data analysis can largely be grouped into; trending, clustering, normal behaviour modelling (NBM) and damage modelling. Trending is arguably less complex method of analysis but as a result is tends to be case specific requiring manual interpretation or if used online, generates frequent false alarms [76]. Clustering techniques can be effective with enough data but can also be difficult to interpret. NBM has become a popular approach to data analysis whereby a model for the normal behaviour is established using training data, and the difference between predicted and actual values of the parameters is then calculated. There are a number of techniques that can be applied to NBM, a prevalent method is neural networks, which has proved a successful means of detecting anomalies [60] [77] [78].

An in-depth review of other NBM machine learning applications can be found in [79], which states how machine learning has evolved in recent research and the advantages and disadvantages of different methods. An alternative to machine learning NBM is demonstrated by [80] who use data standardization and a curve fitting tool to trans-

form the data into a format which can be used for anomaly detection, which worked successfully with a bearing fault.

Finally, damage modelling is an alternative to the "black box" approach of methods discussed previously, where the physical processes relating to failure are modelled. There are few studies who have used this approach successfully [81] [12] and as a result application is yet to be established [76].

2.3.6 Temperature

It is common that WT SCADA systems include temperature sensors installed on components, such as the main bearing, high speed shaft bearing and gearbox oil [82].This exploits temperature measurements to detect abnormal gearbox operating conditions; based on the theory that gearboxes generate power losses in the form of heat. It can be assumed from this that degradation on the contact surface will generate more losses and thus a different thermal behaviour [74]. The coarse time granulation of SCADA data (usually 10 minutes) is well suited to temperature analysis as it naturally "denoises" [83] and, as a result, does not require complex signal processing [40], [73], [74]. However, the simple temperature trending approach alone is rarely successful in highlighting potential failures [84] as operating conditions influence system temperature. [85] argued that, although the temperature signal has good anti-interference performance, for a bearing fault, its linear change trend cannot fully demonstrate nonlinear degradation and the resulting information can be limited.

A comprehensive review of fault detection using temperature measurements was carried out by [74]. They compared research using data from contact sensors and thermography for bearing and gear defects, which is highly relevant for this research. Contact sensors are most commonly used to collect temperature data, and historically, the best diagnostic method was to use threshold values on average temperatures [74]. However, temperature anomalies can be affected by various factors, such as oil temperature, ambient temperature and other operating conditions.

How threshold values are established can be difficult and, if not accurate, can result in false alarms or missed failure warnings. [86] acknowledged these issues and used a

method based on probability estimation to generate confidence intervals to determine whether the oil temperature is abnormal.

Recent studies applied sophisticated NBM machine learning techniques to temperature SCADA data for fault detection. [87] found that using the gearbox temperature collected from SCADA data gave a 68 day early warning of gearbox failure. [83] proposed a method based on an artificial neural network approach, that highlighted fault onsets in advance for three out of the seven turbines using temperature from main bearing. Whether the advance warning is sufficient to prevent failure is unique to WT locations and operators.

A case study on a 2 MW variable speed WT found that oil, bearing and nacelle temperatures, and power output SCADA signals can be used to detect planetary gear failure providing three months warning [39]. Similarly, [11] carried out research using SCADA data from a 2MW WT gearbox. Thermocouples were implemented on the oil circuit and high speed shaft bearing. Oil temperature measurements found a 5°C temperature rise three months before failure. [73] used SCADA temperature measurements plotted against percentage of power with respect to rated power of a 2MW turbine. It was found that their method is capable of highlighting anomalies which could be evolving into faults. This research would be more valuable if it could cross reference with failure history data.

An accurate fault detection and reliable prognosis in WT gearbox remains challenging due to the inherited complexities in their mechanical systems and operation conditions. A multi parameter approach, based on comparison of independent signals would increase the confidence in the fault signal interpretation and thresholds.

2.4 Thermal modelling

Thermal modelling is an important technique to use to understand a system, especially when experimental facilities are not available. Thermal performance is important to understand as it can affect reliability, efficiency and longevity of a system. There are a number of techniques that can be used for thermal modelling with different advantages and disadvantages , depending on the application and detail required.

2.4.1 Finite element methods

Finite Element Methods (FEM) can be used to carry out thermal analysis using Computer Aided Design software, such as AUTODESK, whereby a system is drawn in 3D then split up into a mesh of elements all interacting together. FEM allows for large degrees of freedom and is good if structural deflection and thermal expansion are included, however, this is computationally expensive.

Finite element analysis can generate temperatures that are in good agreement with experimental measurements. Maximum surface temperature and temperature distributions on tooth flank are mainly determined by load and speed as well as gear geometry. Load has more significant effect on surface temperature. Tooth width has important impact on tooth temperature variations. Ambient temperature under operational conditions is an important boundary condition [88].

2.4.2 Computational fluid dynamics

Computational Fluid Dynamics (CFD) can also be used to model thermal behaviour, especially when there are complicated types of convective heat transfer, for example, interaction with the natural environment or cooling systems. CFD can provide a detailed understanding of thermal behaviour of a system, but like FEM, requires large computational resource.

2.4.3 Thermal network modelling

Thermal network modelling can be equated to electrical circuit theory by analogy where resistance to heat transfer is equivalent to electrical resistance, heat flow equates to current, temperature difference is equivalent to potential difference, and thermal mass to capacitance [89]. To create the thermal model, the gearbox components are split into a number of lumped mass isothermal nodes. Linking these nodes are thermal resistances, representing heat transfer by conduction, convection and radiation. Losses are introduced at the respective nodes. Heat flows between nodes can be calculated as temperature differences.

Lumped parameter thermal network modelling is an established method used to model electrical machines, used by many researchers involved in thermal analysis of electrical machines, both for steady-state and transient analyses [90]. A steady state thermal network model of a totally enclosed fan-cooled (TEFC) induction motor was created by [91], to determine loadability of electric machines, as determined by temperature limits. The model comprised of 107 nodes and experimental validation was performed on a 4 kW and a 15 kW induction motor. The resistive losses were calculated using the equivalent circuit of the induction machine. The stator core losses are calculated by a two dimensional, time-stepping finite element method. Comparisons between measured and calculated temperatures show that good agreement can be expected if the heat transfer coefficient between the frame and the ambient and the additional losses were known. Similarly, [92] successfully modelled an induction motor, to calculate temperatures of the stator windings and the rotor at different operating conditions, the model was experimentally validated.

Thermal modelling of a test rig was carried out by [89], which considered gears as isothermal and its temperature is that of oil bath to estimate gear friction coefficients and influence of lubricant. They found that isothermal approaches relying on oil sump temperature may underestimate gearbox efficiency because the contributions of local temperature rises are ignored. A solution to this is to increase fidelity by splitting the casing into three parts to account for temperature variations. This is logical as the different sides of the gearbox casing will have different levels of forced convection.

[93] produced a thermal model of the main mechanical components of a 7MW demonstration turbine. The modelling was integrated with wind field simulation data to replicate the dynamic operation conditions of a WTG gearbox. It found at high wind speeds, load dependant losses dominated. The oil cooling/heating system was simulated, which starts working when the oil temperature reaches a designated value. Using a similar method, [94] generated a thermal model in Simulink of small gearboxes with a splash cooling systems.

[88] found the heat generated is conducted into the gear teeth and is also taken away by the cooling lubricant applied to the gear wheel and tooth flank. Heat transfer

coefficients change with rotational speed, surface location and operational conditions such as flow-rate of lubrication oil, the temperature of the oil inlet and position of oil jet. The frictional heat flux generated on the tooth flank, and heat transfer on the gear surfaces and tooth flanks have a significant influence on the temperature variation and distributions, consequently affecting gear lubrication, performance and service life.

[81] used a 1.5MW WT gearbox operating at 1500 rpm as a case study. A thermo-mechanical model was developed, and diagnosis was made by computing the efficiency from temperature measurement. A clear decrease in efficiency was seen, a 3-5K increase in temperature three months prior to failure. These results show a nonlinearity of the gearbox oil temperature rise with wind speed/output power that can effectively indicate gearbox efficiency degradation, which may be attributed to gear transmission problems such as gear teeth wear.

Gearbox power losses can range from 2-5% of input power, depending on the relative number of epicyclic and parallel shaft stages and on the type of lubrication [95]. [96] found that lubrication type could affect power losses by approximately 22%. It could be argued there are many more factors to take into consideration when estimating gearbox power losses. Firstly, if the appropriate design considerations have been made for the intended application. For example, the test rig gearbox used in this research is an 17kW gearbox used in an 11kW Gaia wind turbine. It is intentionally over-sized for robustness as this was considered more of a priority for these turbines (generally domestic installation, with little to no maintenance). For an operational gearbox, there are number of internal considerations which could affect power losses, such as lubrication type, age and condition of components, their interaction, alignment, inspections and maintenance. Many of these aspects are unknown to us researchers, as we just have access to engineering drawings and SCADA data. We can only make assumptions about condition, maintenance history, alignment and lubrication quality. From industry experience, these assumptions may not be accurate as in practice maintenance, inspections, servicing are done to a varying degree of standard.

Operational conditions have a significant effect on losses. Changes in torque and rotational speed, dictated by the dynamic nature of the wind regime, for example, [97]

found that at low input power the gearboxes have a very low efficiency due to the low oil operating temperature.

Similarly, it is difficult to predict tooth temperature and evaluate thermal behaviour of gear transmission systems, since thermal balance and gear temperature are determined by a number of factors including gear parameters and configuration, applied loads and rotational speeds, as well as lubrication properties and operating conditions [88]. Frictional heat generation during gear meshing is determined by the applied load, rotational speed and lubrication on the tooth flank. The frictional heat flux varies over the tooth flank due to changes of sliding velocity, normal contact pressure and the coefficient of friction along the contact path [50].

2.4.4 Experimental

The effect of different types of lubrication were studied in [98], where the efficiency of an 850kW gearbox test rig, running at full power were compared using oil jet lubrication. The research found power loss measurements were consistent with oil temperature measurements. It was also found that no-load losses are dominant at low operating temperatures. It can be estimated that this is affected by oil viscosity. It was found that power loss reduction has a direct influence on lubrication quality. It promotes lower heat dissipation and lower oil operating temperature. Lowering operating temperature minimises oil oxidation and degradation, impacts lubrication quality and consequently the surface protection against failure.

[99] carried out experiments using a test rig operating at 7150 rpm. Thermocouples were used to measure ambient and lubricant temperature. The influence of churning losses was measured by operating the test rig with no load until thermal equilibrium was reached. It was found that churning power losses decrease as temperature increases and viscosity is reduced, up until high Reynolds number. The study also measured different spur gears and found that at low speeds whilst the module and face parameters are not influential, diameter is. As speed increases, there are larger losses from wider gears.

Infrared (IR) imaging enables non-contact, non-intrusive, single-sensor based temperature measurements, which is ideal for condition monitoring with the aim of au-

tonomously diagnosing faults [100]. Thermography allows estimating and visualizing the temperature distribution over the surface of a mechanical system. The main issue with this method is due to uncertainties introduced by lubrication, as oil may interfere with the infrared emission. It is not generally used for online measurements and generates significant data. To autonomously detect conditions and faults, infrared thermal imaging is mostly used in combination with image processing and machine learning. An interesting study used both infrared thermal imaging and vibration data via feature fusion, wherein model-driven features were extracted from the vibration measurements, and data-driven features were extracted from the infrared thermal imaging data then combined with the outcome of outperforming single sensor-based systems on the study's two datasets [101].

[102] used a 2.5kW test rig, 3600rpm coupling motor, gearbox and generator. A fault was simulated by an unbalancing motor shaft. Infrared camera data was processed with inner and outer temperature sensors from the test bench which were used to estimate bearing and gearbox characteristics temperatures. A temperature rise between healthy and faulted bearing of 1.5K was observed.

[89] used a FZG[1] gear test rig to measure the influence of temperature on gear failure. It was found that high temperature leads to low viscosity and thin oil film thickness formation, high chemical activity and good tribological layer formation. There are unintended benefits from high operating temperatures.

[96] studied a parallel axis and planetary gearbox test rig, operating up to 42kW, monitoring input/output speed and torque, room temperature, oil sump temperature in two locations and external wall temperature in various points. Industrial grade 3 wire pt100 Resistance Temperature Detectors (RTDs) and Type K thermocouples were used. The experimental results indicate that changing the lubricating oil can have a severe impact in the power loss performance and operating temperature. It also found that in the planetary gearbox, the bearing losses were much higher than the gear mesh losses, opposite to that of the parallel axis. A FZG gear test was used by [103] and [104] to compare power losses in relation to theoretical calculation. A range of

[1] *Forschungsstelle fur Zahnrader und Getriebebau* Test evaluates fluid lubricating and wear protection properties at the interface of a loaded set of gears

test operating conditions; varying levels of torque and rotational speed, were carried out. When different gear box oils were implemented and compared, it was found that PAGD[2] saw the lowest power loss, MINR[3] the highest. The studies also demonstrated that torque loss at low speed is clearly influenced by the coefficient of friction of oil.

The data acquisition system itself plays a significant role when interpreting experimental results, and different equipment and methods can yield different results. For example, [74] reports that temperature measurement method influences diagnostic capabilities. Data from thermography was found to be different from data from contact sensor. On bearing condition monitoring, a link between fault initiation and temperature increase was found using a contact sensor. Thermography is more uncertain as oil can affect the infrared emission. Some studies have found indirect temperature measurements successfully detect gear defects. [74] [89] used Type K thermocouple with a precision of $\pm 0.5^{o}$C. It was found that all studies dealing with lubrication failure were conducted by thermography analysis, using a thermal camera rather than point temperature measurements.

2.5 Conclusions

The literature review started at a high level, exploring reliability research which used large population data sets to understand the reliability trends across WFs. There is a general consensus that gearbox has a significant effect on WT reliability, in terms of frequency and downtime. Understanding the factors which cause gearbox failures is an important step to improve reliability. It is understood that the loading characteristics a WT gearbox suffers is a large contributing factor, research in this area explores the effect of the wind regime on the gearbox. There is limited research on the effects of interaction with the downstream topology (generator and the grid).

Using reliability data to understand where the failures occur is important, to develop condition monitoring techniques that can target these problematic components, for example, bearings.

[2]Polyalkylene Glycol
[3]Mineral oil

Existing condition monitoring techniques were explored to identify the strengths and weaknesses. Data driven machine learning approaches are the predominant subject of contemporary research, but this is heavily reliant on historical data and failure history information. An alternative to this is thermal modelling, where most existing research is from a purely tribological perspective, with minimal application being made to WT gearboxes.

Chapter 3

Gearbox reliability analysis for different wind turbine power train configurations

3.1 Introduction

In this chapter, the reliability of different configurations in relation to the gearbox is explored, how the operation strategy can have an effect on the health of different components. Studies which have explored reliability analysis include [32], who compares the overall reliability of DFIG and PMG generators WTs and compares the failure rates in terms of the generators and converters. [105] studied the reliability of wind turbine drivetrains using a large population of offshore wind turbine failure data. The top fault locations in the populations analysed were high speed bearings and generator bearings. The top failure modes for bearings were outer race defects. It was found that the failure rate is high in the first operational years and with a higher rate around year 4, which does not strictly follow the bathtub curve. Failure rates between different datasets can have some discrepancy, depending on the volume of data, location, power rating and turbine configuration.

[106] conducted a reliability analysis of wind-energy systems, focusing on wind-turbine system failures. The modelling used the bathtub curve (Figure 1.10), in addition

to other factors, such as the mean time to repair (MTTR), operation and maintenance cost, weather conditions, grid effects, and load variation. By including other factors, they highlighted the need to enhance the understanding of failure mechanism and effects. In [107] failure rates of critical components were estimated by applying existing industrial standards and datasheets for general mechanical applications. The failure rates of three generic gearbox configurations were predicted using reliability software, to assess the effects of different designs on the overall performance of wind turbines. The research highlighted that field failure data collection and exchange between end-users, WT manufacturers, gearbox manufacturers and bearing manufacturers is essential to estimate the true reliability, to determine and/or to validate. There are few studies which compare the reliability of different WT configurations, this is generally due to lack of data and confidentiality agreements.

Downstream of the gearbox, powertrain topology is a factor that has the potential to affect reliability, and this is yet to be explored in terms of gearbox reliability in existing literature.

Reliability analysis has the potential to provide useful insights for life time extension. It could be used to supplement the methodologies outlined in [108], which conducts reviews of lifetime extension assessment practices executed within a variety of industries, to determine if any of these practices can be implemented or adapted for use on wind turbine drivetrains.

Research questions:

- Does the choice of generator and converter influence gearbox reliability?
- If so, how is this manifested at component/fault type level?
- Are there operational factors that can influence gearbox reliability?

The novelty of this research stems from:

- Consideration of the interdependence of the WT generator and gearbox in relation to gearbox reliability

- Providing gear box reliability analysis at a sub-component level, something which can prove difficult in published research due to confidentiality agreement
- This paper explores how the operating conditions of a WT is affected by the power train configuration, and explores how this relates to gearbox reliability.

3.2 Methodology

This analysis can be used to identify reliability and vulnerabilities of WT powertrain. Work such as [109] can supplement reliability analysis by using vulnerability map to identify which sub-systems/components have the highest failure rates. This can help determine the weak links and conditions of the components.

3.2.1 Power train topology

The different WT power train topologies will be briefly described. This will be useful in understanding the differences in operation and how this might affect the gearbox reliability.

DFIG PRC

A doubly fed induction generator (DFIG), is an induction generator that connects the stator directly to the grid, and a partial-scale frequency power converter (PRC) is attached to the rotor circuit and so is partially decoupled from the grid. A schematic shown in Figure 3.1. Typically, the variable speed range is around $\pm 30\%$ of the synchronous speed [110], but it depends on the size of the frequency converter, larger ones allowing a greater range of speeds. From this point this configuration will be referred to as DFIG PRC.

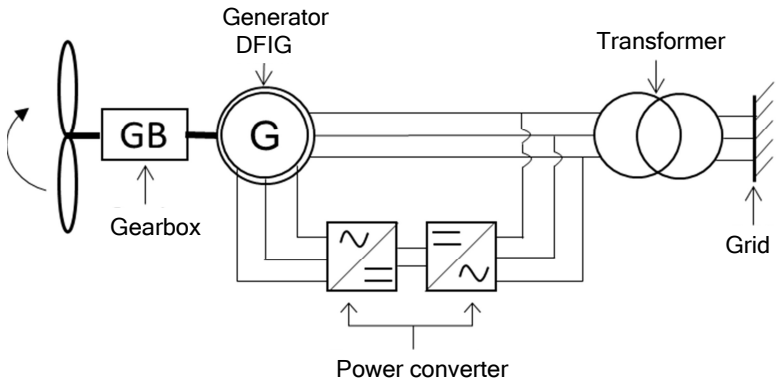

Figure 3.1: DFIG PRC schematic

PMG FRC

A permanent magnet generator (PMG) operates at synchronous speed and is completely decoupled from the grid with a fully rated converter (FRC), a schematic shown in Figure 3.2. A FRC means the WT can operate at a wide range of speeds. Being decoupled from the grid means it does not have to operate reactively to grid conditions. From this point this configuration will be referred to as PMG FRC. All the WTs in this study feature a gearbox, irrespective of the type of generator.

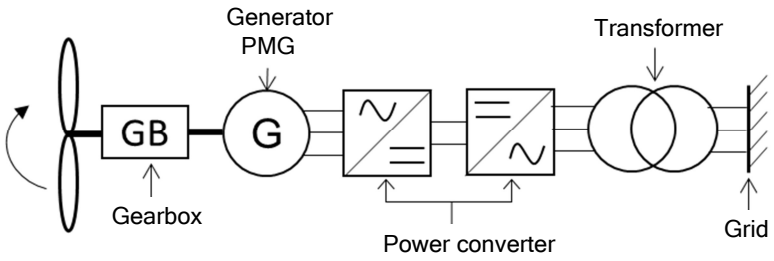

Figure 3.2: PMG FRC schematic

3.2.2 Gearbox

The gearboxes are all of similar configuration. They are multi stage, generally featuring two planetary stages and a parallel stage, as outlined in previous chapters.

3.2.3 Population

To complete this analysis the authors have partnered with a WF operator/developer to analyse a large proportion of their fleet located in the UK and Europe. The population analysed consisted of $\tilde{2}000$ WTs. Of the 2000 turbines $\tilde{8}0\%$ were located in Continental Europe and 20% were located in the UK. Of the population analysed $\tilde{7}5\%$ of the population consisted of drive train configurations that were partially decoupled from the grid through a DFIG PRC configuration and 25% of the population was fully decoupled from the grid through the use of a PMG FRC. The turbines in the DFIG PRC configuration population had on average 4.7 years of operation and the turbines in the PMG FRC configuration population had on average 4.95 years of operation, meaning a comparison between the two types was not affected by a difference in age. All turbines in this analysis had a similar rated power of between 1.5 and 3MW, the exact rated powers cannot be disclosed for confidentially reasons.

3.2.4 Data analysis process

WF operational records are often imperfect and not set up for reliability analysis of components. Consequently, a large amount of work from this analysis consisted of identifying and pulling together orders for replacement gearboxes and confirming the work was carried out through work order analysis for each turbine. The process was manual and slow. A flow chart of the methodology can be seen Figure 3.3.

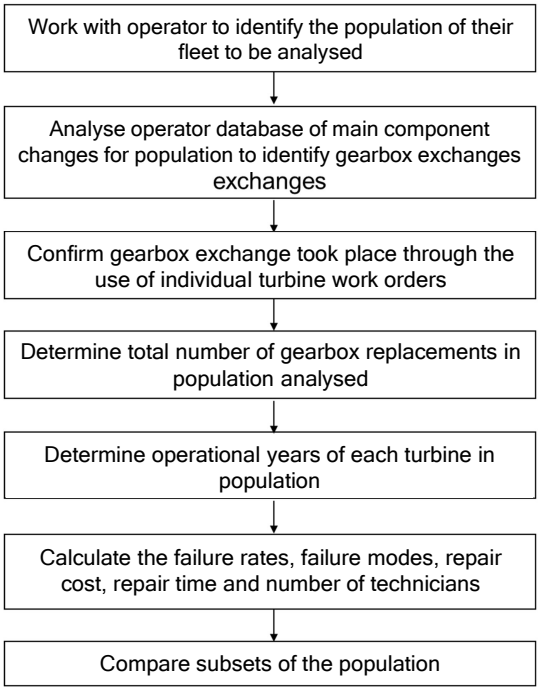

Figure 3.3: Methodology flowchart

Failure: For the purpose of this study a failure is defined as ceasing of turbine operation due to a gearbox fault only to be remedied through the full replacement of a gearbox. The definition of a failure used in this paper is in line with the definition for a "Major Replacement" used in past papers [32].

Repair cost: Cost of replacement gearbox, averaged from material database and converted to Euro as the majority were in Euro, use GBP exchange rate from the dates of the failures for UK costs. These costs are based on material cost only.

Number of technicians: Is the average number of technicians that booked time on the gearbox exchange.

Repair time: Average of total time booked by each technician on a gearbox failure across all gearboxes exchanged in this analysis. Travel time and lead time are not included. Presenting the costs in this manner means repair time is independent of distance from shore.

Calculating failure rate

The formula used to determine failure rate per turbine per year in this analysis is shown in 5.7 [23].

$$\lambda = \frac{\sum_{i=1}^{I} \sum_{K=1}^{K} n_{i,k}/N_i}{\sum_{i=1}^{I} T_i/8760} \tag{3.1}$$

λ	Failure rate per turbine per year
I	Number of intervals for which data are collected
K	Number of subassembles
$n_{i,k}$	Number of failure
N_i	Number of turbines
T_i	Total time period in hours

The numerator is the sum of the number of failures in all periods per turbine. The denominator is the sum of all time periods in hours divided by the number of hours in a year. Details of the failure mode is taken from information included in the work order. The level of detail is variable and so are categorised using the information available.

3.3 Results

3.3.1 Failure rates, repair costs and repair time

The calculated reliability metrics are show in Figure 3.4 for both WT configurations.

Figure 3.4 shows DFIG PRC gearboxes being the worst performing in all reliability metrics; average failure rate, repair costs and repair time.

	Gearbox in DFIG PRC	Gearbox in PMG FRC
Average failure rate (failure/turbine/year)	0.015	0.008
Average repair costs (000 euro/repair)	120	110
Repair time (hours)	227	185

Table 3.1: Summary of failure data

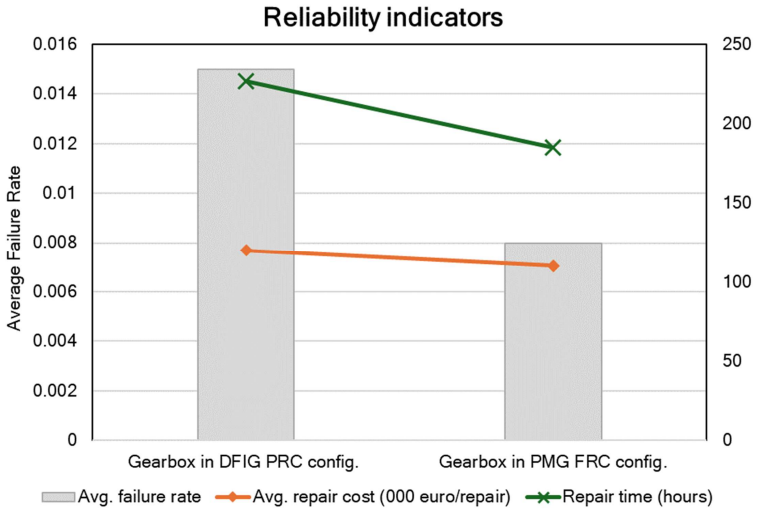

Figure 3.4: Summary of reliability indicators

3.3.2 Failure modes

Figure 3.5 and Figure 3.6 shows the proportion of failures based on components. DFIG PRC appear to suffer more bearing failures, whereas for the PMG FRC, failures from bearings and gears are more equal. However, the proportion of "unknown" is significant, this is where the work order related to the failure does not give enough detail to categorise the failure. Therefore it can be said the failure modes of the two configurations are broadly similar.

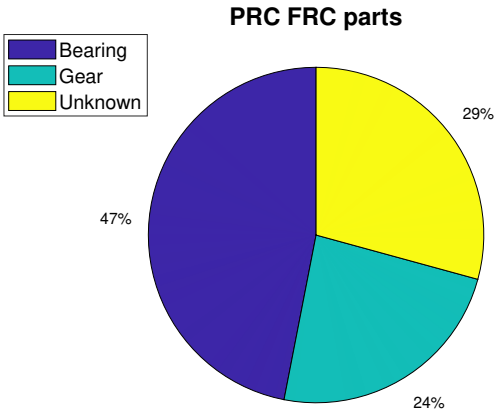

Figure 3.5: Failure mode PMG FRC

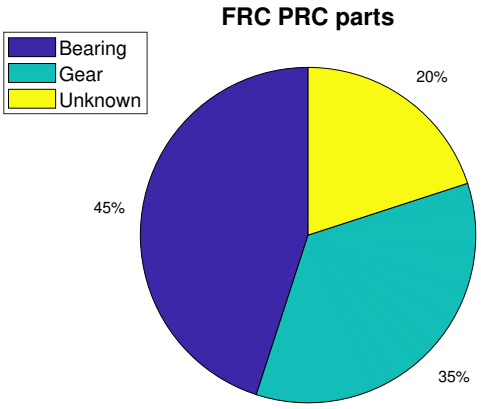

Figure 3.6: Failure mode DFIG PRC

3.3.3 Failure location

The location of failures can be analysed to determine where in the gearbox the failures occur. Figure 3.7 and Figure 3.8 shows both turbine types suffer mostly at the planetary stage. This is in line with what we would expect, which is that that major replacements to take place predominantly planetary stage as generally HS faults can be repairs and do not require major replacement. The presence of HS failures in PMG FRC suggests that HS failure is significant/catastrophic or may have led to further damage to other parts of the gearbox as it needs a major replacement, not just a repair.

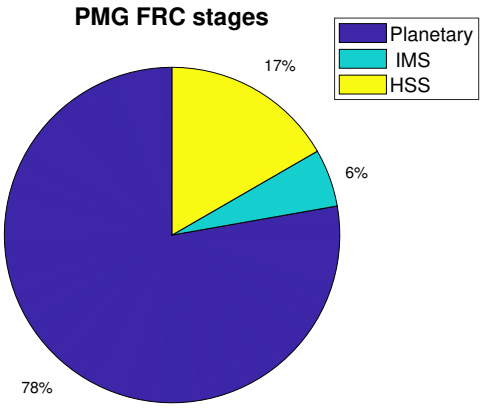

Figure 3.7: Failure location PMG FRC

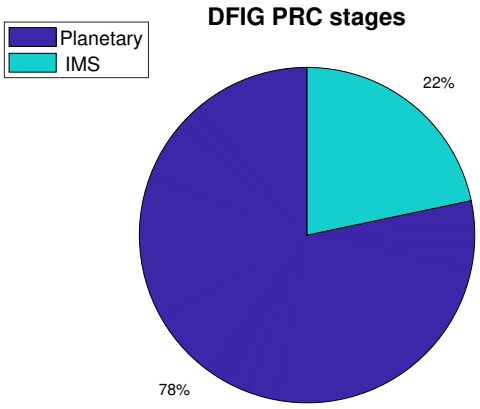

Figure 3.8: Failure location DFIG PRC

3.4 Discussion

The breakdown of reliability data by failure mode and location can give an additional insight into gearbox failure. It could be suggested that the planetary stage is more susceptible to failure due to is complex nature, compared to parallel stage which is generally more robust. This supports the data found in [41] which states that the parallel intermediate speed stage is more reliable than an intermediate planetary stage.

It could be hypothesised that when the generator is connected directly to the grid,

without a power converter, it is exposed to the grid variability which acts as a reaction torque. The power converter can act like a buffer between the grid and turbine. The power converter also allows the turbine to operate more flexibly, in response to wind speed as the power converter will condition the electricity generated to meet grid requirements. The FRC WT configuration sees failure rate lower that PRC failure rate. It can be hypothesised that decoupling from the grid can reduce loading felt upstream on the drive train. The generator plays a key role in wind turbine control, the reaction torque from the generator regulates the rotational speed to follow the power curve. The control inputs that determine the power output, are the wind speed but also the grid setpoint, which is determined by the grid frequency. Generator operating conditions will be compared to test this hypothesis.

3.4.1 Operating conditions

A sample turbine of each configuration has been taken to explore the different operating conditions. The torque and speed of the generator of each has been plotted as a box plot to show the distribution of variables. The mean torque values are similar for both DFIG and PMG but the DFIG has a much wider distribution of values it operates in, as shown by Figure 3.9 . The DFIG also operates at rotational speeds close to its maximum whereas the PMG operates at lower rotational speeds as shown by 3.10.

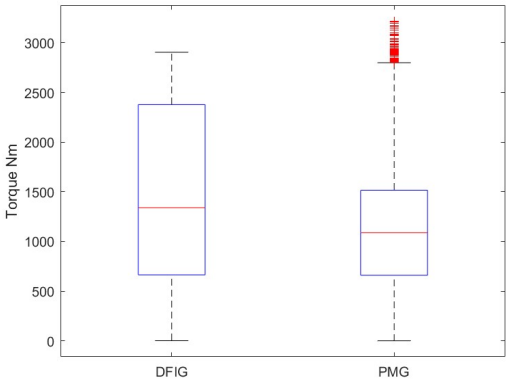

Figure 3.9: Box plot of generator torque

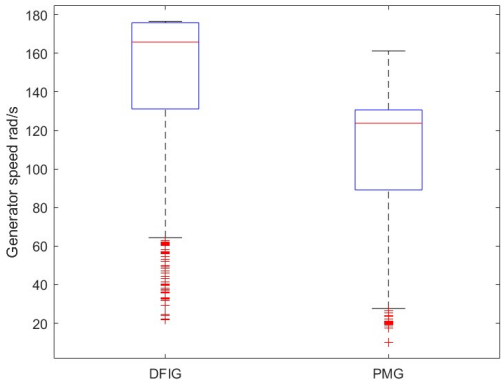

Figure 3.10: Box plot of generator rotational speed

[111] found that non-uniform distributions of temperature and lubricant film thickness over the tooth flank are observed due to the conditions of torque and rotational speed variations and sliding contact along the gear tooth flanks. Varying torque at high speed has a greater effect on increasing the gear tooth flash temperature, the instantaneous temperature at the local contact point. Local contact temperature and lack of lubrication can contribute to micropitting. [112] found that higher torque leads to

greater sliding on gear tooth flanks. By operating at wider ranges of torque and higher rotational speeds, the DFIG PRC gearbox is potentially more susceptible to damage and failure.

3.4.2 Limitations

It should be noted that this analysis covers only major replacement. These costs are based on material cost only. Travel time and lead time are not included in repair times or costs. Presenting the costs and times in this manner means repair costs are independent of distance from shore, but will under-represent the true cost, as lost production from lead time can incur significant costs, but they are generally project specific.

3.5 Conclusions

The results of the reliability analysis found that the DFIG PRC WT configuration experiences greater gearbox failure rates per turbine per year, incur higher costs and have a longer repair time than the PMG FRC WT configuration. The failure locations are similar for both, but the PMG FRC experience HS failures, suggesting the HS failures are catastrophic.

It was hypothesised that the high rate of failure of DFIG PRC can be attributed to the operating conditions it experiences as a result of being partially connected to the grid, and not fully decoupled, as the PMG FRC is. It can be argued that the operation conditions of a DFIG are more structurally demanding that of a PMG, due to its asynchronous operation, where the rotor can spin at variable speeds ($\pm 30\%$ of synchronous speed). This can introduce torque pulsations and mechanical stress on the shaft and bearings, especially during grid faults [113]. [114] found that during simulated grid loss event, the HS bearing torque fully reversed to -60% of rated and experienced relatively low stresses. However, the bearing load zones changed abruptly, and the loads were below the minimum requisite load during the reversals, which can potentially cause roller sliding.

These potential reliability issues should be a consideration in project planning when choosing a WT technology, if the site is located near to known grid congestion regions which could result in regular grid curtailment, thus being exposed to operating condition that can accelerate fatigue and have a negative effect on WT reliability. WF owners receive grid curtailment payments to reduce their output, as part of the balancing mechanism, as required. As they are financially compensated, owners combine grid curtailment into their availability metrics, so it isn't negatively affected. As a result, the impact of grid curtailment is given little consideration, and the potential long-term effects. This would also need to be part of the consideration process when a project comes to lifetime extension.

Chapter 4

Thermal modelling of a wind turbine gearbox for condition monitoring

4.1 Introduction

Most state of the art approaches to WT gearbox condition monitoring use black-box machine learning techniques for normal behaviour modelling as described in Section 2.3.5. This chapter's aim to use thermal modelling to create an alternative normal behaviour model, without the need for historical SCADA data. Thermal modelling techniques have been outlined in the literature review and existing literature relating to thermal network modelling has been detailed in Section 2.4.3. It can be noted that much of the existing research is from a purely tribological perspective, with minimal application being made to WT gearboxes.

In a gearbox, losses are generated by rotating parts, the interaction between the shaft, gears and bearings, and their interaction with the air and lubrication. These losses are assumed to be in the form of heat. The losses of the system can vary significantly depending on the gearbox type and operating conditions. A healthy gearbox has losses, and the same gearbox operating under different conditions may have different losses. The variation of these losses are to be explored from a theoretical physical

model, and then experimentally, as illustrated by Figure 4.1.

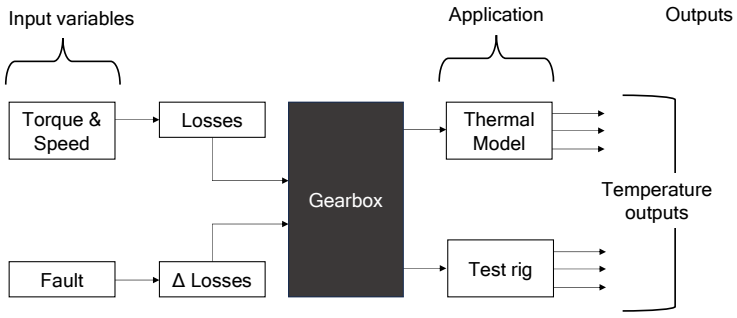

Figure 4.1: Thermal modelling overview

Research questions:

- Can a wind turbine gearbox thermal model imitate the thermal behaviour of a real life gearbox?
- If so, can a thermal model be used to detect and locate gearbox failures?

The Novelty of this research stems from:

- Simulating faults in a WT model to determine how it effects thermal behaviour
- Validating the thermal model with experimental data from a WT gearbox

4.2 Thermal network modelling

To determine the heat propagation of the gearbox, heat needs to be inputted into a system. The losses of a "healthy" gearbox is calculated mathematically using established tribological equations and applied to a thermal network model.

4.2.1 Methodology

Calculating losses

The total losses P_T from different component parts are a combination of load dependent and load independent losses as shown in 4.1 [115]. Each loss type can be estimated numerically, for the different gearbox stages.

$$\sum P_T = \sum P_{GD} + \sum P_{GI} + \sum P_{BD} + \sum P_{BI} + \sum P_S \tag{4.1}$$

P_T	Total losses	W
P_{GD}	Load dependent gear losses	W
P_{GI}	Load independent gear losses	W
P_{BD}	Load dependent bearing losses	W
P_{BI}	Load independent bearing losses	W
P_S	Seal losses	W

For nominal power transmission the load losses of the gear mesh are typically dominant. For part load and HS no load losses dominate total losses [116].

Gear - Load dependent Gear contact losses occur when gear teeth are in contact. The standard ISO/TR 14179-2:2001 [115] for calculating thermal losses uses a method widely used in other literature relating to gearbox efficiency [116] [89] [117] [118] [119] [103]. 4.2 uses a gear loss factor (H_v) which accounts for gear geometry and a mean coefficient of friction (μ_{mz}) and the transmitted power (P_a).

$$\sum P_{GD} = P_a \mu_{mz} H_v \tag{4.2}$$

P_a	Transmitted power	W
H_v	Gear loss factor	$-$
μ_{mz}	Coefficient of friction	$-$

4.3 is used to calculate H_v. It is assumed that the friction coefficient remains constant along the path of contact of the meshing gears [118].

$$H_v = \frac{\pi(u+1)}{z_1 u \cos\beta}(1 - \epsilon_a + \epsilon_1^2 + \epsilon_2^2) \tag{4.3}$$

u	Gear ratio	–
z_1	Number of gear teeth	–
β	Base helix angle	^{o}
ϵ_a	Profile contact ratio	–
$\epsilon_{1,2}$	Tip contact ratio	1 pinion, 2 gear

μ_{mz} is calculated in 4.4 where υ_Σ is a function of tangential velocity $\upsilon_\Sigma = 2\upsilon_t \sin\alpha_t$.

$$\mu_{mz} = 0.048\left(\frac{F/b}{\upsilon_\Sigma \rho_c}\right)^{0.2} \eta_{oil}^{-0.05} Ra^{0.25} X_L \tag{4.4}$$

b	Tooth width	mm
F	Force at pitch circle	N
η_{oil}	Dynamic viscosity of oil	Ns/m^2
Ra	Average roughness of pinion and gear wheel	μm
X_L	Lubrication parameter	–
υ_t	Tangential speed at pitch circle	m/s
ρ_c	Equivalent radius of curvature at pitch point of contact	mm
α_t	Transverse pressure angle	^{o}

Gear - Load independent Windage power loss is defined as the power loss due to the fluid drag experienced by the gear when it is running in air or an air-oil mist; air trapped and expelled of rotating gear. Churning power loss is defined as the power loss when a gear is running in an oil bath. Literature shows a number of ways to calculate windage and churning losses.

Approach 1 Oil churning losses are when the gear is submerged in oil and is dependent on operating conditions, immersion depth in sump as well as lubricant viscosity, as shown in 4.5 and used in [116] [89] [119] [99] [120].

$$P_{GI} = \frac{\rho \omega^2 S_m R_p^3 C_m}{2} \tag{4.5}$$

ρ	Fluid density	kg/m^2
ω	Rotational speed	rad/s
R_p	Pitch radius	m

C_m is dimensionless torque which can be calculated depending of fluid dynamic

properties, Reynolds number (Re) and Froude number (Fr) (the ratio of inertia to external field, used to determine the resistance of a partially submerged object moving through fluid). Calculated using either 4.6 or 4.7.
If $\omega R_p b/\upsilon < 6000$

$$C_m = 1.366\left(\frac{h}{D_p}\right)^{0.45}\left(\frac{V_0}{D_p^3}\right)^{0.1} Fr^{-0.6} Re^{-0.21} \tag{4.6}$$

If $\omega R_p b/\upsilon > 9000$

$$C_m = 3.644\left(\frac{h}{D_p}\right)^{0.1}\left(\frac{V_0}{D_p^3}\right)^{-0.35} Fr^{-0.88}\left(\frac{b}{D_p}\right)^{0.85} \tag{4.7}$$

D_p	Pitch diameter	m
V_0	Oil volume	m^3
b	Tooth width	mm
h	Pinion immersion depth	mm
υ	Kinematic viscosity	mm^2/s

Approach 2 [115] uses a method specific for splash lubrication system, the magnitude of loss is dependent on operating speed, using equations 4.8 - 4.12.

$$P_{GI} = \sum_{i=1}^{stage} T_{Hi}\frac{\pi n_i}{30} \tag{4.8}$$

The total hydraulic loss torque of a gear stage

$$T_H = C_{SP} C_1 e^{c_2\left(\frac{\upsilon_t}{\upsilon_{t0}}\right)} \tag{4.9}$$

$$C_{SP} = \left(\frac{4h_e, max}{3h_c}\right)^{1.5}\frac{2h_c}{l_h} \tag{4.10}$$

$$C_1 = 0.063\left(\frac{h_{e1} + h_{e2}}{h_{e0}}\right) + 0.0128\left(\frac{b}{b_0}\right)^3 \tag{4.11}$$

$$C_2 = \frac{h_{e1} + h_{e2}}{80 h_{e0}} + 0.2 \tag{4.12}$$

$h_{e1,e2}$	Tip circle immersion depth with oil level stationary	mm
h_c	Height of point of contact above the lowest point of the immersing gear	mm
h_{e0}	Reference value of immersion depth	mm
υ_t	Tangential speed	m/s
υ_{t0}	Reference tangential speed	m/s
l_h	Hydraulic length	mm

Where υ_{t0}, h_{e0}, b_0 are all reference values, 10 m/s,10mm and 10mm respectively. No-load losses associated with windage and churning become significant as speeds increases [118]. For splash lubricated gears, oil churning is usually considered major source of power loss which is strongly related to the fluid circulations generated by rotating gears, partly immersed in lubricant [96]. These losses depend on Reynolds number that describes the laminar-turbulent transition. However, [120] found discrepancy between the numerical and experimental results for losses was on the prediction of the gear churning loss.

Generally, the effect of lubricant aeration increases bath temperature. The presence of air in a lubricant manifest itself by the production of a significant number of bubbles whose size and shape are controlled by their surface tension representing the energy of the interface between the air in a bubble, and the surrounding oil. During the churning process, a number of bubbles are split into smaller ones leading to an increase in interface surface area thus requiring more energy; for example generating additional power losses [99].

Approach two is used in this research as it relies on fewer uncertainties related to gearbox parameters.

Bearing

Rolling bearing losses depend on type, size, arrangement, lubricant viscosity and immersion depth. There are a number of methods to calculate bearing power losses. [119] splits it into C_f= friction torque; C_v = viscous torque, as shown in 4.13 where ω is rotational speed (rad/s).

$$P_{bear} = \Big(C_f + C_v\Big)\omega \tag{4.13}$$

[121] uses experimental results to model bearing torque losses. Total frictional torque is made up of rolling friction torque, sliding friction torque, friction torque of drag losses and friction torque of seals; the sliding friction caused by the sliding speed over the contact area, the rolling friction caused by the squeezing of the oil meniscus and the reflow of lubricant at the contact inlet, the aerodynamic drag issued by the passage of elements through a fluid. Other sources of friction can occur such as the shearing of lubricant between the cage and the rings, within the cage pocket [122]. [56] states that a major part of heat generated is evacuated by conduction through raceways, and global thermal resistance of the bearing is not strongly affected by the grease so the grease will not be factored into the model.

Sliding friction torque is dependent on weighting factor and on reference values of the coefficient of friction for oil. In this case coefficients were determined experimentally, so it is unclear whether they can be generalised or specific to that configuration. The equations provided include a number of factors and coefficients which are not provided or explained, making it difficult to use this approach as there are too many unknown variables.

The BS ISO standard [115] for calculating bearing losses will be used, as show in 4.14, applicable for each bearing, where n_i is the rotational speed of gear stage i (rpm), and T_{VL} is total bearing loss torque (Nm).

$$P_B = \sum_{i=1}^{bearing} T_{VLi}\frac{\pi n_i}{30} \tag{4.14}$$

$$T_{VL} = T_{VL0} + T_{VLP1} + T_{VLP2} \tag{4.15}$$

Load dependent

Load dependent bearing losses depend on bearing type, size, load and sliding conditions

in the bearing and lubricant type and can be calculated using 4.14 - 4.17 [115].

$$T_{VLP1} = f_1 P_1^a d_m^b 10^{-3} \tag{4.16}$$

Where P_1^a is related to axial and radial bearing loads, $P_1^a = 2YF_a$

T_{VLP2} is for cylindrical roller bearings with additional thrust loading, otherwise $T_{VLP2} = 0$

$$T_{VLP2} = f_2 F_a d_m 10^{-3} \tag{4.17}$$

Load independent

Load independent losses are a function of bearing type and size, bearing arrangement, lubricant viscosity [116], in addition to rotational speed.

If υ_{oil} x $n < 2000 mm^2/s$

$$T_{VL0} = 1.6 \times 10^{-8} f_0 d_m^3 \tag{4.18}$$

If υ_{oil} x $n \geq 2000 mm^2/s$

$$T_{VL0} = 10^{-10} f_0 (\upsilon_{oil} n)^{2/3} d_m^3 \tag{4.19}$$

Where f_0 is from look up tables in [115] and are dependent on bearing type.

$f_{0,1,2}$	Coefficient for bearing losses from [115]	$-$
d_m	Mean bearing diameter	mm
b	Bearing width	mm
Y	Axial factor from [115]	$-$
F_a	Bearing thrust load	N
υ_{oil}	Kinematic viscosity oil	mm^2/s

Seals

Losses from the seals can be calculated using 4.20 where ϕ is shaft diameter (m) [115].

$$P_{seal} = 7.69 \times 10^{-6} \phi^2 n \tag{4.20}$$

Other losses

There are other losses discussed in literature for example, lubricant trapping, when lubricant is pumped out of gear mesh [17] [123]. These losses are not accounted for at this point, due to the lack of consensus in the literature as to how to calculate the loss.

Heat transfer

Hear transfer, is the transfer of energy due to molecular activity. A temperature gradient is established with energy continuously being transported in the direction of decreasing temperature [124]. The mechanism for this transfer is dependent on the material, whether it is a fluid, or a solid.

Conduction

Conduction is heat transfer that takes place between two solids that are in contact. The rate of heat transfer is dependent on the surface area (A), thickness (L) and material properties. Temperature of one surface when $x = 0$, is T_1, and the temperature of the other surface where $x = L$, is T_2.

$$T_1 = T(x); T_2 = T(x + dx) \tag{4.21}$$

$$T(x + dx) - T(x) = dT \tag{4.22}$$

$$Q = -kA\frac{dT}{dx} \tag{4.23}$$

$$Q = k\frac{A(T_1 - T_2)}{L} \tag{4.24}$$

Thermal conductivity k, is a material property. 4.24 is valid for steady state, constant k and one-dimensional conduction [124]. The minus sign illustrates the fact that the heat flows in the direction of the decreasing temperature as determined by 2^{nd} law of thermodynamics. Thermal conductivity varies with temperature and is limited to isotropic material.

Convection

Convection is heat transfer involving a fluid. It comprises surface area and heat transfer

coefficient (h). Heat transfer coefficient is not a material property [124] but a function of geometry, fluid properties, motion and temperature difference. Convection can be sub-categorised. Surface convection, the energy exchange between a surface and a fluid moving over it. Free convection is caused by a change in density of a fluid due to a temperature change or gradient. It is always present as long as fluid temperature is not uniform and there is an acceleration field such as gravity [124]. Forced convection involves heat transfer being accelerated by fluid motion, fluid motion which can be generated by an external source, for example, a fan. The general form of convection equation.

$$Q = hA(T_1 - T_2) \tag{4.25}$$

Heat transfer coefficient is related to a number of fluid dynamic principles, which can be used to calculate a heat transfer coefficient, for example 4.26 [125]. Which takes into account Reynolds number (the ratio of inertial forces to viscous forces within a fluid) and Prandtl number (the ratio of momentum diffusivity to thermal diffusivity)

$$h = 0.664\frac{k}{L}Re^{\frac{1}{2}}Pr^{\frac{1}{3}} \tag{4.26}$$

Calculating the heat transfer coefficients of the fluids within a gearbox can be difficult due to the limited information available. There are values available to cross reference, listed in 4.1

h (W/m^2K)			
		[126]	[124]
Forced Convection	Gases	10-500	20-300
	Oils	50-1700	50-20000
	Water	300-1200	
Free Convection	Gases	5-30	5-30
	Oils	10-350	20-1000
	Water	100-7000	

Table 4.1: Heat transfer coeffient values

Radiation

Radiation is a form of heat transfer where radiation energy is transmitted by electro-

magnetic waves, maximum possible radiation described by Stefan-Boltzmann law [124].

$$Q = \varepsilon\sigma\Delta T^4 \tag{4.27}$$

Where T= surface temperature, ε= emissivity, σ= Stefan-Boltzman constant ($5.67 \cdot 10^{-8} W/m^2K^4$). Radiation between two surfaces depends on geometry, shape, area, orientation and emissivity of the surfaces. For a real surface, emissivity is a fraction of the maximum black body. It depends on absorptivity of each surface – a property defined as the fraction of radiation energy incident on a surface which is absorbed by the surface.

SIMULINK

MATLAB Simulink was used to apply the theory of heat transfer outlined. The Simscape package has heat transfer blocks can be used to build up the thermal model, with several parameters to input, as listed below in Table 4.2

For all blocks, connection A and B are thermal conserving ports associated with the points between which the energy transportation takes place. Heat flow is positive if it flows from A to B.

It is assumed that radiation between components inside the gearbox are negligible. The only radiation considered is that between the gearbox casing and the outside. The boundary conditions imposed in the thermal modelling are those considered in literature: imposed temperatures at some nodes (ambient temperature) and imposed heat flows at others, in the form of power losses [56]. Oil temperature is set free, the oil operating temperature depends on ambient temperatures and oil/gearbox performance.

Block	Input	Variables	Output	Equation
Conductive heat transfer	Area m^2 Thickness m Thermal conductivity W/mK	Heat flow J/s $T_A - T_B$ = Temperature drop K	Heat transfer W	$Q = k(T_A - T_B)\frac{A}{D}$
Convective heat transfer	Area m^2 Heat transfer coefficient W/m^2K	Heat flow J/s $T_A - T_B$ = Temperature drop K	Heat transfer W	$Q = hA(T_A - T_B)$
Radiative heat transfer	Area m^2 Radiation coefficient W/m^2K^4	Heat flow J/s $T_A - T_B$ = Temperature drop K	Heat transfer W	$Q = kA(T_A^4 - T_B^4)$ where $k = \frac{\sigma}{\frac{1}{\varepsilon_1}+\frac{1}{\varepsilon_2}-1}$
Thermal mass	mass kg Specific heat $J/kg/K$	Heat flow J/s $T_A - T_B$ = Temperature drop K	Heat transfer W	$Q = cm\frac{dT}{dt}$

Table 4.2: Heat transfer block parameters

4.2.2 Application - case study

Input parameters were estimated using engineering drawings and parts list provided by the manufacturer, found in Appendices **??** - **??**. The important specifications can be found in Table 4.3.

Gearbox rated power 17.73kW, the given drivetrain efficiency is 66%. At rated power, the manufacturers predict drive train losses amount to 6.03 kW.

$$P = \frac{1}{2}\rho\pi R^2 V^3 C_P \tag{4.28}$$

Specification	
Rated capacity	11kW
Cut in wind speed	3 m/s
Rated wind speed	9.5m/s
Cut out wind speed	$>$ 25m/s
Rotor diameter	13m
Rotor speed	56rpm / 5.86rad/s
Control	Fixed speed, stall regulated

Table 4.3: 11kW WT specifications

Using 4.28 [127], for the given rated power of $9.5m/s$ and C_P=0.26. The power curve of the rotor side of the WT is shown in Figure 4.2. As losses are load dependent, we can estimate losses as wind speed varies.

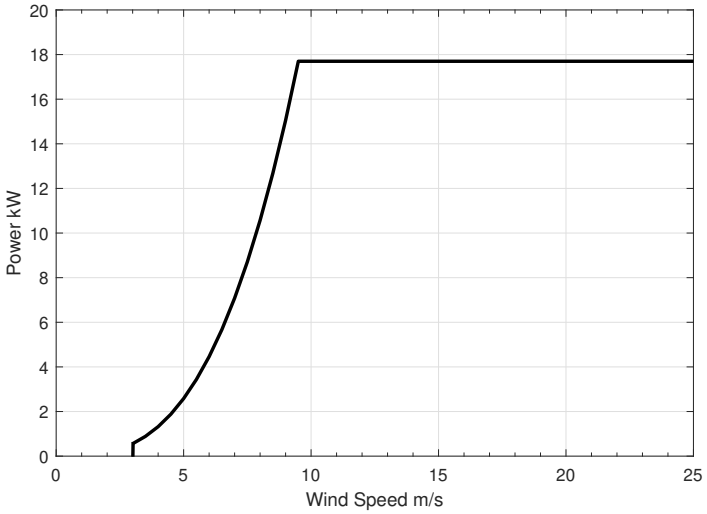

Figure 4.2: 11kW WT power curve

The thermal network model was produced for this gearbox. Figure 4.3 shows the geometry interaction of the gearbox and of the components. The heat transfer between nodes are shown in where the black lines represent the component nodes, labelled at the top of the Figure 4.4.

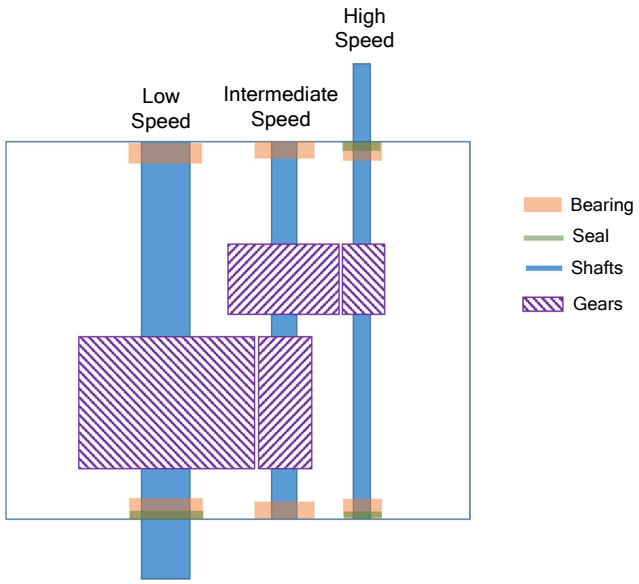

Figure 4.3: Schematic of 11kW gearbox

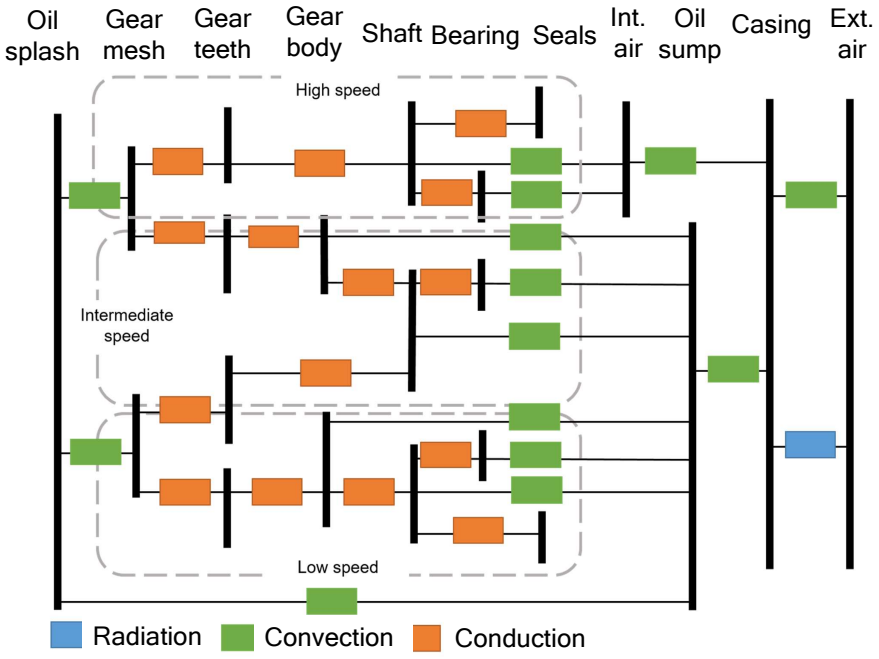

Figure 4.4: Thermal Network Model of 11kW gearbox

4.2.3 Results

A steady state thermal model was created and the simulation run with the rated power input. The results are shown in Figure 4.5 and Figure 4.6.

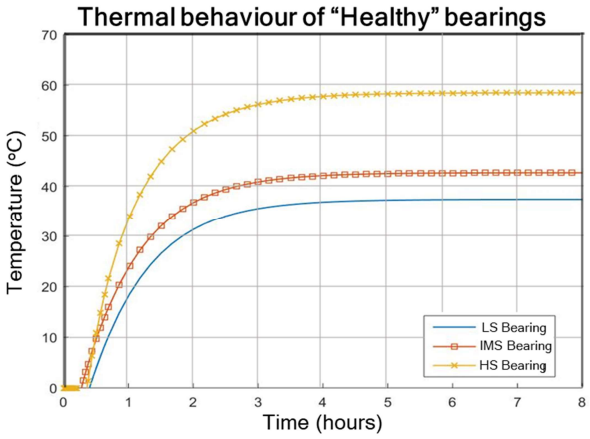

Figure 4.5: Simulated bearing temperatures in a "healthy" gearbox

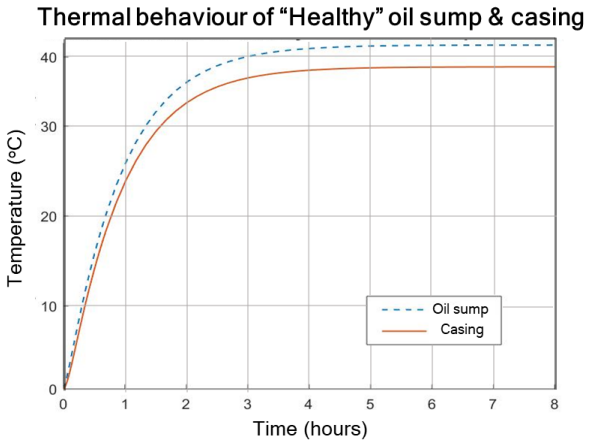

Figure 4.6: Simulated oil sump and casing temperatures in a "healthy" gearbox

As expected, the HS temperature is greater than intermediate (IMS) or low speed (LS), due to the higher rotational speed.

4.2.4 Discussion

The hypothesis that the model can be used to monitor a fault at the component level was tested. To do this, extra heat losses were introduced into the model at the high-speed (HS) bearing nodes to mimic fault heat. The bearing was selected in the first instance as this is a common gearbox failure mode. It is assumed that a fault will affect the friction within the bearing and thus generate heat. However, the magnitude of this additional heat input in real gearboxes is unknown, and does not appear to be covered in available literature.

To model a fault in the high-speed bearing, an estimated approach has been taken, where a step increase in heat flow is added at the HS bearing node at one third of the way into the total simulation when it has reached thermal equilibrium. The temperature increase of different levels of fault are shown in Figure 4.7. An important outcome of the thermal model is to determine if a fault in a component can be detected elsewhere, for example, the oil sump, a location commonly used to monitor temperature in SCADA data. Figure 4.8 shows oil sump temperature as a result of a "fault" at the HS bearing temperature. These fault heat levels (10, 20 and 30W) represent a 12.5, 25 and 37.5% increase in heat that is already present in the healthy gearbox.

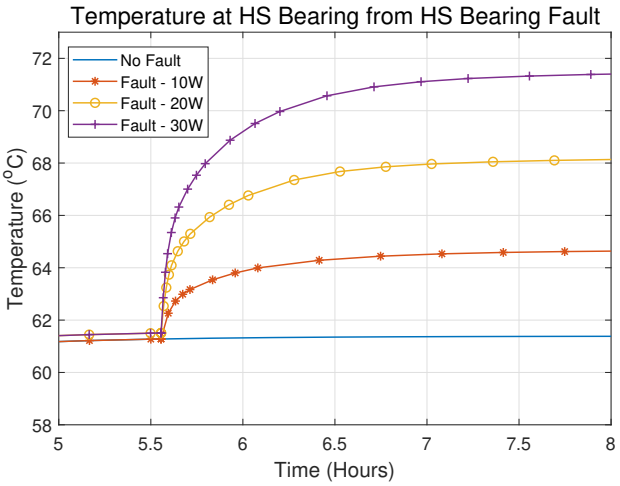

Figure 4.7: Temperature at HS bearing

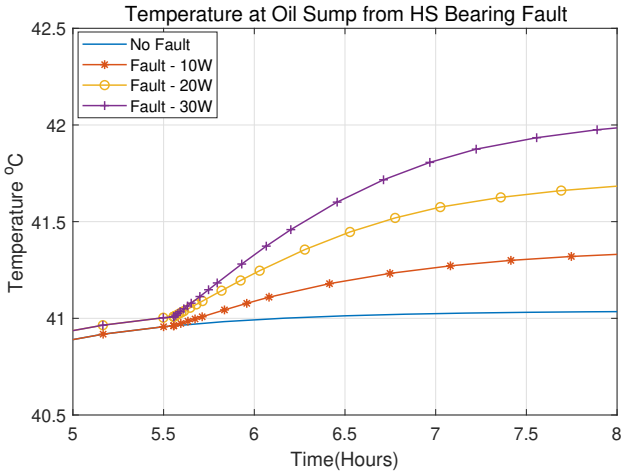

Figure 4.8: Temperature at oil sump from fault

The same "fault" process has been applied to the low-speed (LS) bearing in the model. This gives a similar result, as shown in Figure 4.9 but with a lower equilibrium temperature due to its slower rotational speed, and lower equivalent thermal resistance. The thermal behaviour of the oil sump (Figure 4.10) is almost identical to a fault in the HS bearing.

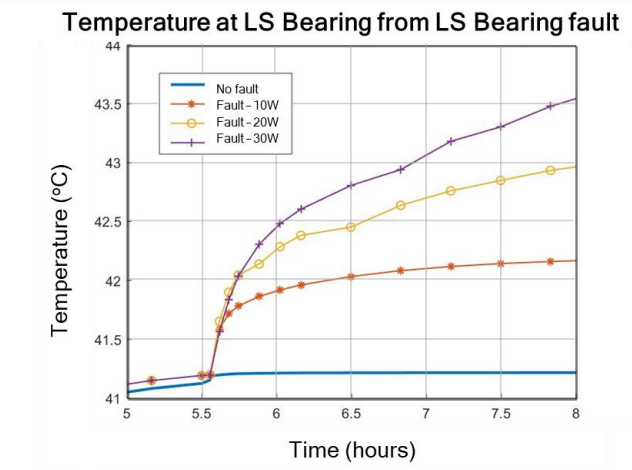

Figure 4.9: Temperature at LS bearing

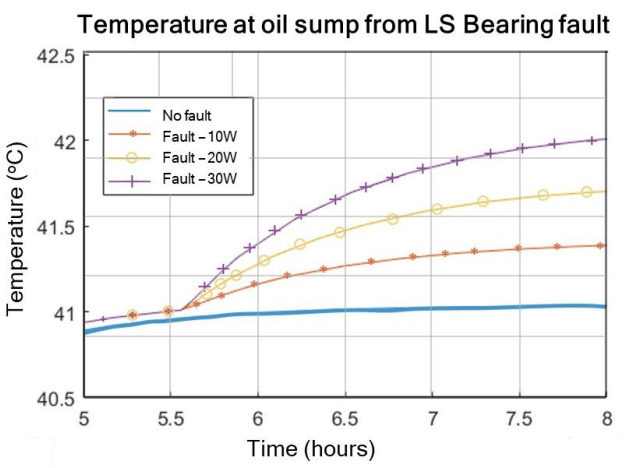

Figure 4.10: Temperature at oil sump from fault

Figure 4.8 and Figure 4.10 show that using a single temperature measurement, such as the oil sump temperature, does not give much information about a fault location. However, if the difference in temperature between two components is used, it shows a more definitive difference. Figure 4.11 and Figure 4.12 show the difference in temperature between nodes, illustrating that faults in different locations produce different thermal behaviour. This suggests that multi-locational measurements alongside a thermal model may be able to locate faults.

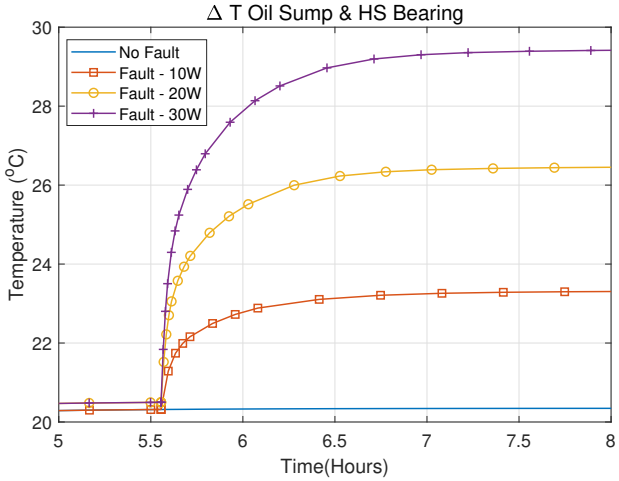

Figure 4.11: Temperature difference between HS bearing and Oil Sump due to fault at HS bearing

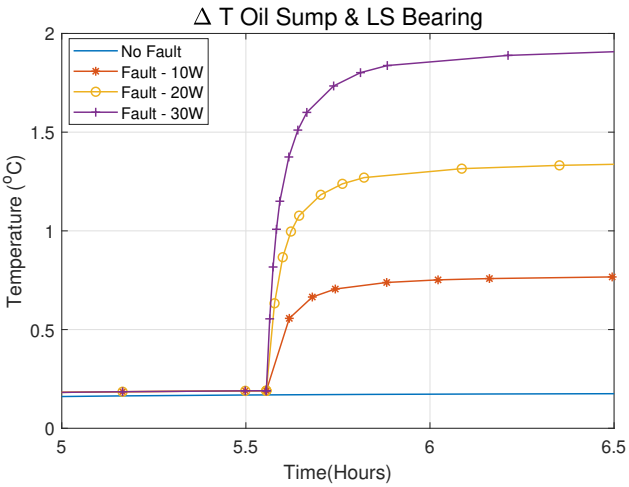

Figure 4.12: Temperature difference between LS bearing and Oil Sump due to fault at LS bearing

Uncertainties

Thermal network models found in literature were found to include other forms of heat transfer. [89] introduced an additional thermal resistance, heat removal by centrifugal fling off. [128] included a thermal resistance for striction, a constriction of the thermal current from surface to the gear centre. These mechanisms are not easy to model in the Simulink set-up given the simplified nature of the thermal network modelling method. If temperature is controlled, how would you consider that in your model?

Limitations

Calculating losses for planetary type gears are not included in British Standard so further research is needed to move onto these types of gearboxes. The gear meshing is the same source of losses, but as multiple elements are in contact at the same time, speed and torque will need to be calculated for each element of the planet gear.

A more sophisticated cooling system used in complex gearboxes will need to be accounted for,as it will change the way the heat propagates through the gearbox as the heat transfer mechanism is different from a splash lubrication system. For the splash lubrication in the model, the oil temperature was unconstrained, but to model an active cooling system, an additional heat source which is activated when oil temperature reaches a certain temperature. This done by [93], where the a smooth control of oil temperature was achieved.

There is minimal information in literature that estimates the additional losses or temperature increased as a result of a fault. [129] found that micropitting can increase gear tooth friction by 10% and friction coefficient has a direct influence on gear power losses as shown by the ISO TR 14179-2 expression [115]. Yet, in the perspective of health monitoring, the defect magnitude estimation (i.e. the micropitted area) based on temperature measurements remains a complex task. It is not possible at this point to propose a law that could directly link the temperature variations to the micropitting severity [129]. Experimental validation is required to determine how well the thermal network model can imitate the thermal behaviour of a gearbox.

4.3 Experimental

The experimental set-up of the test rig is outlined. The reliability of the results will be discussed based on the set-up and equipment used.

4.3.1 Methodology

The test rig is made up of two identical gearboxes back-to-back, driven by a motor, controlled by a torque and speed control unit, as shown by Figure 4.13. The test rig

step up was an existing one in the university's engineering laboratory. It already had a torque meter fitted to the output shaft. The set up involved in this research was to fit one of the gearboxes with temperature sensors to collect temperature data.

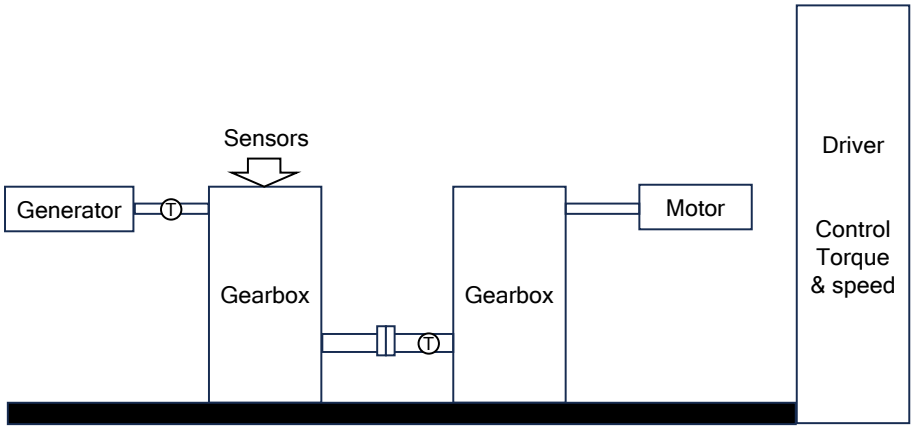

Figure 4.13: Schematic of test rig

Preliminary set up

An existing data acquisition system was used for preliminary part of this research. This consisted of thermocouple sensors with an uncertainty of $\pm 2^{o}$C. Allowing for restrictions in the geometry of the gearbox, a sensor system was used which corresponded to the individual gears and shafts. The configuration is shown in Figure 4.14.

1	High speed shaft
2	Intermediate speed gear
3	Intermediate speed shaft
4	Low speed gear
5	Low speed shaft

Figure 4.14: Preliminary set up

The data acquisition instrumentation was made up of TMP35/6/7 temperature sensors connected to an Arduino Mega. Operating conditions were set at 968 Nm and 57 rpm, giving an output power of 5.8kW, approximately half the rated power of the small WT for which it is designed. The output of this preliminary experiment is shown in Figure 4.15.

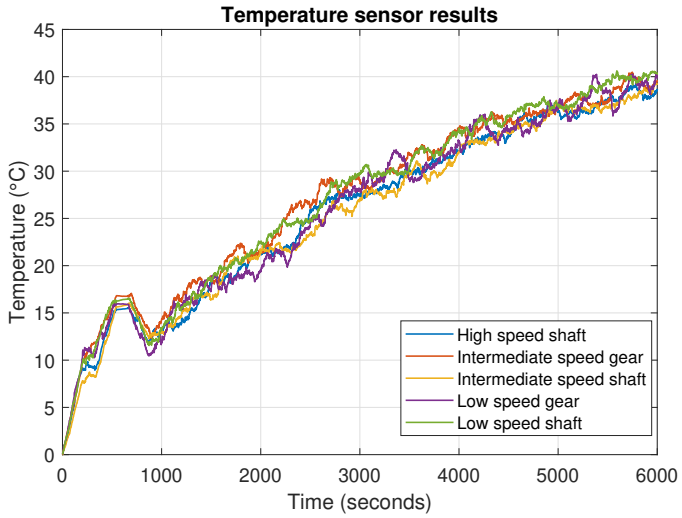

Figure 4.15: Preliminary results

This data acquisition system was used as a simple and low cost solution to collect preliminary data, and because of this, there was a potential for significant uncertainties

in the results:

- Metal prongs housing the sensors add additional heat path and thermal capacity.
- Proximity to corresponding components is approximate.
- Temperature sensor accuracy not being ideal

Experiment Redesign

Literature has found temperature measurement methods influence diagnostic capabilities, for example, data from thermography was found to be different from data from contact sensor [74]. Therefore, subsequent research considers a more sophisticated data acquisition system, with the aim of improving precision by repeating experiments and using sensors with increased sensitivity. With products chosen to fit our application; the selection process will now be discussed. The design of the system needs to account for the compact nature of the gearbox, the accessibility and the level of disturbance required. The measurement system can be broken down into a number of components which can loosely represent different products required for the data acquisition system shown in Figure 4.16.

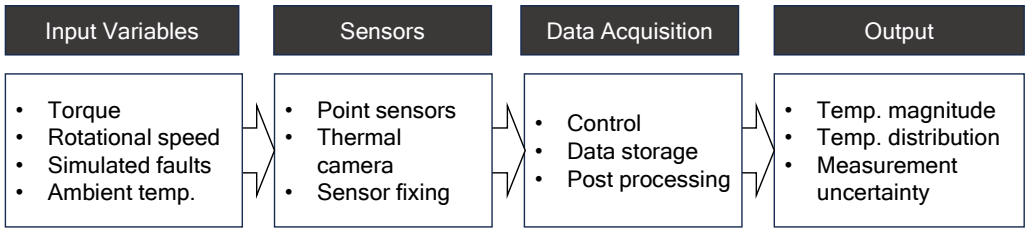

Figure 4.16: Data acquisition considerations

Sensors

The physical variable to be measured is temperature, the "primary transducer" is the temperature sensor. There are a number of primary transducers that can be used to measure temperature, all with different advantages and disadvantages as listed in Table 4.4 [130].

This information can be used to determine which characteristics are most important for this application. These are accuracy, stability and sensitivity. Durability and range are less important. The sensors also need to withstand vibration and exposure to oil splash. Considering all these factors, RTD sensors are most appropriate. They have been used for many years to measure temperature in laboratory and industrial processes, and have developed a reputation for accuracy, repeatability, and stability. The large temperature range offered by a thermocouple is not required for this application.

RTD sensors are temperature sensors that contain a resistor that changes resistance value as its temperature changes. Passing current through an RTD generates a voltage

Type	Advantages	Disadvantages
Thermocouple	Simple Rugged Low cost Wide temperature range	Non linear Small sensitivity Least stable Required cold-junction compensation
RTD (resistance temperature detector)	Most stable Good linearity Most accurate	Low sensitivity Externally powered Self-heating error
Thermistor	Fast High output	Limited temperature range Externally powered Nonlinear fragile

Table 4.4: Temperature sensor options

across the RTD. By measuring this voltage, one can determine its resistance and, thus, its temperature. RTDs exhibit the most linear signal with respect to temperature of any electronic temperature sensor. RDT sensors are available in three configurations: 2,3 and 4 wire. 2-lead constructions result in lead wire resistance being added to the element resistance. Consequently, the temperature reading is artificially high. 4-wire resistance measurement will effectively cancel lead wire resistance. The 4-wire circuit is a true 4-wire bridge, which works by using wires 1 & 4 to power the circuit and wires 2 & 3 to read. This true bridge method will compensate for any differences in lead wire resistances [131].

Temperature is measured using voltage or resistance as a proxy. There is a near linear relationship between resistance and temperature for using RTD sensors, as shown in Figure 4.17. Also, as the resistance of the sensor is being read, the distance between the sensor and the instrumentation should be kept to a minimum so that wire resistance does not affect the signal.

Platinum resistance temperature detector PT100 sensor of Accuracy class A is defined as having an accuracy of $\pm$ 0.15^{o}C at 0^{o}C, as directed by the IEC standard [132]. The difference between Class A and Class B is demonstrated by Figure 4.18. For this application, between 0^{o}C and 200^{o}C, Class A tolerance values are acceptable.

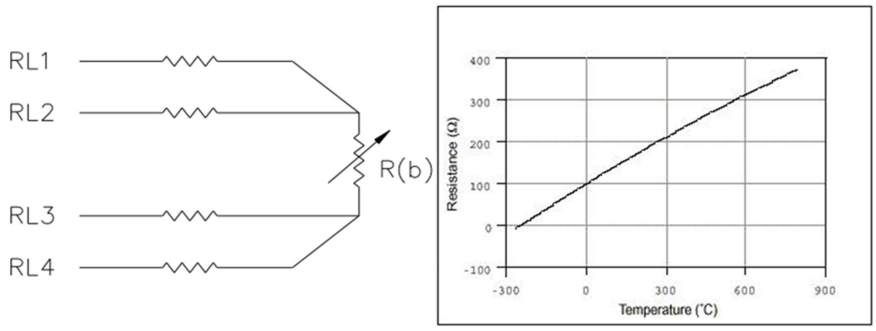

Figure 4.17: RDT sensor

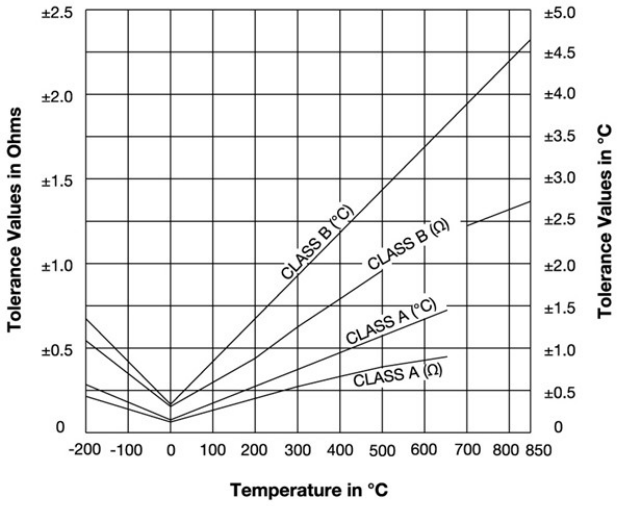

Figure 4.18: Tolerance of RTD sensor, Class A and Class B

Several signal conditioning considerations must be made, including:

- Amplification
- Filtering

- Excitation
- Scaling to temperature units

There are a number of collection and processing data acquisition units available that can address these considerations. A National Instruments cRIO[1] is the data acquisition unit selected for this application. The unit comprises a chassis frame with a number of slots for sensor modules, an FPGA[2] and a controller.

RTDs can be calibrated by comparing their resistance to the resistance of a secondary standard at several points over the temperature range of interest. The secondary standard's resistance is well-known and stable over time. Calibration of an RTD can be done by comparing its readings at a known, controlled temperature (like the freezing point of water) to the expected resistance value. This should be done periodically to ensure accurate readings.

Calibrating the RTDs in the actual environment where it will be used can help account for self-heating. Most RTDs can measure temperatures from about -200°C to 850°C, a much greater range than for this application.Self-heating is typically specified as the amount of power that will raise the RTD temperature by 1°C, or 1 mW/°C.

Self-heating can be minimized by using the smallest possible excitation current. The amount of self-heating also depends heavily on the medium in which the RTD is immersed. An RTD can self heat up to 100 times higher in still air than in moving water [133]. The RTDs placed in the gearbox will benefit from heat being immersed in moving oil from the splash lubrication. This would also be the case in utility scale wind turbine gearboxes, whereby the sensor placements would either have contact with the cooling system fluid, or near a cooling fan.

Sensor placement

Sensors were selected that had the capability of being submerged in oil. The ideal placement of sensors are as close to the component as possible without interfering with the running of the gearbox. The sensors therefore had to be robustly fixed in place.

[1] Compact reconfigurable input output system
[2] Field-programmable gate array

The externally located sensors (shown in Figure 4.19) were fixed with a thermally conductive glue, which is designed to maximise heat transfer from the surface to the sensor, without being affected by adhesive.

The internal sensors were fixed in place using strong magnets to ensure that they

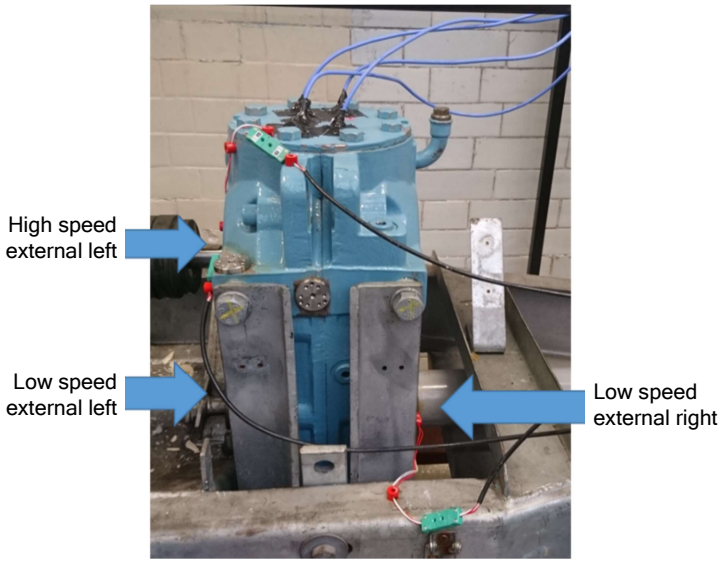

Figure 4.19: External sensor placement

would stay in place. Using an adhesive was considered too risky, as it may not be strong enough to keep the sensors in place while the gearbox is in operation. The sensors were fixed while the gearbox was empty of oil (as shown in Figure 4.20). This also meant that fresh oil would be used for the experiments. The magnet set-up ensured there was no interference with the equipment. This was difficult to ensure when the casing lid was re-attached for operation, but periodic checking to maintain their placement was planned. The other interference would be to the oil splash, but as that is a chaotic system by design, it is assumed impact negligible. It should be noted that the magnets could be adding to the thermal mass of the casing.

The cRIO and the laptop were located as close to the gearbox as safely possible so that the resistance of the wire did not affect the signal. An ambient temperature sensor was located away from any potential sources of heat, as shown in Figure 4.21

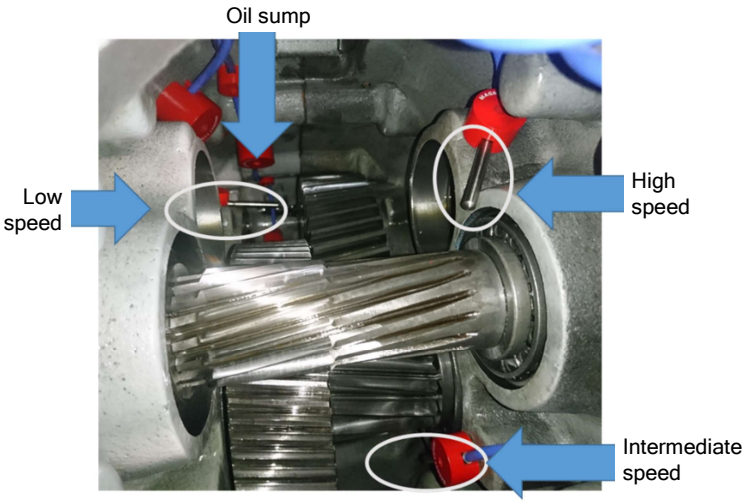

Figure 4.20: Internal sensor placement

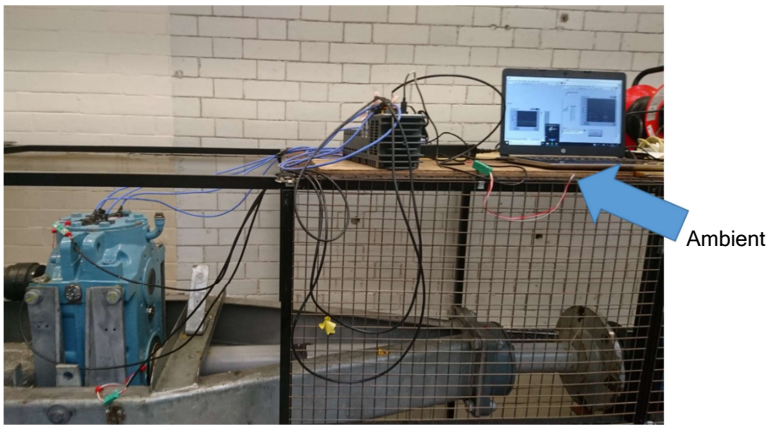

Figure 4.21: cRIO and laptop location

Software – LabVIEW

As National Instruments hardware is used in the data acquisition, the associated programme was chosen to interface with the cRIO to collect and store the data, LabVIEW.

LabVIEW is a systems engineering software for applications that require test, measurement, and control with configuration with hardware. Programs-subroutines are termed virtual instruments (VIs). Each VI has three components: a block diagram, a front panel, and a connector pane. The last is used to represent the VI in the block diagrams of other, calling VIs. The front panel is built using controls and indicators. Controls are inputs: they allow a user to supply information to the VI. Indicators are outputs: they indicate, or display, the results based on the inputs given to the VI.

The back panel, which is a block diagram, contains the graphical source code. All of the objects placed on the front panel will appear on the back panel as terminals. The back panel also contains structures and functions which perform operations on controls and supply data to indicators.

In this application DAQmx driver is used with LabVIEW. NI-DAQmx is National Instruments' current-generation data acquisition driver. NI-DAQmx is a driver complete with its own functions and development tools to control National Instruments data acquisition devices (DAQ).

Several VIs are used to establish a connection to the sensors, select their characteristics, and dictate the sampling frequency, which was set to 10Hz. This is then fed into a For- Loop to read data from the sensors at the set frequency.

As the cRIO is field programmable, it acts like a separate PC that requires applications on it. The cRIO does not have the storage capacity to hold all of the data. Data from the cRIO then needs to passed back to the host PC (laptop) to continuously store the data in a readable form. Network streams use a one-way, point-to-point buffered communication model to transmit data between applications. This means that one of the endpoints is the writer of data and the other is the reader.

This process is summarised in the Figure 4.22 with the corresponding VI configurations for the cRIO Figure 4.23 and PC host Figure 4.24.

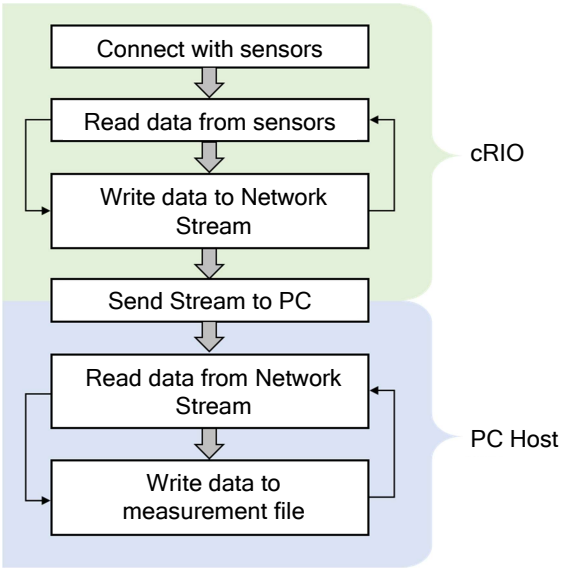

Figure 4.22: labVIEW data acquisition and storage process

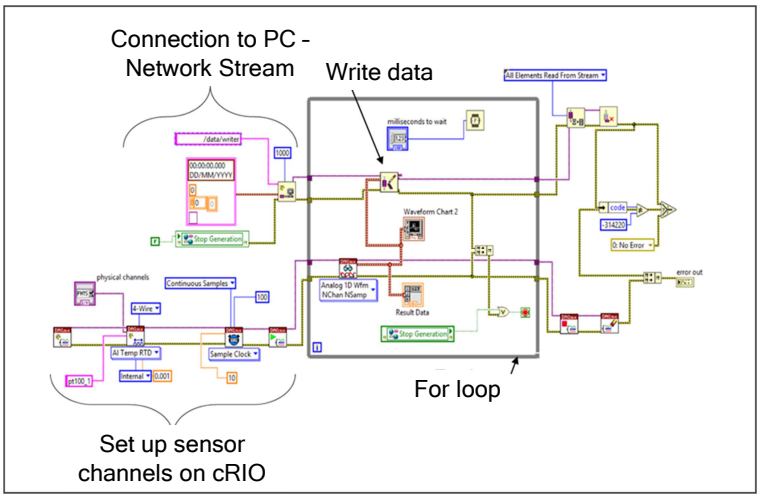

Figure 4.23: labVIEW software configuration - cRIO

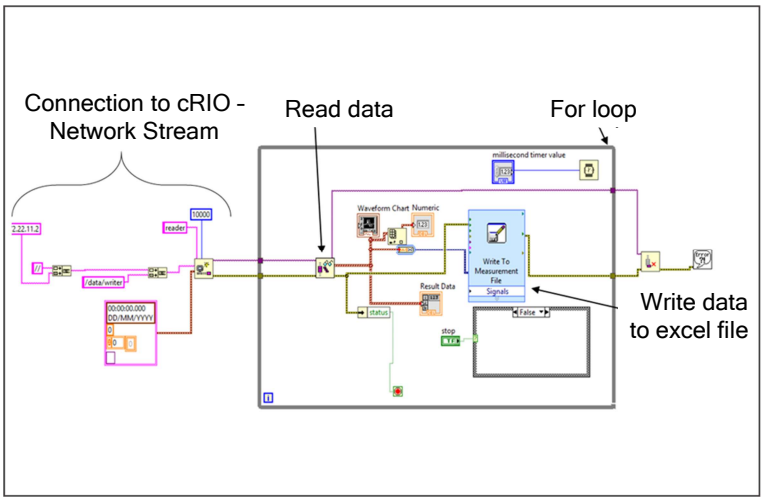

Figure 4.24: labVIEW software configuration - PC Host

Additional data collection

A thermal imaging camera was used to supplement the point sensor temperature measurement data. The specifications are as follows [134]:

- 160 × 120 (19,200 pixels) thermal resolution
- Thermal sensitivity: <0.06°C at 30°C
- Spatial resolution (IFOV): 3.7 mrad

Temperature and strain-rate are variables of fundamental importance in the prediction of the mechanical response of materials. When a material is heated or cooled, it will expand or contract. This dimensional change creates strain. If the material can't expand freely, the thermal strain results in stress, leading to thermo-mechanical stress, which can cause cracks or fatigue over time. Different components may have different coefficients of thermal expansion leading to thermal mismatch and strain at interfaces. Gearboxes are also under mechanical strain from torque loads. When combined with thermal strain, thermo-mechanical strain occurs which can lead to fatigue over time, affects gear meshing accuracy, and impact gear alignment and efficiency.

Research by NREL [114] used strain gauges to monitor high-speed shaft bearing

loads on tapered roller bearings. This involved machining slots into the bearing outer race and the HSS itself was instrumented with strain gauges. It was tested under various conditions, including normal operation, generator misalignment, simulated braking, and grid loss events. The condition which had the most significant effect on loading was braking events, where gearbox torque increased abruptly to 70% above rated and resulted in maximum stresses in the bearings 45% to 60% above rated. The research is valuable in understanding root causes of gearbox failures. However, the instrumentation is difficult, with machining needing to take place, and it is not something available for this research.

Moreover, the purpose of this research is to validate a thermal model, for condition monitoring applications. There for want to replicate data available in real life WT. It would be unusual to have strain measurement in SCADA data.

Operating conditions

To understand the thermal behaviour of the WT gearbox, it should be run for different operating conditions, as torque and speed both have an effect on losses. Initially the rotational speed was fixed as this replicates the operation of the GAIA WT, the gearbox from a fixed speed stall regulated WT. The torque was varied to give a range of power outputs. The initial set of experiments were performed to test the new sensor set-up and data acquisition system, the operating conditions are show in Table 4.5.

	Speed input	rpm output	Torque input	Nm output	Power (kW)	Start	Total (mins)
8/7/19	56	1000	0	0	0	12:47	236.5
10/7/19	56	1000	682	38.2	4	11:57	238.9
11/7/19	56	1000	556	21.9	3.3	14:24	149
17/7/19	56	1000	872	39.3	5	10:42	167
19/7/19	56	1000	929	41.2	5.44	10:27	163.2

Table 4.5: Experimental operating conditions

The operating conditions were set by the control panel for the drive motor (motor 1 on Figure 4.25). The RPM was set using the gauge. The torque is more difficult as the gauge displays it as a % So the dial must be adjusted and then compared to the torque meter reading, shown in Figure 4.26.

Figure 4.25: Test rig control panel

Figure 4.26: Torque meter output displays

4.3.2 Results

At this point, it is important to note that the data collection was disrupted by technical problems arising with the test rig. This led to troubleshooting and repairs, resulting in the test rig being offline for long periods of time. The issues include:

1. The shaft between the two gearboxes decoupled and jammed, resulting in the entire test rig being moved to free the parts and reposition (see Figure 4.27).

2. Torque and speed measurement device on low speed shaft became jammed so shaft could no longer freely rotated inside. The test rig again had to be taken apart to free the device.

3. The input torque was not being supplied constantly; it was oscillating as shaft rotated. This made it difficult to accurately control the torque input. It was found to be caused by a loose connection from the drive controller.

4. The test rig had to be moved to a different location due to space constraints in the originally allocated University laboratory.

It is believed that the issues experienced by the test rig are caused by shaft misalignment between the two gearboxes, as a result of the design and installation of the support structure (years prior to this research). It was proposed that with the relocation of the test rig, repairs could be made and the test rig would operate as required.

However, during the move and recommissioning process, the university closed due to Covid lockdown restrictions. Finally, with the long term uncertainty, it was decided to abandon any further experimental work.

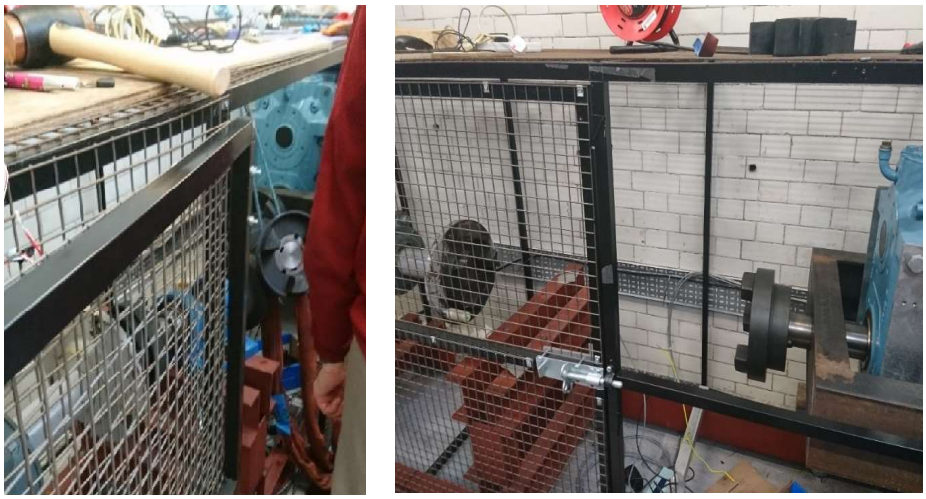

Figure 4.27: Test rig under repair

The following results are those that were managed to be gathered, prior to the test rig being taken offline for relocation and later University closure.

Post processing of the temperature data involved using a moving average filter, with a sliding window of length 1000 across neighbouring elements. The results of 0kW run is shown in 4.28.

Results from all runs are grouped by component sensor and normalised by the ambient temperature. As expected, the higher the power input, the higher the temperature readings. These are shown in Figures 4.29- 4.34.

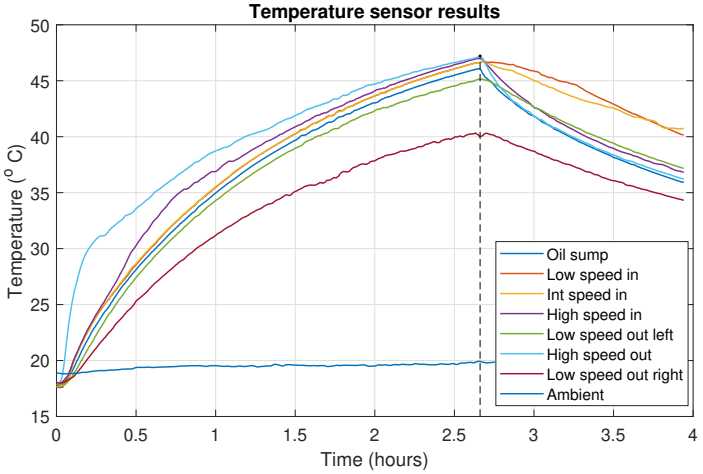

Figure 4.28: Results from running the test rig

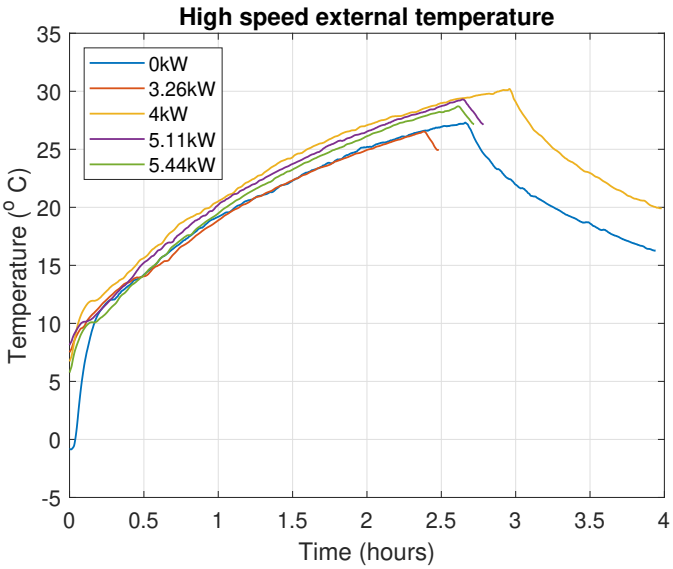

Figure 4.29: High speed external results

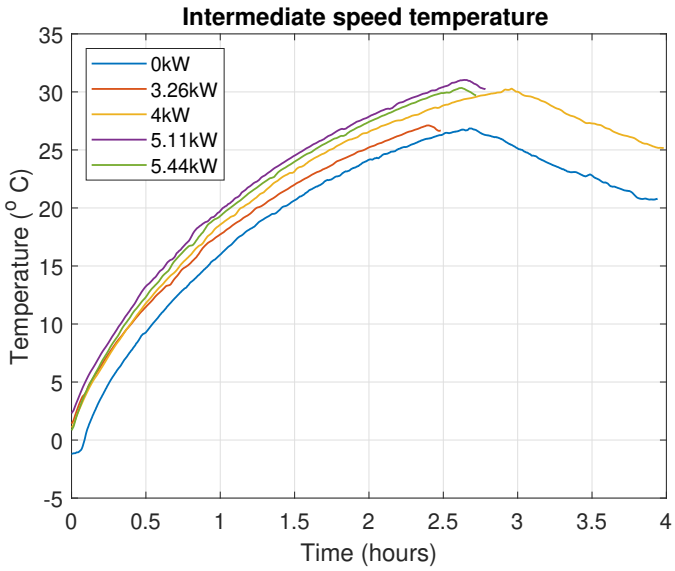

Figure 4.30: Intermediate speed internal results

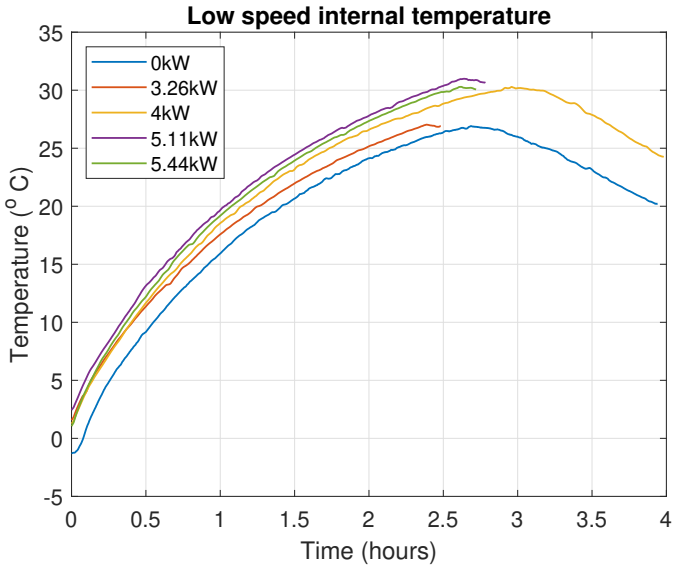

Figure 4.31: Low speed internal results

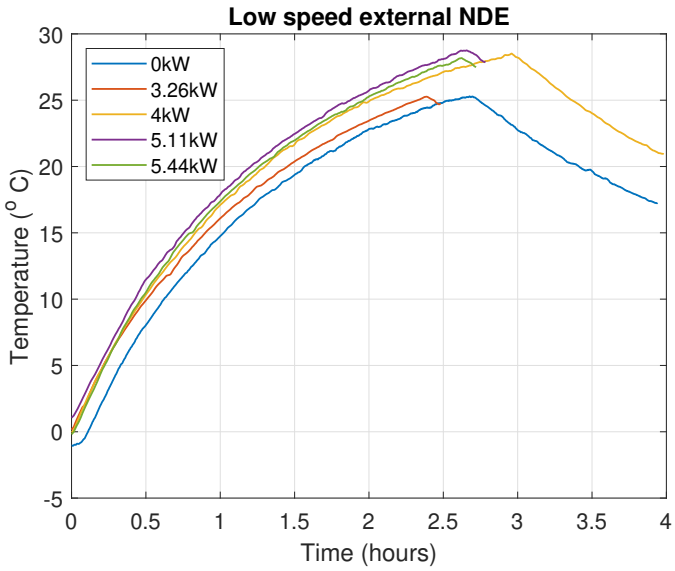

Figure 4.32: Low speed external NDE results

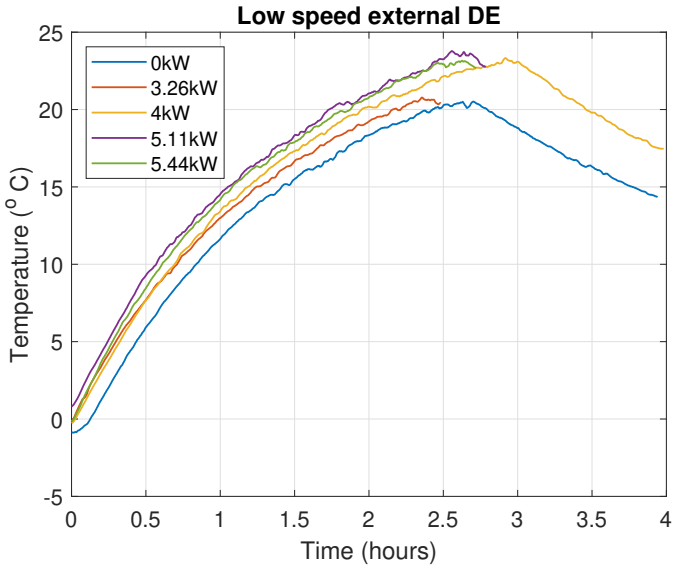

Figure 4.33: Low speed external DE results

IR Thermal image

Thermal camera images were also taken during experiments as shown by Figure 4.35. These demonstrate how hot the casing gets during the gearbox operation. It also provides a temperature reading for the rotating shaft, where it meets the seal and bearing, a location which was not possible to add a point sensor.

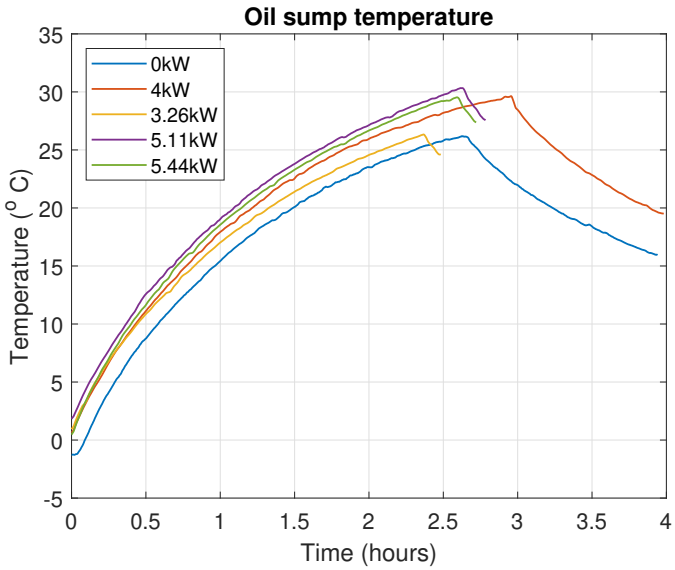

Figure 4.34: Oil sump results

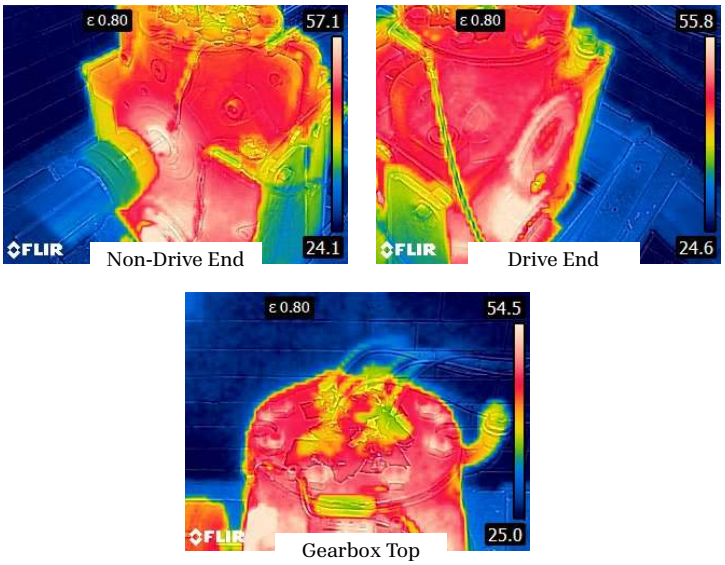

Figure 4.35: Thermal image of gearbox

Figure 4.35 shows the top of the gearbox reaching temperatures of 40°C − 50°C, even with no connection to sources of heat generation. It is assumed the oil splash was causing this.

4.3.3 Discussion

The oil sump and casing provide a significant thermal mass. As demonstrated by the test rig took taking longer to reach equilibrium than expected (a limitation of lone working meant that the test rig couldn't be run unsupervised, so had to be turned off). When the test rig was turned off, the external sensors and those not submerged in oil, cool much quicker due to the heat retained in the oil and the lack of active convection.

The IR images suggest that the bearing temperature readings are not capturing the highest temperatures, as the sensors were not placed where highest temperatures were located.

Comparing the experimental results with the analytical model suggests that the model may be overestimating the losses. In comparing the model oil sump temperature at 2 hours, to the experimental data, we find the experimental data to be 10°C lower. The model found that the difference between the LS and the HS to be 20°C, but in the experimental data, the difference between the two is much less. In the experimental data, there is a discrepancy between the LS external sensor temperatures, the right sensor reads temperatures 5°C less than the left. As they start at the same temperature, it is assumed that it isn't a calibration issue, it could be because the right side is the input shaft. The input shaft could be acting as a thermal mass, absorbing heat from the bearing. This was not factored into the model but is something that should be.

The HS stage in Figure 4.29, show that, for these experiments, torque does not play a significant a role in varying the operating temperature (2°C) when compared to that of the LS stage (5°C). These experiments are all relatively low torque, the maximum being 5.5kW, compared with the rated torque input, which is 17kW. Without more experimental data operating at higher torque, it is difficult to quantify its effect.

Figure 4.33 shows the LS outside right sensor output as noisy, which may have been caused by the issue found with torque controller, as that is the side being driven.

The limited experimental results show the temperature of casing is much higher than in the thermal model. This suggests that the heat transfer between where the heat is generated and the casing is underestimated, proving the difficulty in modelling the chaotic nature of oil splash systems. Moveover, [91] found in their research, that

when it comes to the modelling of the frame, the heat transfer coefficient must be measured; it is not easy to calculate it from geometry data

4.3.4 Limitations

There are a number of limitations in the experimental work. The limitation of lone working in the lab meant that the test rig was switched off before it had reached equilibrium, as it could not be left unattended. There were plans to allow the test rig to run for longer with help from a colleague, but this was cancelled as stated earlier (due to Covid lockdown). The lack of experimental data has meant that there is limited information to use to update the thermal model.

4.4 Conclusions

This chapter demonstrates the potential for thermal modelling to be used as a wind turbine gearbox condition monitoring tool by understanding changes in thermal behaviour. A "healthy" gearbox thermal model has been developed, modelling losses and heat transfer. The model was used to mimic a component fault. It was found that single temperature measurements cannot necessarily detect or locate faults, but potentially a combination of temperature measurements could be used together to identify a gearbox fault. The step up of an experimental data acquisition system was detailed, with information on equipment selection to meet the highest standard of data reliability as possible.

The thermal network model was one-way coupled. The calculated losses are irrespective of the temperature of the component. It could be argued that the temperature variations of a component will influence the losses generated. For example, churning losses will change as temperature changes due to the effect temperature has on fluid viscosity. Further work could add a feedback look whereby temperature is used as an input to potentially alter how a loss is calculated.

Moreover, the thermal model is steady state, as opposed to dynamic. To more accurately represent a WT, the transient nature of operation should be replicated. [93]

research used a wind regime as input and losses were calculated dynamically as the wind speed changed. [135] found that simulating deterministic non-steady events, there were important interactions between wind conditions, dynamics/timescales of the wind turbine controller, and the structural dynamics of the turbine itself that impacted main-bearing loads. Rapid main-bearing unloading and reloading events were observed for gusts in above-rated conditions. These loading conditions would filter through to the drivetrain and effect the losses and thermal behaviour. The NREL study [114] described previously, tested HS bearing under transient conditions (simulated braking, and grid loss events) and found these to have significant effects on loading, which would in term effect thermal behaviour. It could be argued these transient effects (wind gusting, or breaking) could be the root cause of a component failure whose condition was degrading. This could also be integrated into future thermal modelling research.

A limited amount of experimental data was collected from the test rig due to unforeseen circumstances; which had a knock-on effect of limiting the validation of the thermal model. The experimental data did show that the heat transfer between the oil splash and the casing is greater than modelled. This interaction may need a different approach to thermal modelling.

Chapter 5

Combination of thermal modelling and machine learning approaches for fault detection

5.1 Introduction

Temperature has historically been a used as a proxy for gearbox health. However, internal and external environment and machine conditions can influence temperature measurements, so by analysing the evolution of temperature, it is important to note whether the increased temperature is from a fault, or from higher load. This is why temperature differences due to faults are not always visible through temperature trends alone.

Research using temperature SCADA data for fault detection or remaining useful life (RUL) predictions have briefly been discussed in Section 2.3.5 and Section 2.3.6. Research which applied machine learning methods to SCADA data for this purpose, will now be discussed in more detail. [136] used a regression tree ensemble model with three SCADA input parameters: power, rotor speed and nacelle temperature, along with a component temperature, to wind farm data spanning multiple years. The predicted component temperature could be calculated, which could then be compared to the actual temperature. Applied to a population of 6 turbines, the results of this research

provide a method which can help the operator to identify problematic components over time.

[137] used artificial neural networks to provide the most accurate failure and RUL prediction out of three machine learning techniques trialed. Demonstrates that SCADA data can be used to predict failure up to a month before it occurs, and high frequency vibration data can be used to extend that accurate prediction capability to 5 to 6 months before failure. This paper demonstrates that two class neural networks can correctly predict gearbox failures between 72.5% and 75% of the time depending on the failure mode when trained with SCADA.

[138] applied a convolutional neural network to a fleet of eight WTs monitored for over 11 years, to evaluate the suitability of SCADA-based condition monitoring for fault diagnosis. A weakly supervised (limited information) method was used to model the normal behaviour of the turbine component. The method, instantiated as a threshold-based method, proved to be suitable for diagnosis, however, with a wide variability between the detection time and the fault is observed, suggests its limited suitability for prognosis.

[139] describes black-box models applied solely on SCADA data as useful for diagnosing wind turbine drivetrain faults; however, further developments are required regarding the precise fault location and prognosis. They state that combining normal-behaviour modelling with a physics-based mode, provides a powerful indication of how much information the purely black-box models are missing. This is in reference to the published work from this chapter [140].

This chapter will apply the methods of three different approaches used to analyse SCADA temperature data, one based on physical modelling, the other, using machine learning techniques and the last combining the physical model and machine learning approach through feature engineering. The results from these three approaches will be compared to see if they provide a better understanding of how the thermal behaviour of a gearbox is affected by a fault, and if temperature data can reliably be used for fault detection. The high level process can be seen in Figure 5.1.

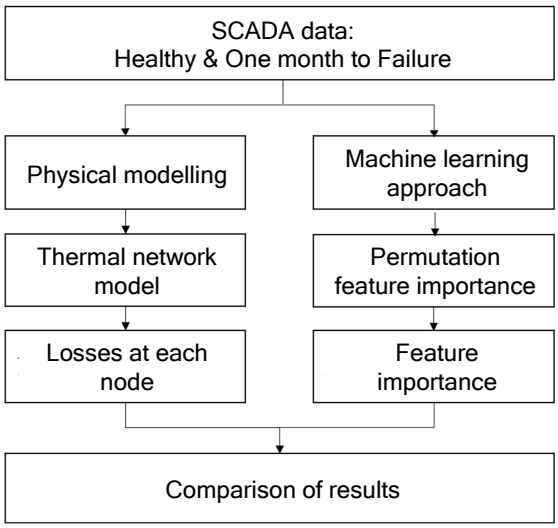

Figure 5.1: High level methodology

This research is based on analysing SCADA data from multi MW, utility scale WTs. In this study datasets from two test cases are used, the test cases are from commercial operational WTs, each case features the same sensor configuration and failure mode. The number and location of temperature sensors dictates the number and location of nodes to be used in the model, and based on this the heat transfer between nodes can be deduced.

For each dataset, SCADA data is available for when the turbine is considered "healthy" (one year from failure), and when the turbine is one month before failure (1M2F). The SCADA data is pre-processed prior to analysis. This took the form of separating out relevant temperature data from the rest of the SCADA data. Data points where the power was recorded as below zero, and any anomalous data points were removed. The power curves of the turbines were compared for healthy and 1M2F, to check for de-rating or other power curve deviations so that the same turbine could be compared for healthy and with fault, as shown in Figure 5.2.

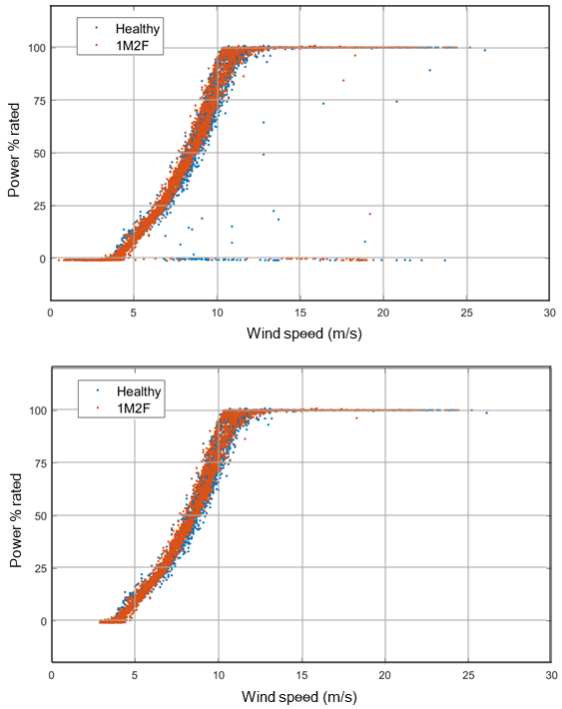

Figure 5.2: Power curve data cleaning

Dataset 1 includes a number of turbines of the same type, that all share the same failure mode. Dataset 2 includes a number of turbines of the same type which differ from those of dataset 1. They share a common failure, different from dataset 1. This allowed for different types of gearboxes to be modelled with different failure modes. This is summarized in Table 5.1.

All the gearboxes had a conventional set up for multi MW WT, 3-stages, two planetary and one parallel.

	Dataset 1	Dataset 2
Number of turbines	5	6
Fault location	HS bearing	Planetary bearing
Sensor locations	IMS bearing (IMS) HS bearing (HSA) HS bearing (HSB) HS bearing (HSC) Oil inlet	HS rotor end (HSrtr) HS mid (HSmid) HS generator end (HSgen) HS-lower speed shaft rotor end (Hlwrtr) HS-lower speed shaft generator end (Hlwgen) Oil inlet

Table 5.1: Summary of data sets

Research questions:

- Can a thermal model be applied to SCADA data and be used to detect gearbox failures?
- Does the efficacy depend on the number (and spread) of temperature measurement nodes?

The novelty of this research stems from:

- Applying a thermal network modelling approach to a WT gearbox failure identification using real word data.
- Comparing the output of thermal network modelling with temperature measurements to determine what has the greatest effect on gearbox health classification.
- Using and combining both physical modelling and machine learning approach through feature engineering to improve understanding of WT gearbox thermal behaviour for failure prediction

5.2 Thermal network modelling

The inverse of previous chapter, using temperature to estimate losses. Thermal network modelling has the potential to estimate the heat losses generated within the gearbox, using available SCADA data and engineering drawings. This was carried out using a dataset from a turbine that is healthy and a dataset from the same turbine, that is

known to be one month before a gearbox component failure. The estimated losses can then be compared to see if it could successfully identify a fault, as demonstrated by Figure 5.3.

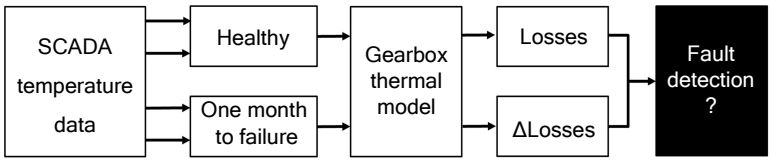

Figure 5.3: Thermal modelling approach

5.2.1 Methodology

The gearbox components are split into a number of lumped mass isothermal nodes, and an energy balance is applied to each node, assuming steady state conditions, shown in 5.1 [141].

$$\sum Q_{in} + \sum Q_{out} = 0 \tag{5.1}$$

Where Q_{in} is any heat energy generated at the node, for example, from friction. Q_{out} is heat moving away from the node via heat transfer. Q is a function of temperature difference (ΔT) and thermal resistance between two nodes, as shown in 5.2. Thermal resistance R_{a-b} is characterised by the type of heat transfer- conduction (5.3) or convection (5.5) [**?**]. Where A and L are related to component geometry, k and h are heat transfer properties.

$$Q_{a-b} = \frac{(T_a - T_b)}{R_{a-b}} \tag{5.2}$$

$$R_{conduction} = \frac{L}{A \times k} \tag{5.3}$$

$$R_{convection} = \frac{1}{A \times h} \tag{5.4}$$

Figure 5.4 shows the process of thermal modelling, general to all gearbox applications.

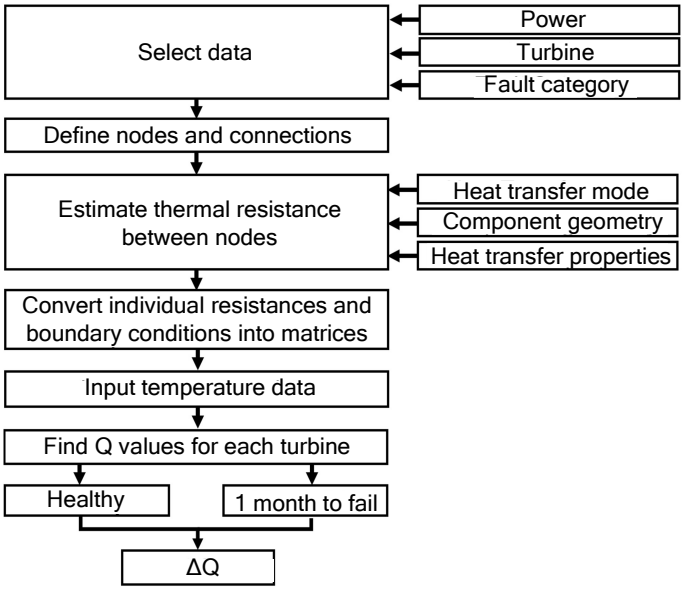

Figure 5.4: TNM methodology flowchart

A thermal network diagram for an example gearbox is shown in Figure 5.5, where gearbox components are connected by the thermal resistances.

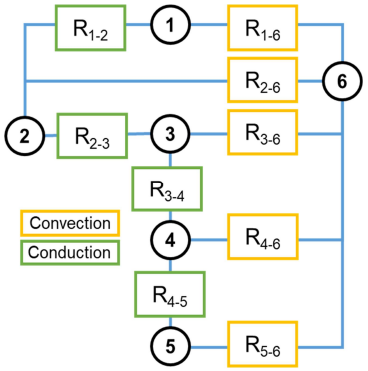

Figure 5.5: Thermal network model of gearbox for dataset 1

Sensor number	Location (node)
1	LS main bearing
2	IMS bearing (IMS)
3	HS bearing A (HSA)
4	HS bearing B (HSB)
5	HS bearing C (HSC)
6	Oil inlet

Table 5.2: Dataset 1 gearbox node labels

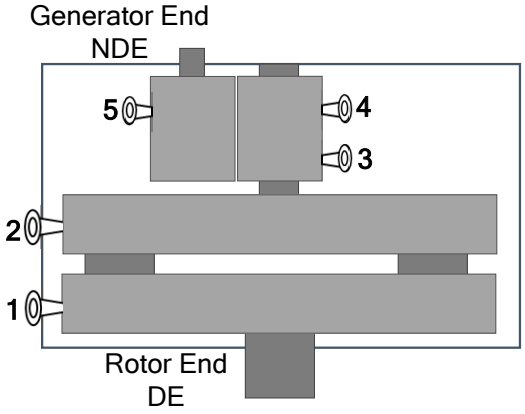

Figure 5.6: Thermal network model of gearbox for dataset 1

Carrying out an energy balance on each node results in a number of simultaneous equations as shown by 5.5 - 5.9 [140], where C is the inverse of the calculated resistances. Arranging these equations into simultaneous equations gives the following for each node.

$$\textbf{Node 1: } Q_1 + T_6 C_{1-6} = T_1(C_{1-2} + C_{1-6}) - T_2 C_{1-2} \tag{5.5}$$

$$\textbf{Node 2: } Q_2 + T_6 C_{2-6} = -T_1 C_{1-2} + T_2(C_{1-2} + C_{2-3} + C_{2-4} + C_{2-6}) - T_3 C_{2-3} - T_4 C_{2-4} \tag{5.6}$$

$$\textbf{Node 3: } Q_3 + T_6 C_{2-6} = -T_2 C_{2-3} + T_3(C_{2-3} + C_{3-4} + C_{3-6}) - T_4 C_{3-4} \tag{5.7}$$

$$\textbf{Node 4: } Q_4 + T_6 C_{4-6} = -T_3 C_{3-4} + T_4(C_{3-4} + C_{2-4} + C_{4-5} + C_{4-6}) - T_2 C_{2-4} - T_5 C_{4-5} \tag{5.8}$$

$$\textbf{Node 5: } Q_5 + T_6 C_{5-6} = -T_4 C_{4-5} + T_5(C_{4-5} + C_{5-6}) \tag{5.9}$$

Node 6, the oil inlet, is treated as independent from the other nodes as its temperature is not affected by the temperature changes of the other nodes. This is because it is just after the oil has been through the heat exchanger to cool, and it is assumed that the auxiliary cooling system keeps the oil at a set temperature. These simultaneous equations can be rearranged into matrix form and solved, using the temperature SCADA data as demonstrated by 5.10 [140].

$$\begin{bmatrix} T_1 \\ \vdots \\ T_n \end{bmatrix} \begin{bmatrix} (C_1 + C_2) & \cdots & -C_n \\ \vdots & \ddots & \vdots \\ -C_n & \cdots & (C_2 + C_n) \end{bmatrix} = \begin{bmatrix} Q_1 \\ \vdots \\ Q_n \end{bmatrix} \tag{5.10}$$

The thermal network model of dataset 2's gearbox configuration is shown in Figure 5.7, with Figure 5.8 and Table 5.3 showing the node locations. The sensor placement is based on assumptions made from limited engineering drawings and information from the OEM. These assumptions are best estimates, sensitivity analysis could be done to determine the impact of the assumptions. Sensors are usually RTD sensors (PT100), with a threaded probe which is inserted into the gearbox wall.

For all turbines in dataset 1, the temperature sensors were located at the fault location. For dataset 2, all turbines have suffered with an IMS planetary bearing fault,

but the gearbox configuration meant that the sensors were only located at the HS stage, not at the fault location, as is dataset 1. This will allow us to see if the method works when there are multiple heat transfer mechanisms in between the sensors and a fault.

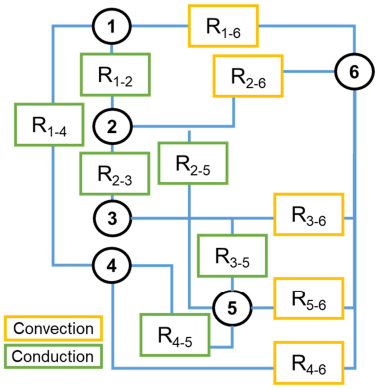

Figure 5.7: Thermal network model of gearbox for dataset 2

Sensor number	Location (node)
1	HS rotor end (HSrtr)
2	HS mid (HSmid)
3	HS generator end (HSgen)
4	HS low speed shaft rotor end (Hlwrtr)
5	HS low speed shaft generator end (Hlwgen)
6	Oil inlet

Table 5.3: Dataset 2 gearbox node labels

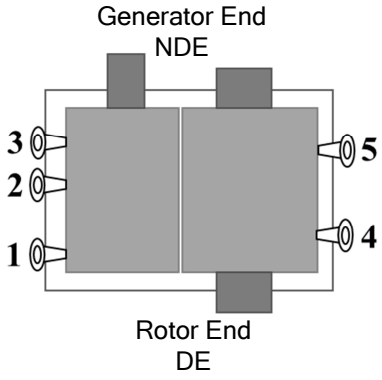

Figure 5.8: Schematic of gearbox HS end with sensor locations

5.2.2 Results

Dataset 1

Dataset 1 is a group of turbines of the same type that have a suffered a HS bearing failure. The losses for each turbine is calculated when it it considered healthy, and again using the data that is one month before the HS bearing failure (1M2F). To determine the change in losses when the component is damaged, compared to when it is healthy, the difference is calculated, as shown in 5.11. The ΔQ values are plotted for each node, across all turbines, shown in Figure 5.9.

$$Q_{1M2F} - Q_{healthy} = \Delta Q \tag{5.11}$$

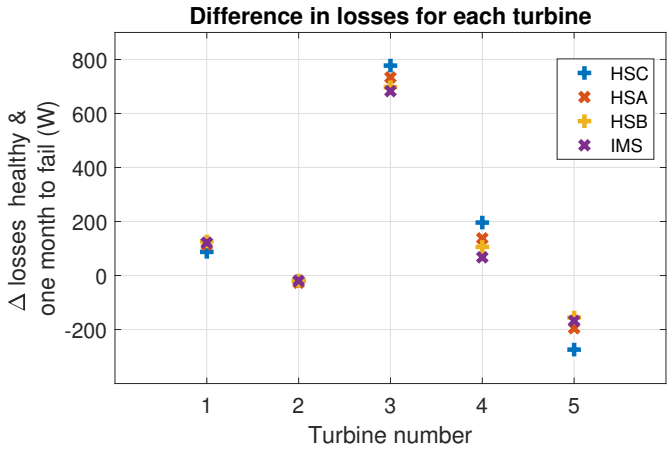

Figure 5.9: Dataset 1 thermal network model results

Based on the thermal modelling a difference in losses between the healthy data and 1M2F data can be seen in three out of five cases. The negative difference in losses suggest that the healthy turbine generates higher losses than it does one month before failure, which is not as would be expected. Of the turbines with a positive difference in losses, HSC has the greatest difference for two out of three turbines.

Dataset 2

Figure 5.10 show the difference in mean calculated losses for healthy and one month to fail for each turbine in the dataset. The data modelling was carried out on the whole

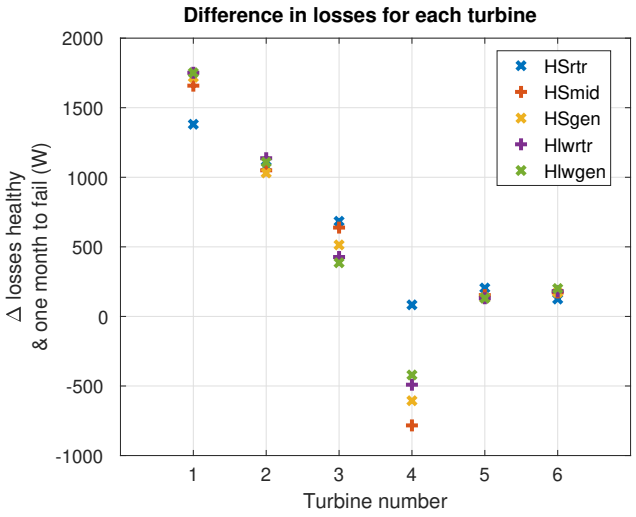

Figure 5.10: Dataset 2 thermal network model results

dataset initially. The results for dataset 2 show that the range of loss differential is much larger across the turbines than dataset 1, indicating that there may be factors in the data affecting the results, the most obvious factor being power, as power is a function of torque and rotational speed, and gearbox losses are also a function of torque and rotational speed. To explore this further the modelling was carried out on data split by power output, to see if it has an effect on the calculated losses, as shown by Figure 5.11 and Figure 5.12 for above and below rated power, respectively.

Figure 5.11 shows a much-reduced range in terms of difference in losses, giving more uniform results and in most cases, an increase in losses is shown for one month to failure. It can be seen that HSrtr has the highest change in losses for three out of six turbines and HSmid also has consistently high change in losses, suggesting these locations (HSrtr, HSmid) could be used to indicate fault. The difference in the losses between healthy and one month to failure with the planetary bearing are consistently less apparent than with the HS bearing fault. The results do show a difference in losses at one gearbox component or more.

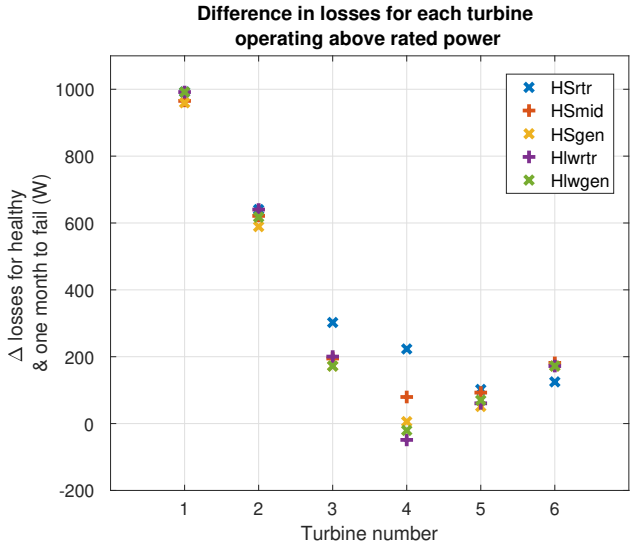

Figure 5.11: Dataset 2 thermal network model results - Above rated power

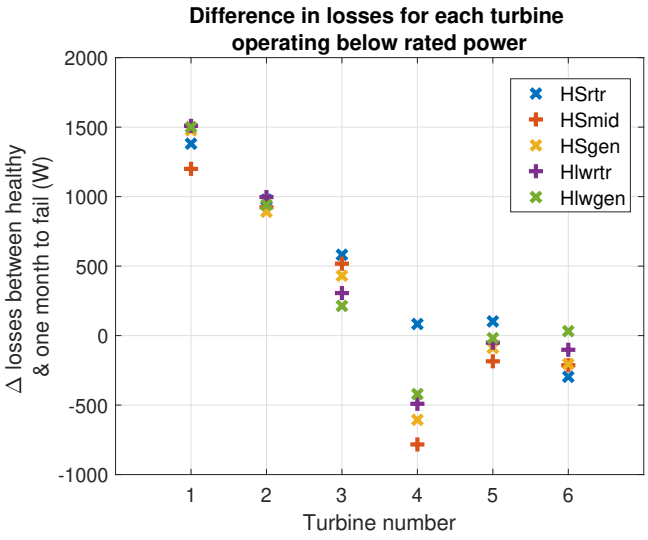

Figure 5.12: Dataset 2 thermal network model results - Below rated power

The difference in results between above rated and below rated data could be a result of the operating conditions. Above rated power sees fluctuations in torque, but rotational speed is maintained constant, whereas, below rated would see changes in torque and rotational speed to maintain optimal power output for a given wind speed.

By applying SCADA temperature data to the thermal model, a change in heat losses can be seen to an extent. This change is losses at component level can provide

an understand of how a fault can affect the thermal behaviour of a gearbox. It has been found that when the fault is located close to the sensor, the thermal model shows the change more clearly. To increase confidence in the model, a weighting analysis is carried out using machine learning techniques, to see if the results from the physical model align with purely data driven analysis.

5.3 Permutation feature importance

Weighting analysis is the form of permutation feature importance (PFI) was undertaken to provide an insight into how the input variables affect classification of the turbines in terms of healthy or one month to fail. In this case, to see which temperature sensors had the greatest effect on the classification.

5.3.1 Methodology

The PFI implementation steps followed are shown in Figure 5.14. A random forest classifier was used. Random forests are made up of a number of decision trees. Decision trees seek to find the best split to subset the data. Questions make up the decision nodes in the tree, acting as a means to split the data. Each question helps an individual to arrive at a final decision, which would be denoted by the leaf node. Observations that fit the criteria will follow the "Yes" branch and those that don't will follow the alternate path. Decision trees are common supervised learning algorithms, they can be prone to bias and overfitting [142]. However, when multiple decision trees form an ensemble in the random forest algorithm, they predict more accurate results. A depiction of a random forest algorithm is illustrated by Figure 5.13 adapted from [142]. For classification tasks, the output of the random forest is the class selected by most trees. Random forest algorithms have three main hyperparameters, which need to be set before training. These include node size, the number of trees, and the number of features sampled. A Bayesian optimization was used to optimise hyperparameter selection. The hyperparameter optimised the number of trees and the complexity (depth) of the trees in the forest [105] to eliminate over or under-fitting.

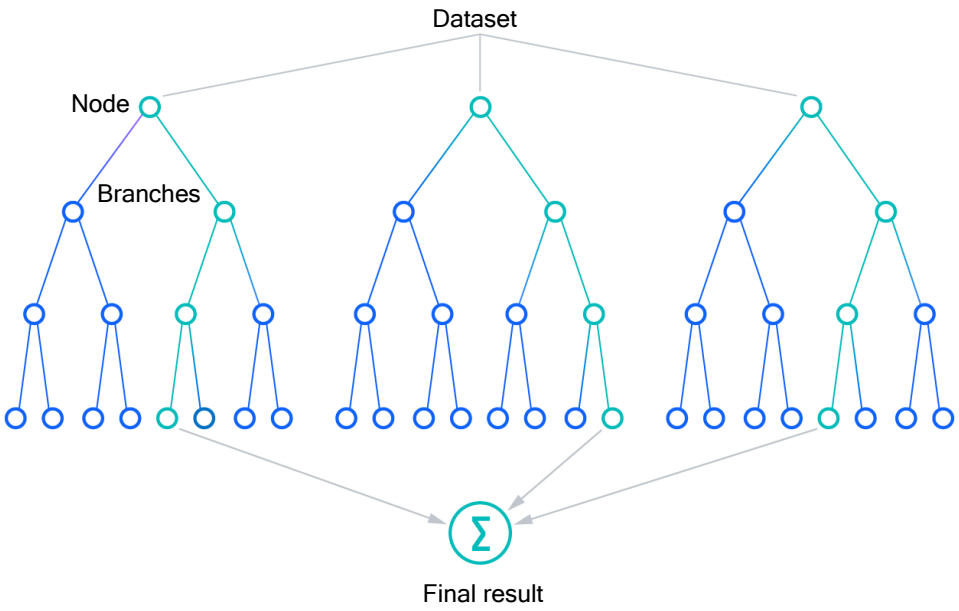

Figure 5.13: Random forest classifier

The random forest classifier is used in this method, as it can be used for evaluating the impact of each feature on the model's performance, providing insights into which features are most influential. As opposed to other classifiers which don't have this functionality, for example Naive Bayes classifier works on the assumption that each feature makes an independent and equal contribution to the outcome. Or Artificial Neural Network which it can be challenging to train and adjust, due to its complexity, and it often requires large amounts of training data.

Extracting feature importance through permutation estimates the value of how influential the predictor variables in the model are at predicting the response. The influence of a predictor increases with the value of this measure. If a predictor is influential in prediction, then permuting its values should affect the model error. If a predictor is not influential, then permuting its values should have little to no effect on the model error. In this application, the temperature node with the highest value, has the greatest effect on the classification outcome, and could be used to indicate if a

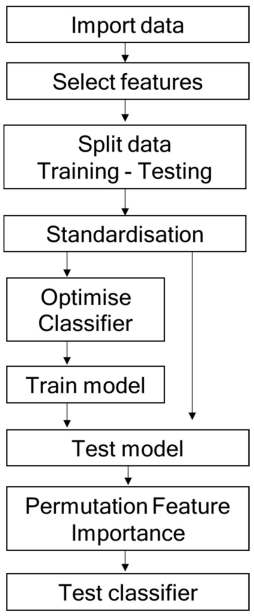

Figure 5.14: PFI process

gearbox is healthy or close to failure.

5.3.2 Results

Dataset 1

The PFI algorithm is run with the same data, as shown in Figure 5.15. The PFI of dataset yields HSC node as most important in most turbines, suggesting it is the location most effected by a HS fault. The results for dataset 1 suggests the thermal modelling can detect a fault one month before failure in the majority of turbines studied. The highest losses can be seen at a node in the same stage as the fault, HSC, this result is validated by the PFI confirming it most frequently has the highest feature importance for classification.

Dataset 2

The PFI model was applied to the turbine data to identify which variables had the greatest effect on the health classification, as with the thermal modelling, it was also split by power output, as shown in Figure 5.16 - 5.18.

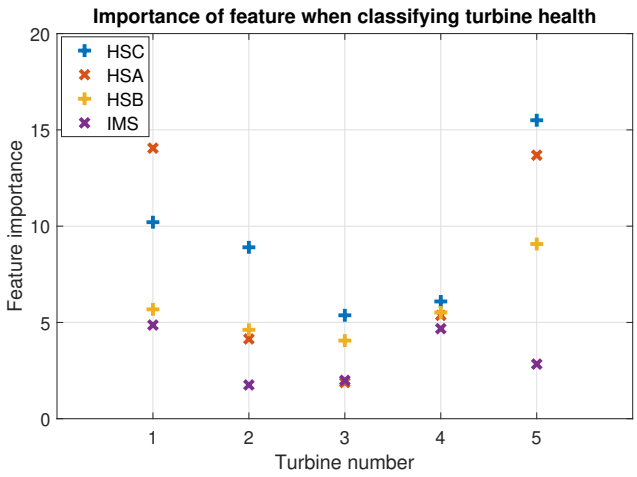

Figure 5.15: PFI results dataset 1

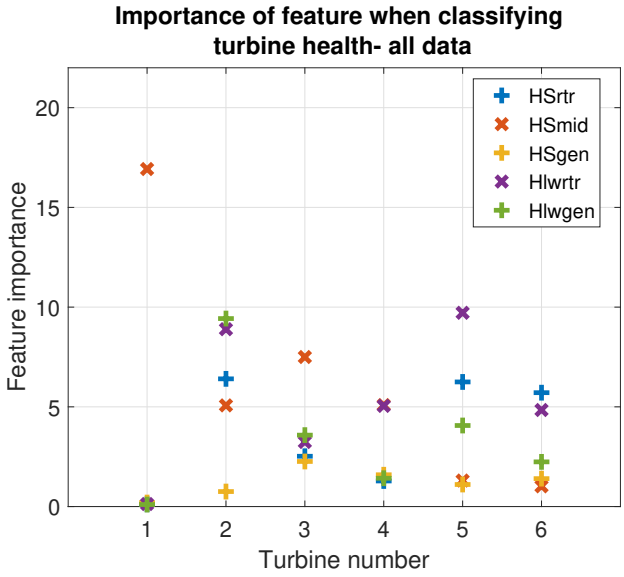

Figure 5.16: PFI results dataset 2 - all data

Contrary to dataset 1 PFI which showed the same node being the most important feature for all but one turbine, dataset 2 has weaker trends. It can be seen that HSmid and HSrtr appear as important features in some cases, but not significantly or consistently for different power level. The PFI analysis on dataset 2, does not give a clear indication of which variable has the greatest effect on classification and there is a

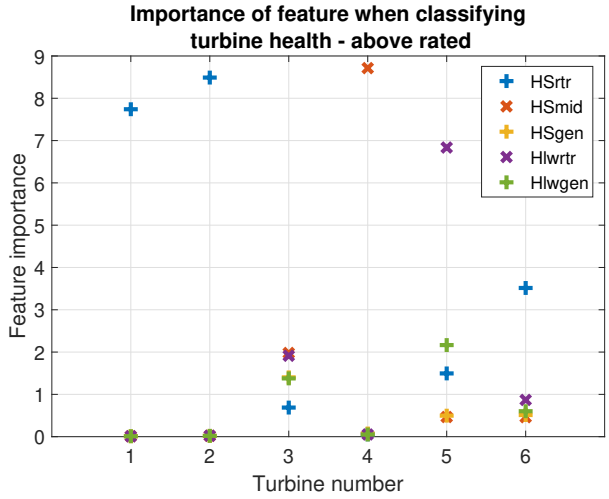

Figure 5.17: PFI results dataset 2 - above rated power

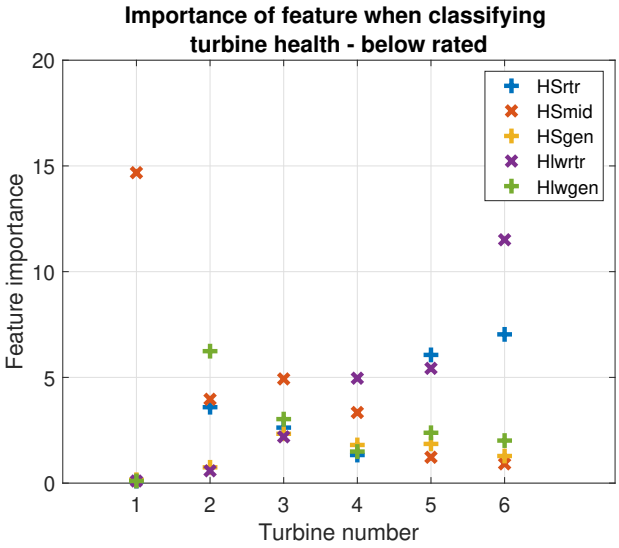

Figure 5.18: PFI results dataset 2 - below rated power

weak correlation between PFI and thermal modelling results. This could be explained by the difference in failure location, at the planetary stage and sensor locations, in the HS stage.

5.4 Combining thermal modelling and machine learning approach

To compare the effectiveness of thermal modelling for fault detection, the thermal loss data from the node with the greatest increase in losses one month to failure for each turbine is selected and added as a feature to the classification data set and the PFI algorithm is run.

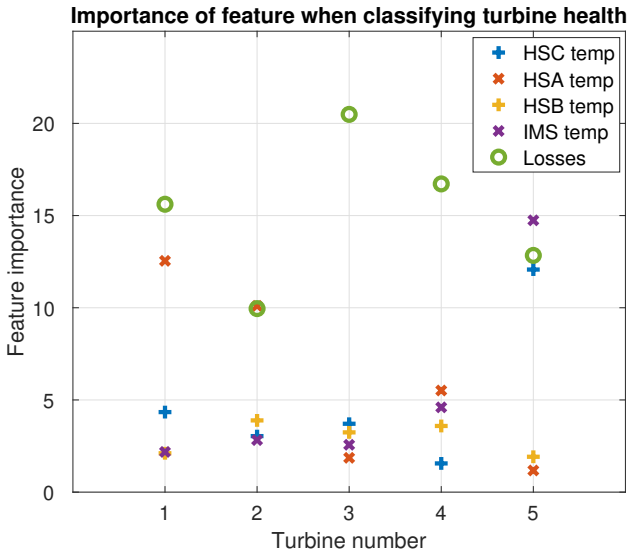

Figure 5.19: PFI results including thermal modelling losses dataset 1

The results are shown in Figure 5.19 and Figure 5.20 for dataset 1 and 2, respectively. These shows that the losses are the most important feature when determining classification for dataset 1, for turbine 3 the importance is significant. This suggests that differences between healthy and unhealthy gearboxes are clearer in the heat and power domain, than they are in the temperature domain. For dataset 2 the loss importance is not the same. The loss data is the most important for only 1 turbine, but scores highly for three of the five other turbines. The fact that the engineered feature based on losses becomes the most or one of the important features for a correct classification demonstrates the value of combining the thermal model approach with the machine learning approach through feature engineering.

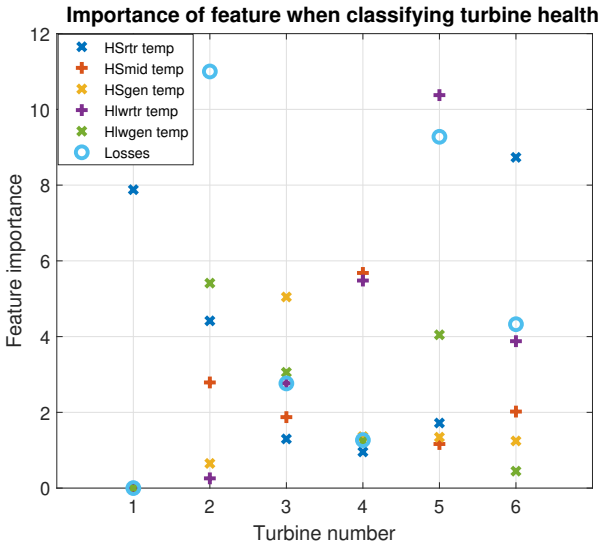

Figure 5.20: PFI results including thermal modelling losses dataset 2

5.5 Discussion

As the thermal modelling and PFI did not yield definitive results for dataset 2, there may be other factors influencing results. To briefly explore this, operational conditions were analysed to see if any patterns could be seen between conditions and simulation results.

5.5.1 Contribution of environmental conditions

From the available SCADA data, Weibull distribution for each turbine was plotted using the method outlined in [143]. Figure 5.21 shows T5 in dataset 1 having a narrow Weibull distribution, suggesting a low wind speed standard deviation so high probability for a single consistent wind speed. T5 behaved differently in all analyses. It was the only turbine in dataset 1 to have a detectable temperature difference between healthy and one month to failure,and showed a significant negative loss differential in the thermal modelling. These conditions could be affected by the operation of the cooling system as the thermal model accounted for cooling by including the temperature after the heat exchanger.

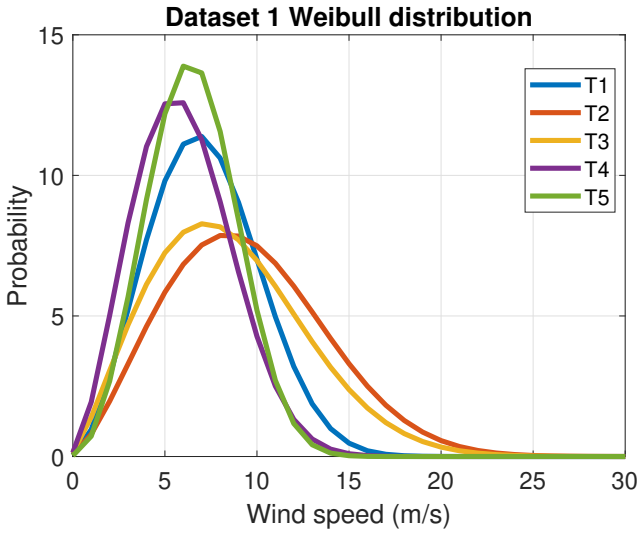

Figure 5.21: Weibull distribution of turbines in dataset 1

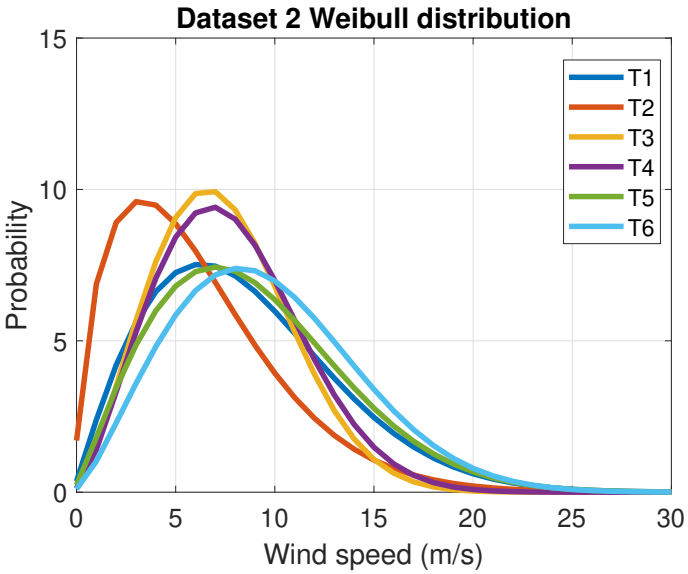

Figure 5.22: Weibull distribution of turbines in dataset 2

Figure 5.22 shows T1, T5 and T6 in dataset 2 have similar Weibull distribution and T5 and T6 have similar thermal model results. The Weibull distribution has a flatter curve, suggesting that there is similar probability of the turbine experiencing a wide range of wind speeds, but from the results of dataset 2 it is difficult to draw many similarities and conclusions.

5.6 Conclusions

The aim of this chapter was to use the thermal modelling theory explored in previous chapters, and apply it to real life SCADA data to see if it could be used to understand the behaviour of a wind turbine gearbox. Weighting analysis was used as a form of validation in terms of which temperature measures have the more impact on health classification.

The results of this research suggest that overall, when a fault is not obvious in a difference in temperature data, thermal modelling can detect a fault. For dataset 1, results from thermal network modelling were significantly more influential in turbine healthy classification.

Results show an agreement between thermal modelling and PFI to an extent, but this agreement seems to be impacted by the failure mode examined and the distance of sensors from the failure. The HS failure with sensors at the HS stage gave more agreeable results as opposed to the planetary failure, with sensors located only at the HS stage.

The two methods were then combined. The thermal loss data from the node with the greatest increase in losses one month to failure for each turbine is selected and added as a feature to the classification data set. It was found in many turbines that the losses were one of, or the most important classification feature suggesting differences between healthy and unhealthy gearboxes are clearer in the heat and power domain, than they are in the temperature domain. The fact that the engineered feature based on losses becomes the most or one of the important features for a correct classification demonstrates the value of combining the thermal model approach with the machine learning approach through feature engineering.

The results of the thermal modelling and PFI were reconciled with wind speed data to explore if environmental conditions impacted the results. Further work could be undertaken to explore other environmental or operational conditions to determine if they have an effect on the results of the thermal network modelling.

Machine learning could be used to calibrate the thermal model from Chapter 4

to improve model accuracy by tuning parameters. This is particularly useful for parameters that were estimated with minimal information, for example, heat transfer coefficients. A supervised regression analysis could be done to learn the relationship between model parameters and observed temperatures. This could then be used for normal behaviour modelling, as a baseline "healthy" model to compare real world data to, as described in Figure 5.3.

The application of this theory has the potential to set condition monitoring threshold values for operational WT gearboxes, by applying thermal modelling and gearbox power loss calculations for a healthy gearbox. This would be applied to gearboxes of different configurations, without the need for historical operational data and failure history.The application of this theory has the potential to set condition monitoring threshold values for operational WT gearboxes, by applying thermal modelling and gearbox power loss calculations for a healthy gearbox. This would be applied to gearboxes of different configurations, without the need for historical operational data and failure history. This could be particularly useful for newly installed WTs, which can be known to suffer gearbox failures shortly after commissioning, with no warning. Otherwise, the operator must wait 3-6 months for enough data to produce black box machine learning models. Additionally, the approach outlined in this paper allows for new high weight features to be engineered through thermal modelling for data driven failure prediction using classification.

Chapter 6

Conclusions

The conclusions of each chapter will be explored in relation to the research questions identified previously. Based on this, further work will be outlined. Overall thesis conclusions will then be drawn.

6.1 Conclusions from Chapter 2

Aim of the literature review is to explore the general topic of WT operation & maintenance in relation to reliability and ways in which it can be improved through predictive maintenance strategies.

The literature review of reliability studies found a general consensus that gearbox have a significant effect on WT reliability, in terms of frequency and downtime. Existing research in this area explores the effect of the wind regime on the gearbox. There is limited research on the effects of interaction with the downstream topology (generator, power converter and the grid). Using reliability data to understand where the failures occur is important, to develop condition monitoring techniques that can target these problematic components, to improve reliability.

Existing condition monitoring techniques, such as vibration, electrical signal analysis and SCADA data analysis were explored in terms of methodology and accuracy in fault detection among other benefits and drawbacks. Data driven machine learning approaches rely heavily on historical data and failure history information. An alterna-

tive to this is thermal modelling, most existing research is from a purely tribological perspective, with minimal application being made to WT gearboxes. The findings from the literature review helps shape the direction and novelty of the research in this thesis

6.2 Conclusions from Chapter 3

The research in this chapter applies a similar methodology as a high impact paper [32], using a large data population to explore reliability of WT gearboxes in relation to the downstream power train configuration.

6.2.1 Research Question 1: Does the choice of generator and converter influence gearbox reliability?

The results of the reliability analysis found that the DFIG PRC WT configuration experiences greater gearbox failure rates per turbine per year, incur higher costs and have a longer repair time than the gearbox in the PMG FRC WT configuration. These metrics suggest that the choice in generator does influence gearbox reliability

6.2.2 Research Question 2: If so, how is this manifested at component/fault type level?

The failure locations are similar for both configurations, with the exception of the PMG FRC experienced HS failures. HS failures are usually replaced in isolation, whereas this research was only categorising major replacement failure, suggesting the HS failures are catastrophic.

6.2.3 Research Question 3: Are there operational factors that can influence gearbox reliability?

It was hypothesised that the high rate of failure of DFIG PRC WT gearboxes can be attributed to the operating conditions it experiences as a result of being partially connected to the grid, and not fully decoupled, as the PMG FRC WT is, which puts more loading up through the gearbox. This could be a consideration in project planning

when choosing a WT technology, if the site is located near to known grid congestion regions which could result in regular grid curtailment.

6.2.4 Further work

Further work could use the same method, but researching major repair and even minor repair, to see if a similar trend is seen. This would be interesting, especially if repair costs could factored in distance from shore in, as frequent trips offshore could prove as significant as a single major replacement.

As detailed in the respective chapter, it would appear that the operation of the gearbox and generator can affect the reliability of one another. The connecting and disconnecting of the generator creates torque reversals and bouncing effects along the shaft. However, [114] investigated the effect operational misalignment due to rotor moments and induced generator misalignment on the bearing loads. Neither changed the loads appreciably compared with pure-torque conditions; thus, it is not likely that rotor moments and generator misalignment are drivers of axial cracking in wind turbine gearbox bearings. As this is one of the only studies that has investigated the effect of this operating condition on bearing strain, it is difficult to corroborate or disprove. This shows that further research is needed that can connect findings from reliability analysis and tribological investigations.

6.3 Conclusions from Chapter 4

A 'healthy' gearbox thermal model has been developed, modelling losses and heat transfer. The model was used to mimic a component fault to see how the thermal behaviour of the gearbox changed. The gearbox test rig was set up to collect temperature data when running.

6.3.1 Research Question 1: Can a wind turbine gearbox thermal model imitate the thermal behaviour of a real life gearbox?

To determine if the thermal model can imitate a real life gearbox, experimental validation is needed. A limited amount of experimental data was collected from the test rig due to unforeseen circumstances; this had a knock-on effect of limiting the validation of the thermal model. The experimental data did show a generally agreement of temperature outputs with the exception, that the heat transfer between the oil splash and the casing is greater than modelled.This was shown by the difference in time taken to reach thermal equilibrium. The test rig took longer than the model. This was identified as the oil splash from thermal imaging photographs taken, which show the gearbox casing reaching higher temperatures than expected. This interaction may need a different approach to thermal modelling.

Therefore, it can be answered that a thermal model can imitate the thermal behaviour of a real-life gearbox to an extent, with the exception of the heat transfer between the oil splash and casing being underestimated by the model. These complex interactions are difficult to be modelled accurately.

6.3.2 Research Question 2: Can a thermal model be used to detect and locate gearbox failures?

The model was used to mimic a component fault by adding additional heat to a component and reviewing how this heat propagated through the gearbox. It was found that single temperature measurements cannot necessarily detect or locate faults, but potentially a combination of temperature measurements could be used together to identify a gearbox fault. This chapter demonstrates the potential for thermal modelling to be used as a wind turbine gearbox condition monitoring tool by understanding changes in thermal behaviour.

6.3.3 Further work

Further work which would improve the confidence in the thermal model, would be to carry out more experimental validation. Running the gearbox with a range of operating

conditions, varying the torque and the speed. This may provide better insight to the oil splash heat transfer.

Additional experimental validation could be carried out on a gearbox with a planetary stage which could potentially allow the application to more complex gearbox configurations. Particularly as there is limited existing experimental research applied to planetary gearboxes. This would be highly relevant to utility scale WT gearboxes.

6.4 Conclusions from Chapter 5

This chapter uses a reverse of thermal modelling method applied in previous chapter. Temperature data is used as the input which generates heat energy as the output. The data used is from a turbine classified as healthy and then the same turbine classified as one month to failure. The comparison of these two datasets determined if a thermal modelling approach can be used to detect gearbox failures. It was applied to a real life utility scale gearbox. As an experimental validation of the thermal model is not possible, a weighting analysis (PFI) was used as a form of validation. This can determine which temperature measurements indicate changes between healthy and one month to failure, using a data driven method.

6.4.1 Research Question 1: Can a thermal model be applied to SCADA data and be used to detect gearbox failures?

The results of this research suggest that overall, when a fault is not obvious from trending temperature data, thermal modelling could detect a fault. For dataset 1, results from thermal network modelling were significantly more influential in turbine healthy classification. Results show an agreement between thermal modelling and PFI to an extent. The quality of the thermal model depends on the gearbox specifications available, for example, dimensions and material of components.

6.4.2 Research Question 2: Does the efficacy depend on the number (and spread) of temperature measurement nodes?

The efficacy of the thermal model, and its agreement with the PFI results seems to be impacted by the failure mode examined and the distance of sensors from the failure. The HS failure with sensors at the HS stage gave more agreeable results as opposed to the planetary failure, with sensors located only at the HS stage. The results of the thermal modelling and PFI were reconciled with wind speed data to explore if environmental conditions impacted the results.

6.4.3 Further work

This thermal modelling approach could be applied to other gearboxes of different configurations, to test the efficacy of the approach as an alternative to purely data driven analysis. Further work could be undertaken to explore other environmental or operational conditions to determine if they have an effect on the results of the thermal network modelling.

The application of this theory has the potential to set condition monitoring threshold values for operational WT gearboxes, by applying thermal modelling and gearbox power loss calculations for a healthy gearbox. This would be applied to gearboxes of different configurations, without the need for historical operational data and failure history. Additionally, the approach outlined in this paper allows for new high weight features to be engineered through thermal modelling for data driven failure prediction using classification.

The sensor placement is based on assumptions made from limited engineering drawings and information from the OEM. These assumptions are best estimates. Further work could be to conduct a sensitivity analysis to determine the impact of the assumptions. Alternative sensing technologies could be explored. For example, fibre optic sensors. They use optical fibres—thin strands of glass or plastic Light travels through the fibre, and when external conditions (like strain or temperature) change the fibre's properties, the light's characteristics (wavelength, intensity, etc.) are altered. These changes are detected and interpreted by photodetectors or interrogators. Intrinsic sen-

sors such as Fiber Bragg Grating (FBG) sensors, where the fibre reacts to strain or temperature or Distributed Temperature Sensing (DTS) which are long fibres can monitor temperature along their entire length. Extrinsic sensors transmit light to and from an external sensing element. Fibre optic sensors have advantages such as being immune to electromagnetic interference, lightweight and small, capable of remote sensing and can withstand harsh environments (corrosion, temperature, etc.). However, the drawbacks are that fibres must be ruggedized and protected from oil and mechanical wear. They are more expensive than basic thermocouples or strain gauges and they need specialized equipment to read the signals [144].

With unstable wholesale electricity prices and WF subsidies being phased out, there should be more focus on improving WT reliability to maintain utility scale WF development. The quality of the sensing could play a significant role in this to improve the efficacy of condition monitoring.

6.5 Overall thesis conclusions

Research Question: How can thermal modelling of a wind turbine gearbox be used for condition monitoring and fault detection to improve reliability?

This research brings together theoretical thermal modelling, experimental research, and machine learning data analysis applied specifically for WT gearbox condition monitoring. The results shown that the application of this theory has the potential to set condition monitoring threshold values for operational WT gearboxes, by applying thermal modelling and gearbox power loss calculations for a healthy gearbox. This could be applied to gearboxes of different configurations, without the need for historical operational data and failure history. The research has shown that the efficacy of detecting failures in different parts of the gearbox, would be dependent on temperature sensor locations in the gearbox.

Thermal modelling of a wind turbine gearbox has the potential to be combined with machine learning methods through feature engineering, to produce a more accurate condition monitoring system than when applied individually. This would mean potential gearbox failures can be identified ahead of time, avoiding unexpected failure and the resulting downtime, improving WT reliability and reducing O&M costs.

The results of this research has outlined the importance of appreciating that a WT operates as number of interdependent components, the operation of which can affect the system up and down stream. To improve reliability, components cannot be considered isolation.

Appendix A

Gearbox Specifications

Appendix A. Gearbox Specifications

This figure has been removed for copyright reasons

Appendix A. Gearbox Specifications

This figure has been removed for copyright reasons

Appendix A. Gearbox Specifications

This figure has been removed for copyright reasons

Appendix A. Gearbox Specifications

This figure has been removed for copyright reasons

Appendix A. Gearbox Specifications

This figure has been removed for copyright reasons

Appendix A. Gearbox Specifications

This figure has been removed for copyright reasons

Appendix A. Gearbox Specifications

This figure has been removed for copyright reasons

Appendix B

Data Acquisition equipment specifications

Appendix B. Data Acquisition equipment specifications

This figure has been removed for copyright reasons

Appendix B. Data Acquisition equipment specifications

This figure has been removed for copyright reasons

Appendix B. Data Acquisition equipment specifications

This figure has been removed for copyright reasons

Appendix B. Data Acquisition equipment specifications

This figure has been removed for copyright reasons

Bibliography

[1] "What is climate change? - met office." https://www.metoffice.gov.uk/weather/climate-change/what-is-climate-change. Accessed: Oct. 07, 2020 [Online].

[2] "Climate action – united nations sustainable development." https://www.un.org/sustainabledevelopment/climate-action/. Accessed: Oct. 07, 2020 [Online].

[3] WorldEnergyCouncil, "World energy trilemma index." www.worldenergy.org. Accessed: Apr. 08, 202 [Online].

[4] "Renewable energy directive — energy." https://ec.europa.eu/energy/en/topics/renewable-energy/renewable-energy-directive/overview. Accessed Nov. 21, 2019 [Online].

[5] IEA, "World energy outlook." https://www.iea.org/weo/. Accessed: Oct. 15, 2018 [Online].

[6] IEA, "Installed power generation capacity by source in the stated policies scenario, 2000-2040." https://www.iea.org/data-and-statistics/charts/installed-power-generation-capacity-by-source-in-the-stated-policies-scenario-2
Accessed: May 05, 2020 [Online].

[7] M. Liebreich, "London summit 2017 breaking clean." https://data.bloomberglp.com/professional/sites/24/2017/09/BNEF-Summit-London-2017-Michael-Liebreich-State-of-the-Industry.pdf. Accessed: Oct. 07, 2020 [Online].

[8] J. Serrano-González and R. Lacal-Arántegui, "Technological evolution of onshore wind turbines—a market-based analysis," *Wind Energy*, vol. 19, pp. 2171–2187, 12 2016.

[9] C. Nutakor, A. Kłodowski, J. Sopanen, A. Mikkola, and J. I. Pedrero, "Planetary gear sets power loss modeling: Application to wind turbines," *Tribology International*, vol. 105, pp. 42–54, 1 2017.

[10] V. L. Jantara and M. Papaelias, *Non-Destructive Testing and Condition Monitoring Techniques for Renewable Energy Industrial Assets*, ch. Wind turbine gearboxes: Failures, surface treatments and condition monitoring. Butterworth-Heinemann, 2020.

[11] Y. Feng, Y. Qiu, C. J. Crabtree, H. Long, and P. J. Tavner, "Monitoring wind turbine gearboxes," *Wind Energy*, vol. 16, pp. 728–740, 7 2013.

[12] C. S. Gray and S. J. Watson, "Physics of failure approach to wind turbine condition based maintenance," *Wind Energy*, vol. 13, pp. 395–405, 8 2009.

[13] C. Crabtree, Y. Feng, and P. Tavner, "Detecting incipient wind turbine gearbox failure: A signal analysis method for on-line condition monitoring," *European Wind Energy Conference*, 2010.

[14] S. McFadden and B. Basu, "Wind turbine gearbox design with drivetrain dynamic analysis," *Offshore Wind Farms: Technologies, Design and Operation*, pp. 137–158, 3 2016.

[15] C. Chen and J. Chen, "Power analysis of two-dof epicyclic gear transmission and experimental validation," in *International Gear Conference 2014: 26th–28th August 2014, Lyon* (P. Velex, ed.), pp. 646–658, Oxford: Chandos Publishing, 2014.

[16] Z. Liu and L. Zhang, "A review of failure modes, condition monitoring and fault diagnosis methods for large-scale wind turbine bearings," *Measurement*, vol. 149, p. 107002, 2020.

[17] A. R. Nejad, Y. Guo, Z. Gao, and T. Moan, "Development of a 5 mw reference gearbox for offshore wind turbines," *Wind Energy*, vol. 19, pp. 1089–1106, 6 2016.

[18] E. Hart, B. Clarke, G. Nicholas, A. K. Amiri, J. Stirling, J. Carroll, R. Dwyer-Joyce, A. McDonald, and H. Long, "A review of wind turbine main bearings: Design, operation, modelling, damage mechanisms and fault detection," *Wind Energy Science*, vol. 5, pp. 105–124, 1 2020.

[19] M. I. Blanco, "The economics of wind energy," *Renewable and Sustainable Energy Reviews*, vol. 13, pp. 1372–1382, 2009.

[20] "Wind farm costs - guide to an offshore wind farm bvg associates." `https://guidetoanoffshorewindfarm.com/wind-farm-costs`. Accessed: Sep. 08, 2020. [Online].

[21] M. Rausand and A. Høyland, *System reliability theory : models, statistical methods, and applications*. Wiley-Interscience, 2004.

[22] DNV-GL, "Definitions of availability terms for the wind industry." `https://www.ourenergypolicy.org/wp-content/uploads/2017/08/Definitions-of-availability-terms-for-the-wind-industry-white-paper-09-08-2017.pdf`, 2017. Accessed: Oct. 12, 2020. [Online].

[23] J. Carroll, A. McDonald, and D. McMillan, "Failure rate, repair time and unscheduled o&m cost analysis of offshore wind turbines," *Wind Energy*, vol. 19, pp. 1107–1119, 6 2016.

[24] A. R. Nejad, Z. Gao, and T. Moan, "Fatigue reliability-based inspection and maintenance planning of gearbox components in wind turbine drivetrains," *Energy Procedia*, vol. 53, pp. 248–257, 2014. EERA DeepWind 2014, 11th Deep Sea Offshore Wind RD Conference.

[25] J. Nilsson and L. Bertling, "Maintenance management of wind power systems using condition monitoring systems—life cycle cost analysis for two case studies," *IEEE Transactions on Energy Conversion*, vol. 22, pp. 223–229, 3 2007.

[26] F. Spinato, P. J. Tavner, G. J. V. Bussel, and E. Koutoulakos, "Reliability of wind turbine subassemblies," *IET Renewable Power Generation*, vol. 3, pp. 387–401, 2009.

[27] S. Sheng and R. O'Connor, "Chapter 15 - reliability of wind turbines," in *Wind Energy Engineering* (T. M. Letcher, ed.), pp. 299–327, Academic Press, 2017.

[28] I. S. Al-Tubi and H. Long, "Prediction of wind turbine gear micropitting under variable load and speed conditions using iso/tr 15144-1: 2010," *Proceedings of the Institution of Mechanical Engineers, Part C: Journal of Mechanical Engineering Science*, vol. 227, pp. 1898–1914, 9 2013.

[29] NREL, "Report on wind turbine subsystem reliability - a survey of various databases." = https://www.nrel.gov/docs/fy13osti/59111.pdf, 2013. Accessed: Mar. 05, 2021. [Online].

[30] E. Artigao, S. Martín-Martínez, A. Honrubia-Escribano, and E. Gómez-Lázaro, "Wind turbine reliability: A comprehensive review towards effective condition monitoring development," *Applied Energy*, vol. 228, pp. 1569–1583, 10 2018.

[31] C. Dao, B. Kazemtabrizi, and C. Crabtree, "Wind turbine reliability data review and impacts on levelised cost of energy," *Wind Energy*, vol. 22, pp. 1848–1871, 12 2019.

[32] J. Carroll, A. McDonald, and D. McMillan, "Reliability comparison of wind turbines with dfig and pmg drive trains," *IEEE Transactions on Energy Conversion*, vol. 30, pp. 663–670, 6 2015.

[33] D. Cevasco, S. Koukoura, and A. J. Kolios, "Reliability, availability, maintainability data review for the identification of trends in offshore wind energy applications," *Renewable and Sustainable Energy Reviews*, vol. 136, 2 2021.

[34] U. Bhardwaj, A. Teixeira, and C. G. Soares, "Reliability prediction of an offshore wind turbine gearbox," *Renewable Energy*, vol. 141, pp. 693–706, 10 2019.

[35] G. Wilson, D. McMillan, and G. Ault, "Modelling the effects of the environment on wind turbine failure modes using neural networks," vol. 2012, pp. 42–42, Institution of Engineering and Technology, 2012.

[36] A. Dhanola and H. Garg, "Tribological challenges and advancements in wind turbine bearings: A review," *Engineering Failure Analysis*, vol. 118, p. 104885, 2020.

[37] A. R. Nejad, Z. Gao, and T. Moan, "On long-term fatigue damage and reliability analysis of gears under wind loads in offshore wind turbine drivetrains," *International Journal of Fatigue*, vol. 61, pp. 116–128, 4 2014.

[38] H. Al-Hamadani, T. An, M. King, and H. Long, "System dynamic modelling of three different wind turbine gearbox designs under transient loading conditions," *International Journal of Precision Engineering and Manufacturing*, vol. 18, pp. 1659–1668, 11 2017.

[39] V. L. Jantara and M. Papaelias, "Chapter 5 - wind turbine gearboxes: Failures, surface treatments and condition monitoring," in *Non-Destructive Testing and Condition Monitoring Techniques for Renewable Energy Industrial Assets* (M. Papaelias, F. P. G. Márquez, and A. Karyotakis, eds.), pp. 69–90, Boston: Butterworth-Heinemann, 2020.

[40] Y. Feng, Y. Qiu, C. Crabtree, H. Long, and P. Tavner, "Use of scada and cms signals for failure detection & diagnosis of a wind turbine gearbox," *European Wind Energy Conference and Exhibition 2011*, pp. 17–19, 01 2011.

[41] "Statistics — gearbox reliability database." `https://grd.nrel.gov/#/stats`. Accessed: Oct. 15, 2020. [Online].

[42] F. P. G. Márquez, J. M. P. Pérez, A. P. Marugán, and M. Papaelias, "Identification of critical components of wind turbines using fta over the time," *Renewable Energy*, vol. 87, pp. 869–883, 2016.

[43] NREL, "Gearbox typical failure modes, detection, and mitigation methods (presentation)." https://www.nrel.gov/docs/fy14osti/60982.pdf, 2014. Accessed: Aug. 14, 2018. [Online].

[44] H. D. M. de Azevedo, A. M. Araújo, and N. Bouchonneau, "A review of wind turbine bearing condition monitoring: State of the art and challenges," *Renewable and Sustainable Energy Reviews*, vol. 56, pp. 368–379, 4 2016.

[45] M. Nie and L. Wang, "Review of condition monitoring and fault diagnosis technologies for wind turbine gearbox," *Procedia CIRP*, vol. 11, pp. 287–290, 1 2013.

[46] "Premature bearing failures in wind gearboxes and white etching cracks." https://https://evolution.skf.com/premature-bearing-failures-in-wind-gearboxes-and-white-etching-cracks-wec/#. Accessed: Apr. 07, 2020 [Online].

[47] "Improving bearing life." https://www.timken.com/wp-content/uploads/2021/05/Timken-TDI-Bearings-White-Paper-Improving-Bearing-Life-in-Wind-Turbine-pdf. Accessed: Apr. 04, 2025 [Online].

[48] C. Zhou, M. Xing, H. Wang, and B. Hu, "A novel thermal network model for predicting the contact temperature of spur gears," *International Journal of Thermal Sciences*, vol. 161, p. 106703, 2021.

[49] A. Dyson, "Scuffing - a review," *Tribology International*, vol. 8, pp. 77–87, 1975.

[50] H. Long, A. Lord, D. Gethin, and B. Roylance, "Operating temperatures of oil-lubricated medium-speed gears: Numerical models and experimental results," *Proceedings of the Institution of Mechanical Engineers, Part G: Journal of Aerospace Engineering*, vol. 217, 02 2003.

[51] B.-R. Hoehn and K. Michaelis, "Influence of oil temperature on gear failures," *Tribology International - TRIBOL INT*, vol. 37, pp. 103–109, 02 2004.

[52] "Six factors affecting the life of a lubricant." https://www.stle.org/shared_content/end_users/lube_fundamentals/basics_of_lube_fundamentals_

articles_full/six_factors_affecting_the_life_of_a_lubricant.aspx. Accessed: Apr. 07, 2025 [Online].

[53] B. Graça, J. Castro, R. Martins, C. Fernandes, and J. Seabra, "Failure and oil analysis in wind turbine gearboxes," 11 2013.

[54] Y. Sinha, J. A. Steel, J. A. Andrawus, and K. Gibson, "Significance of effective lubrication in mitigating system failures — a wind turbine gearbox case study," *Wind Engineering*, vol. 38, no. 4, pp. 441–449, 2014.

[55] M. Wu, X. Han, Y. Tao, and J. Pei, "Lubrication reliability analysis of wind turbine main bearing in random wind field," *Tribology International*, vol. 179, p. 108181, 2023.

[56] A. Neurouth, C. Changenet, F. Ville, and A. Arnaudon, "Thermal modeling of a grease lubricated thrust ball bearing," *Proceedings of the Institution of Mechanical Engineers, Part J: Journal of Engineering Tribology*, vol. 228, no. 11, pp. 1266–1275, 2014.

[57] J. P. Salameh, S. Cauet, E. Etien, A. Sakout, and L. Rambault, "Gearbox condition monitoring in wind turbines: A review," *Mechanical Systems and Signal Processing*, vol. 111, pp. 251–264, 10 2018.

[58] T. Wang, Q. Han, F. Chu, and Z. Feng, "Vibration based condition monitoring and fault diagnosis of wind turbine planetary gearbox: A review," *Mechanical Systems and Signal Processing*, vol. 126, pp. 662–685, 7 2019.

[59] S. Koukoura, J. Carroll, and A. Mcdonald, "Wind turbine intelligent gear fault identification," PHM Society, 2017.

[60] P. Bangalore, S. Letzgus, D. Karlsson, and M. Patriksson, "An artificial neural network-based condition monitoring method for wind turbines, with application to the monitoring of the gearbox," *Wind Energy*, vol. 20, pp. 1421–1438, 8 2017.

[61] Y. Zhang, W. Lu, and F. Chu, "Planet gear fault localization for wind turbine gearbox using acoustic emission signals," *Renewable Energy*, vol. 109, pp. 449–460, 8 2017.

[62] A. Qu, D. He, J. Yoon, B. Hecke, E. Bechhoefer, and J. Zhu, "Gearbox tooth cut fault diagnostics using acoustic emission and vibration sensors - a comparative study," *Sensors (Basel, Switzerland)*, vol. 14, pp. 1372–93, 01 2014.

[63] F. Elasha, M. Greaves, D. Mba, and D. Fang, "A comparative study of the effectiveness of vibration and acoustic emission in diagnosing a defective bearing in a planetry gearbox," *Applied Acoustics*, vol. 115, pp. 181–195, 1 2017.

[64] Y. He, M. Li, Z. Meng, S. Chen, S. Huang, Y. Hu, and X. Zou, "An overview of acoustic emission inspection and monitoring technology in the key components of renewable energy systems," *Mechanical Systems and Signal Processing*, vol. 148, p. 107146, 2 2021.

[65] F. Cheng, L. Qu, W. Qiao, C. Wei, and L. Hao, "Fault diagnosis of wind turbine gearboxes based on dfig stator current envelope analysis," *IEEE Transactions on Sustainable Energy*, vol. 10, pp. 1044–1053, 7 2019.

[66] E. Artigao, S. Koukoura, A. Honrubia-Escribano, J. Carroll, A. McDonald, and E. Gómez-Lázaro, "Current signature and vibration analyses to diagnose an in-service wind turbine drive train," *Energies*, vol. 11, p. 960, 4 2018.

[67] G. Jiang, C. Jia, S. Nie, X. Wu, Q. He, and P. Xie, "Multiview enhanced fault diagnosis for wind turbine gearbox bearings with fusion of vibration and current signals," *Measurement*, vol. 196, p. 111159, 6 2022.

[68] S. Sheng, "Monitoring of wind turbine gearbox condition through oil and wear debris analysis: A full-scale testing perspective," *Tribology Transactions*, vol. 59, pp. 149–162, 1 2016.

[69] R. Golafshan, D. Verbeek, and S. Markert, "Development of an oil monitoring and filtration system for industrial gearboxes," 05 2023.

[70] M. Fox, *The Degradation of Lubricants in Service Use*, pp. 2–1. 10 2008.

[71] NREL, "Wind turbine drivetrain condition monitoring - an overview (presentation)." `https://www.nrel.gov/docs/fy13osti/58774.pdf`, 2013. Accessed: May 22, 2019. [Online].

[72] A. Zaher, S. McArthur, D. Infield, and Y. Patel, "Online wind turbine fault detection through automated scada data analysis," *Wind Energy*, vol. 12, pp. 574–593, 9 2009.

[73] D. Astolfi, F. Castellani, and L. Terzi, "Fault prevention and diagnosis through scada temperature data analysis of an onshore wind farm," *Diagnostyka*, vol. 15, 2014.

[74] T. Touret, C. Changenet, F. Ville, M. Lalmi, and S. Becquerelle, "On the use of temperature for online condition monitoring of geared systems – a review," *Mechanical Systems and Signal Processing*, vol. 101, pp. 197–210, 2 2018.

[75] A. Verma, D. Zappalá, S. Sheng, and S. J. Watson, "Wind turbine gearbox fault prognosis using high-frequency scada data," *Journal of Physics: Conference Series*, vol. 2265, 2022.

[76] J. Tautz-Weinert and S. Watson, "Using scada data for wind turbine condition monitoring - a review," *IET Renewable Power Generation*, vol. 11, pp. 382–394, 03 2017.

[77] M. Schlechtingen and I. F. Santos, "Comparative analysis of neural network and regression based condition monitoring approaches for wind turbine fault detection," *Mechanical Systems and Signal Processing*, vol. 25, pp. 1849–1875, 7 2011.

[78] Z.-Y. Zhang and K.-S. Wang, "Wind turbine fault detection based on scada data analysis using ann," *Advances in Manufacturing*, vol. 2, pp. 70–78, 3 2014.

[79] X. Xu, X. Huang, H. Bian, J. Wu, C. Liang, and F. Cong, "Total process of fault diagnosis for wind turbine gearbox, from the perspective of combination

with feature extraction and machine learning: A review," *Energy and AI*, vol. 15, p. 100318, 1 2024.

[80] D. Ferguson, A. McDonald, J. Carroll, and H. Lee, "Standardisation of wind turbine scada data for gearbox fault detection," *The Journal of Engineering*, vol. 2019, pp. 5147–5151, 7 2019.

[81] Y. Qiu, Y. Feng, J. Sun, W. Zhang, and D. Infield, "Applying thermophysics for wind turbine drivetrain fault diagnosis using scada data," *IET Renewable Power Generation*, vol. 10, pp. 661–668, 2016.

[82] H.-s. Zhao and X.-t. Zhang, "Early fault prediction of wind turbine gearbox based on temperature measurement," pp. 1–5, 10 2012.

[83] M. Mana, E. Piccioni, and L. Terzi, "Wind turbine fault diagnosis through temperature analysis: an artificial neural network approach," *DIAGNOSTYKA*, vol. 18, 2017.

[84] J. Carroll, S. Koukoura, A. McDonald, A. Charalambous, S. Weiss, and S. McArthur, "Wind turbine gearbox failure and remaining useful life prediction using machine learning techniques," *Wind Energy*, vol. 22, pp. 360–375, 3 2019.

[85] M. Lv, S. Liu, X. Su, and C. Chen, "General log-linear weibull model combining vibration and temperature characteristics for remaining useful life prediction of rolling element bearings," *Shock and Vibration*, vol. 2020, 2020.

[86] X. J. Zeng, M. Yang, and Y. F. Bo, "Gearbox oil temperature anomaly detection for wind turbine based on sparse bayesian probability estimation," *International Journal of Electrical Power and Energy Systems*, vol. 123, 12 2020.

[87] H. Rashid, E. Khalaji, J. Rasheed, and C. Batunlu, "Fault prediction of wind turbine gearbox based on scada data and machine learning," pp. 391–395, 9 2020.

[88] H. Long, A. A. Lord, D. T. Gethin, and B. J. Roylance, "Operating temperatures of oil-lubricated medium-speed gears: Numerical models and experimental

results," *Proceedings of the Institution of Mechanical Engineers, Part G: Journal of Aerospace Engineering*, vol. 217, pp. 87–106, 2 2003.

[89] J. D. de Gevigney, C. Changenet, F. Ville, and P. Velex, "Thermal modelling of a back-to-back gearbox test machine: Application to the fzg test rig," *Proceedings of the Institution of Mechanical Engineers, Part J: Journal of Engineering Tribology*, vol. 226, pp. 501–515, 6 2012.

[90] A. Boglietti, A. Cavagnino, D. Staton, M. Shanel, M. Mueller, and C. Mejuto, "Evolution and modern approaches for thermal analysis of electrical machines," *IEEE Transactions on Industrial Electronics*, vol. 56, pp. 871–882, 2009.

[91] G. Kylander, *Thermal modelling of small cage induction motors*. PhD thesis, Chalmers University of Technology, 1995.

[92] P. N. Phuc, H. Vansompel, D. Bozalakov, K. Stockman, and G. Crevecoeur, "Inverse thermal identification of a thermally instrumented induction machine using a lumped-parameter thermal model," *Energies*, vol. 13, p. 37, 12 2019.

[93] P. Jaen-Sola and A. McDonald, "Equivalent electrical circuit derivation of a 7mw offshore wind turbine gearbox," *The Journal of Engineering*, 2018.

[94] D. Morrison, "Thermal modelling of a wind turbine gearbox with a view to condition monitoring, msc thesis," Master's thesis, University of Strathclyde, Glasgow (UK), 2017.

[95] T. Burton, D. Sharpe, N. Jenkins, and E. Bossanyi, *Wind Energy Handbook*, ch. Gearbox Efficiency. Wiley, 2001.

[96] C. M. Fernandes, P. M. Marques, R. C. Martins, and J. H. Seabra, "Gearbox power loss. part iii: Application to a parallel axis and a planetary gearbox," *Tribology International*, 2015.

[97] C. M. C. G. Fernandes, L. Blazquez, J. Sanesteban, R. C. Martins, and J. H. O. Seabra, "Energy efficiency tests in a full scale wind turbine gearbox," *Tribology International*, vol. 101, pp. 375–382, 9 2016.

[98] C. M. Fernandes, R. C. Martins, and J. H. Seabra, "Coefficient of friction equation for gears based on a modified hersey parameter," *Tribology International*, vol. 101, pp. 204–217, 9 2016.

[99] C. Changenet, G. Leprince, F. Ville, and P. Velex, "A note on flow regimes and churning loss modeling," *Journal of Mechanical Design*, vol. 133, pp. 121009–121009–5, 12 2011.

[100] O. Janssens, R. Schulz, V. Slavkovikj, K. Stockman, M. Loccufier, R. de Walle, and S. V. Hoecke, "Thermal image based fault diagnosis for rotating machinery," *Infrared Physics 'I&' Technology*, vol. 73, pp. 78–87, 11 2015.

[101] O. Janssens, M. Loccufier, and S. V. Hoecke, "Thermal imaging and vibration-based multisensor fault detection for rotating machinery," *IEEE Transactions on Industrial Informatics*, vol. 15, pp. 434–444, 1 2019.

[102] J. A. Ramirez-Nunez, L. A. Morales-Hernandez, R. A. Osornio-Rios, J. A. Antonino-Daviu, and R. J. Romero-Troncoso, "Self-adjustment methodology of a thermal camera for detecting faults in industrial machinery," pp. 7119–7124, 10 2016.

[103] C. M. Fernandes, P. M. Marques, R. C. Martins, and J. H. Seabra, "Gearbox power loss. part ii: Friction losses in gears," *Tribology International*, vol. 88, pp. 309–316, 2015.

[104] P. M. T. Marques, R. Camacho, R. C. Martins, and J. H. O. Seabra, "Efficiency of a planetary multiplier gearbox: Influence of operating conditions and gear oil formulation," *Tribology International*, vol. 92, pp. 272–280, 12 2015.

[105] S. Koukoura, *Wind turbine gearbox diagnostics using artificial intelligence*. PhD thesis, University of Strathclyde, 2019.

[106] L. Alhmoud and B. Wang, "A review of the state-of-the-art in wind-energy reliability analysis," *Renewable and Sustainable Energy Reviews*, vol. 81, pp. 1643–1651, 2018.

[107] K. Smolders, H. Long, Y. Feng, and P. Tavner, "Reliability analysis and prediction of wind turbine gearboxes," vol. 4, pp. 2660–2682, 01 2010.

[108] *On Lifetime Extension of Wind Turbine Drivetrains*, vol. Volume 9: Ocean Renewable Energy of *International Conference on Offshore Mechanics and Arctic Engineering*, 06 2021.

[109] K. Tartt, A. Kazemi-Amiri, A. R. Nejad, A. McDonald, and J. Carroll, "Development of a vulnerability map of wind turbine power converters," *Journal of Physics: Conference Series*, vol. 2265, p. 032052, may 2022.

[110] H. Li, "Overview of different wind generator systems and their comparisons," *IET Renewable Power Generation*, vol. 2, pp. 123–138(15), June 2008.

[111] I. S. Al-Tubi and H. Long, "Prediction of wind turbine gear micropitting under variable load and speed conditions using iso/tr 15144-1: 2010," *Proceedings of the Institution of Mechanical Engineers, Part C*, vol. 227, no. 9, pp. 1898–1914, 2013.

[112] S. Li and A. Anisetti, "On the flash temperature of gear contacts under the tribo-dynamic condition," *Tribology International*, vol. 97, pp. 6–13, 5 2016.

[113] J. Yao, T. Zhang, X. Wang, D. Zeng, and P. Sun, "Control strategy for suppressing the shafting oscillation of the grid-connected dfig-based wind power generation system," *International Transactions on Electrical Energy Systems*, vol. 29, 06 2019.

[114] Y. Guo and J. Keller, "Investigation of high-speed shaft bearing loads in wind turbine gearboxes through dynamometer testing," *Wind Energy*, vol. 21, no. 2, pp. 139–150, 2018.

[115] B. Standard, "Bs iso/tr 14179-2:2001 gears - thermal capacity - part 2: Thermal load carrying capacity," 2001.

[116] B.-R. Hoehn, K. Michaelis, and M. Hinterstoißer, "Optimization of gearbox efficiency," *GOMABN*, vol. 4883301843, pp. 441–480, 1 2009.

[117] A. W. Wemekamp and Y. Luo, *Efficiency and thermal gearbox calculation*, pp. 1069–1077. Chandos Publishing, 2014.

[118] P. Velex and F. Ville, "An analytical approach to tooth friction losses in spur and helical gears—influence of profile modifications," *Journal of Mechanical Design*, vol. 131, pp. 101008–101008–10, 9 2009.

[119] C. Changenet, X. Oviedo-Marlot, and P. Velex, "Power Loss Predictions in Geared Transmissions Using Thermal Networks-Applications to a Six-Speed Manual Gearbox," *Journal of Mechanical Design*, vol. 128, pp. 618–625, 08 2005.

[120] P. M. T. Marques, C. M. C. G. Fernandes, R. C. Martins, and J. H. O. Seabra, "Power losses at low speed in a gearbox lubricated with wind turbine gear oils with special focus on churning losses," *Tribology International*, vol. 62, pp. 186–197, 6 2013.

[121] C. M. C. G. Fernandes, P. M. T. Marques, R. C. Martins, and J. H. O. Seabra, "Gearbox power loss. part i: Losses in rolling bearings," *Tribology International*, vol. 88, pp. 298–308, 8 2015.

[122] P. Brossier, D. Niel, C. Changenet, F. Ville, and J. Belmonte, "Experimental and numerical investigations on rolling element bearing thermal behaviour," *Proceedings of the Institution of Mechanical Engineers, Part J: Journal of Engineering Tribology*, vol. 235, pp. 842–853, 4 2021.

[123] H. Liu, H. Liu, C. Zhu, and R. G. Parker, "Effects of lubrication on gear performance: A review," *Mechanism and Machine Theory*, vol. 145, p. 103701, 2020.

[124] L. M. Jiji, *Basic Concepts*, pp. 1–23. Springer, Berlin, Heidelberg, 2009.

[125] "Introduction to engineering heat transfer." `https://ocw.mit.edu/courses/16-050-thermal-energy-fall-2002/87d9f4544b7fd64a77201382500d057c_10_part3.pdf`. Accessed: Apr. 07, 2025 [Online].

[126] J. Taler and P. Duda, *Mass and Energy Balance Equations*, pp. 7–27. Berlin, Heidelberg: Springer Berlin Heidelberg, 2006.

[127] "Wind energy and power calculations." https://www.e-education.psu.edu/emsc297/node/649. Accessed: Apr. 04, 2025 [Online].

[128] J. D. de Gevigney, C. Changenet, F. Ville, P. Velex, and S. R. G. Becquerelle, "Analysis of no-load dependent power losses in a planetary gear train by using thermal network method," 2014.

[129] T. Touret, C. Changenet, F. Ville, and J. Cavoret, "Experimental investigation on the effect of micropitting on friction - part 2: Analysis of power losses evolution on a geared system," *Tribology International*, vol. 153, p. 106551, 1 2021.

[130] NationalInstruments, "Overview of temperature sensors - national instruments." http://sine.ni.com/np/app/main/p/ap/daq/lang/en/pg/1/sn/n17:daq,n21:17557/fmid/6681/. Accessed: Aug. 13, 2018 [Online].

[131] InstrumentationTools, "How 3 wire rtd lead wire resistance eliminated?." https://instrumentationtools.com/how-3-wire-rtd-lead-wire-resistance-eliminated/?utm_content=cmp-true. Accessed: Dec. 16 2019 [Online].

[132] I. E. COMMISSION, "Iec 60751:2002 industrial platinum resistance thermometers and platinum temperature sensors," 2022.

[133] "Measuring temperature with rtds – a tutorial." https://newton.ex.ac.uk/teaching/CDHW/Sensors/an046.pdf. Accessed: Apr. 07, 2025 [Online].

[134] FLIR, "Handheld thermal cameras — flir industrial — teledyne flir." https://www.flir.co.uk/browse/industrial/handheld-thermal-cameras/. Accessed: Mar. 13, 2024. [Online].

[135] E. Hart, A. Stock, G. Elderfield, R. Elliott, J. Brasseur, J. Keller, Y. Guo, and W. Song, "Impacts of wind field characteristics and non-steady deterministic wind events on time-varying main-bearing loads," *Wind Energy Science*, vol. 7, no. 3, pp. 1209–1226, 2022.

[136] K. Tartt, A. Kazemi-Amiri, A. Nejad, J. Carroll, and A. McDonald, "Life extension of wind turbine drivetrains by means of scada data: case study of generator bearings in an onshore wind farm," vol. 24, Dec. 2024.

[137] J. Carroll, S. Koukoura, A. McDonald, A. Charalambous, S. Weiss, and S. McArthur, "Wind turbine gearbox failure and remaining useful life prediction using machine learning techniques," *Wind Energy*, vol. 22, no. 3, pp. 360–375, 2019.

[138] A. Murgia, R. Verbeke, E. Tsiporkova, L. Terzi, and D. Astolfi, "Discussion on the suitability of scada-based condition monitoring for wind turbine fault diagnosis through temperature data analysis," *Energies*, vol. 16, no. 2, 2023.

[139] D. Astolfi, "Wind turbine drivetrain condition monitoring through scada-collected temperature data: Discussion of selected recent papers," *Energies*, vol. 16, no. 9, 2023.

[140] B. Corley, S. Koukoura, J. Carroll, and A. Mcdonald, "Combination of thermal modelling and machine learning approaches for fault detection in wind turbine gearboxes," 2021.

[141] I. Dincer and C. Zamfirescu, "Chapter 1 - fundamental aspects," in *Sustainable Hydrogen Production* (I. Dincer and C. Zamfirescu, eds.), pp. 1–63, Elsevier, 2016.

[142] "What is random forest? - ibm." `https://www.ibm.com/think/topics/random-forest`. Accessed: Apr. 04, 2025 [Online].

[143] B. Standard, "Bs en iec 61400-2:2019 wind energy generation systems," 2019.

[144] "Fiber-optical sensors for condition monitoring of wind turbines." `https://www.hbkworld.com/en/knowledge/resource-center/articles/strain-measurement-basics/optical-strain-sensor-fundamentals/tips-and-tricks-fiber-optical-sensors-for-condition-monitoring`. Accessed: Apr. 07, 2020 [Online].